uOttawa

L'Université canadienne
Canada's university

FACULTÉ DES ÉTUDES SUPÉRIEURES ET POSTOCTORALES

uOttawa

L'Université canadienne
Canada's university

FACULTY OF GRADUATE AND POSDOCTORAL STUDIES

Derek Prosser
AUTEUR DE LA THÈSE / AUTHOR OF THESIS

Ph.D. (Neuroscience)
GRADE / DEGREE

Department of Cellular and Molecular Medicine
FACULTÉ, ÉCOLE, DÉPARTEMENT / FACULTY, SCHOOL, DEPARTMENT

Novel links between protein sorting and cytoskeletal dynamics in the secretory pathway

TITRE DE LA THÈSE / TITLE OF THESIS

Johnny Ngsee
DIRECTEUR (DIRECTRICE) DE LA THÈSE / THESIS SUPERVISOR

CO-DIRECTEUR (CO-DIRECTRICE) DE LA THÈSE / THESIS CO-SUPERVISOR

EXAMINATEURS (EXAMINATRICES) DE LA THÈSE / THESIS EXAMINERS

Antonio Colavita

Wayne Sossin

Stephen Gee

Xiaohui Zha

Gary W. Slater
Le Doyen de la Faculté des études supérieures et postdoctorales / Dean of the Faculty of Graduate and Postdoctoral Studies

Novel links between protein sorting and cytoskeletal dynamics in the secretory pathway

Derek C. Prosser

Thesis submitted to the Faculty of Graduate and Postdoctoral Studies in partial fulfillment of the requirements for the Ph.D. degree in Neuroscience

Department of Neuroscience

Faculty of Medicine

University of Ottawa

Your file Votre référence
ISBN: 978-0-494-46518-9
Our file Notre référence
ISBN: 978-0-494-46518-9

Abstract

Sorting of proteins and lipids is an essential process for maintaining organelle composition and integrity in eukaryotic cells. In many compartments, proteins are sequestered into membrane subdomains from which vesicle budding and scission occur, thereby allowing transport to other compartments. Protein sorting and vesicle transport are closely coupled to the cytoskeleton, where actin and/or tubulin dynamics are involved in multiple steps of this process. However, links between sorting and the cytoskeleton remain unclear.

Within the endocytic pathway, sorting nexins (SNXs) play a role in sorting of internalized receptors for recycling or degradation. In this study, SNX1 and SNX2 are shown to interact with Kalirin-7 (Kal7), a neuronal guanine nucleotide exchange factor (GEF) that activates the actin-modulating GTPases Rac1 and RhoG. Overexpression of either SNX with Kal7 in epithelial cells potentiated lamellipodia formation in a GEF- and RhoG-dependent manner, while SNX depletion inhibited this phenotype. Furthermore, SNX2 enhanced Kal7-dependent neurite extension in nerve growth factor-treated PC12 cells. Finally, SNX1 and SNX2 interact with inactive RhoG, and could thus recruit the small GTPase to its GEF.

In the exocytic pathway, proteins are synthesized at the endoplasmic reticulum (ER), where they are folded prior to transport and maturation in post-ER compartments. ER tubules extend along the microtubule network, and this link is critical for ER structure and function. The VAMP-associated proteins VAPA and VAPB are ER transmembrane proteins that interact with microtubules through a conserved major sperm protein (MSP) domain. This link between ER and microtubules could create immobile obstacles in the

ER membrane, which could adversely affect membrane protein diffusion. In this study, overexpression of VAPA, but not VAPB, inhibited lateral diffusion of the transmembrane cargo VSVG, suggesting differential effects on cargo sorting. Furthermore, a P56S mutation in the VAPB MSP domain, which is linked to adult-onset amyotrophic lateral sclerosis, caused ER aggregation that blocked anterograde VSVG transport. These defects could be rescued by co-expression of a FFAT (two phenylalanines in an acidic tract) motif found in numerous VAP-interacting proteins, which dissociated VAPs from microtubules. Overall, these findings demonstrate novel links between protein sorting and cytoskeletal dynamics in multiple transport processes.

Table of Contents

List of Figures

List of Tables

List of Abbreviations

Throughout this study, the standard three- or one-letter code is used for abbreviation of amino acids unless otherwise stated. Where specified within the text, Φ refers to a bulky, hydrophobic amino acid, A refers to an aliphatic amino acid, and X refers to any amino acid.

Nonstandard abbreviations used are:

ALS	amyotrophic lateral sclerosis
β-ME	β-mercaptoethanol
BAR	Bin/amphiphysin/Rvs
CERT	ceramide transfer protein
CgB	Chromogranin B
CHAPS	3-(3-cholamidopropyl)diethylammonio-1-propanesulfonate
CHO	Chinese hamster ovary
CLIMP-63	cytoskeleton-linking membrane protein of 63 kDa
CMV	cytomegalovirus
CPY	carboxypeptidase Y
DH	Dbl homology
DMEM	Dulbecco's modified Eagle's medium
DMSO	dimethyl sulfoxide
EEA1	Early endosomal antigen 1
EGFR	epidermal growth factor receptor
Endo H	Endoglycosidase H
ER	endoplasmic reticulum
ERAD	ER-associated degradation
ERGIC	ER-Golgi intermediate complex
ESCRT	endosomal sorting complex required for transport
F-BAR	Fes/CIP4 homology-BAR
FBS	fetal bovine serum
FFAT	two phenylalanines in an acidic tract
FRAP	fluorescence recovery after photobleaching
GAP	GTPase activating protein
GAPDH	glyceraldehyde 3-phosphate dehydrogenase
GDF	GDI displacement factor
GDI	GDP dissociation inhibitor
GDPβS	guanosine 5'-(β-thio)diphosphate
GEF	guanine nucleotide exchange factor
GFP	green fluorescent protein
GTPase	guanosine triphosphatase
GTPγS	guanosine 5'-(γ-thio)triphosphate
HA	hemagglutinin
HD	Huntington's disease
HAP1	huntingtin-associated protein 1
Hrs	hepatocyte growth factor-regulated tyrosine kinase substrate

Htt	huntingtin
I-BAR	inverse BAR
iNOS	inducible nitric-oxide synthase
IRSp53	insulin receptor substrate of 53 kDa
Kal7	Kalirin-7
MIM	missing-in-metastasis
MLC	myosin light chain
mRFP	monomeric red fluorescent protein
MSP	major sperm protein
MVB	multivesicular body
NGF	nerve growth factor
Ni-NTA	Ni-nitrilotriacetic acid
NP-40	Nonidet P-40
N-WASP	neural Wiscott-Aldrich syndrome protein
ORP	OSBP-related protein
OSBP	oxysterol-binding protein
PAK	p21-activated kinase
PAR1	protease-activated receptor 1
PBS	phosphate-buffered saline
PDZ	PSD-95/discs large/ZO1
PH	Pleckstrin homology
PI	phosphoinositide
PI(3)P	phosphatidylinositol 3-phosphate
$PI(3,5)P_2$	phosphatidylinositol (3,5)-bisphosphate
$PI(4,5)P_2$	phosphatidylinositol (4,5)-bisphosphate
PIPES	1,4-piperazinebis(ethanesulfonic acid)
PMSF	phenylmethylsulfonyl fluoride
polyQ	polyglutamine
PX	Phox homology
RGS	regulator of G-protein signaling
RT-PCR	reverse transcriptase-polymerase chain reaction
SGEF	SH3-containing GEF
SH3	Src homology 3
siRNA	small interfering RNA
SNAP-25	synaptosome-associated protein of 25 kDa
SNARE	soluble N-ethylmaleimide-sensitive factor attachment protein receptor
SNX	sorting nexin
SOD1	superoxide dismutase 1
TAP	tandem affinity purification
TGN	*trans*-Golgi network
UPR	unfolded protein response
VAMP	vesicle-associated membrane protein
VAP	VAMP-associated protein
VSVG	vesicular stomatitis virus glycoprotein G
WAVE	WASP family verprolin-homologous protein

Acknowledgements

There are many people who have supported me throughout my studies, and without whom this work would not have been possible. Above all, I owe a great debt of gratitude to Dr. Johnny Ngsee for his excellent guidance, mentorship and friendship throughout the years. His vast wealth of knowledge and passion for science have been a constant source of inspiration, and have strongly influenced my own desire to pursue a career in science. Secondly, I would like to thank all of the present and former members of the lab for helping to create such a great work environment. It has been an honor to work with such a great group of people. I would especially like to thank Dr. Pierre-Yves Gougeon, Duvinh Tran and Carine Verly for their contributions to the VAP project. Yves performed a number of preliminary studies, while Duvinh and Carine conducted additional experiments that made publication of the work possible.

I would also like to thank my thesis advisory committee, Drs. Antonio Colavita, Heidi McBride and Luc Sabourin, for their excellent advice and insight, which greatly strengthened and focused this study. In addition, I would like to acknowledge the NSERC and OGSST postgraduate scholarship programs for supporting me in my studies.

Finally, I would like to express my gratitude to my friends and family, who have always supported me in all of my efforts. I would especially like to thank Yulia Artemenko, who has always been there to share this experience with and to remind me of what is important in life. Yulia's kindness and understanding – even during the most difficult times – have meant the world to me. She has been the most important person in my life throughout this entire process, and I couldn't have accomplished any of this without her support.

Authorizations

Figures 1 and 2 are reprinted from J. S. Bonifacino and B. S. Glick. (2004) The mechanisms of vesicle budding and fusion. *Cell* 116:153-166, with permission from Elsevier. The following summary appears in the limited license:

ELSEVIER LIMITED LICENSE
TERMS AND CONDITIONS
Jul 08, 2008

This is a License Agreement between Derek C Prosser ("You") and Elsevier Limited ("Elsevier Limited"). The license consists of your order details, the terms and conditions provided by Elsevier Limited, and the payment terms and conditions.

Supplier	Elsevier Limited The Boulevard,Langford Lane Kidlington,Oxford,OX5 1GB,UK
Registered Company Number	1982084
Customer name	Derek C Prosser
Customer address	Ottawa Health Research Institute Ottawa, ON K1Y 4E9
License Number	1984361194286
License date	Jul 08, 2008
Licensed content publisher	Elsevier Limited
Licensed content publication	Cell
Licensed content title	The Mechanisms of Vesicle Budding and Fusion
Licensed content author	Juan S. Bonifacino and Benjamin S. Glick
Licensed content date	23 January 2004
Volume number	116
Issue number	2
Pages	14
Type of Use	Thesis / Dissertation
Portion	Figures/table/illustration/abstracts
Portion Quantity	2
Format	Print
You are an author of the Elsevier article	No
Are you translating?	No
Purchase order number	
Expected publication date	Aug 2008
Elsevier VAT number	GB 494 6272 12

Portions of data presented in chapters II and IV appear in the following publication:

D. C. Prosser, D. Tran, P.-Y. Gougeon, C. Verly and J. K. Ngsee. (2008) FFAT rescues VAPA-Mediated Inhibition of ER-to-Golgi Transport and VAPB-Mediated ER Aggregation. *J. Cell Sci.* 121:3052-3061.

The following statement appears on the author information page of the Journal of Cell Science website:

Author rights

Authors remain the owners of the copyright to the article and retain the following non-exclusive rights (for further details, please refer to the licence agreement that accompanies article proofs):

(1) authors may reproduce the article, in whole or in part, in any printed book (including thesis) of which they are author.

The full copyright and reproduction policy can be found at the following website:

http://www.biologists.com/web/submissions/jcs_information.html

Introduction

Vesicular trafficking regulates organelle homeostasis in eukaryotes

Eukaryotic cells have evolved a complex system of organelles in order to compartmentalize numerous biosynthetic, degradative, metabolic and regulatory functions. Maintenance of the structural and functional integrity of organelles requires constant delivery of new proteins and lipids, as well as removal of non-functional material. Vesicular trafficking is the principal method used to co-ordinate this process, where material buds from a donor compartment in the form of membrane-bounded vesicles, and is transported to an acceptor compartment for fusion (Bonifacino and Glick, 2004). In this manner, it is possible to precisely regulate the composition of a compartment. Although vesicle budding, transport and fusion have been extensively studied, many aspects of this field are not fully understood. Among these, the regulation of protein sorting has generated particular interest, where mechanisms exist to differentiate between proteins that are destined for other compartments and those that must be retained. The following study characterizes novel functions for proteins involved in sorting at multiple transport steps, and examines the relationship between protein sorting and interaction with or modulation of the cytoskeleton.

Intracellular transport pathways

Vesicle transport events are generally divided into the exocytic and endocytic pathways, although there is extensive cross-talk between the two systems (Figure 1). In the exocytic pathway, membrane-associated and secreted proteins are synthesized at the endoplasmic reticulum (ER), where they are inserted into the ER membrane or are

Figure 1: Intracellular transport pathways. Transmembrane and secreted proteins are synthesized at the ER, where they are inserted into or translocated across the membrane. Following folding and assembly, proteins destined for transport through the secretory pathway are sequestered into ER exit sites for COPII-dependent budding and transport to the Golgi complex via the ER-Golgi intermediate compartment (ERGIC). Following processing within the Golgi complex, proteins are sorted for COPI-dependent retrieval to the ER or clathrin-mediated budding from the TGN for transport to the cell surface or endocytic pathway. Cell surface proteins can be internalized via clathrin-dependent and independent endocytosis for delivery to early endosomes. Subsequently, proteins are transported to late endosomes and/or multivesicular bodies, which fuse with lysosomes for degradation. Within the endocytic pathway, there are multiple opportunities for cargo sorting and recycling to the TGN or back to the cell surface, and as-yet unidentified coat proteins might mediate these processes. Reprinted from Bonifacino and Glick (2004) *Cell* 116: 153-166, with permission from Elsevier.

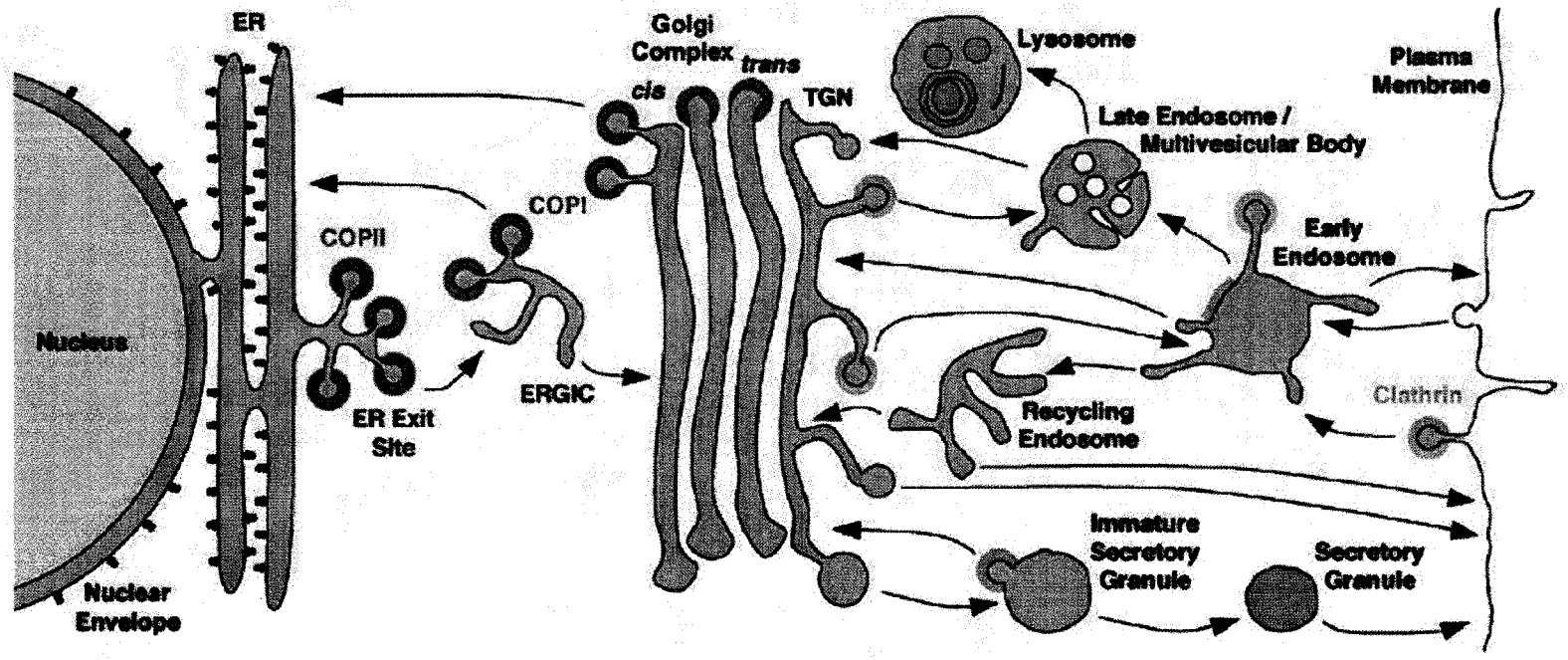
ER
Golgi Complex
cis
trans
TGN
Lysosome
Plasma Membrane
Late Endosome / Multivesicular Body
COPI
COPII
Early Endosome
Nucleus
ER Exit Site
ERGIC
Clathrin
Recycling Endosome
Immature Secretory Granule
Secretory Granule
Nuclear Envelope

translocated to the lumen. From the ER, proteins are transported to the Golgi complex via the ER-Golgi intermediate compartment (ERGIC). After further maturation in the Golgi complex, proteins proceed to the *trans*-Golgi network (TGN), where they are sorted for transport to the plasma membrane or endocytic pathway, or alternatively for secretion into the extracellular space. Within the secretory pathway, there are additional retrograde transport steps within the Golgi complex and from the Golgi back to the ER, which allow retrieval of ER proteins from post-ER compartments. The ER is also a site of lipid synthesis, thus anterograde transport along the secretory pathway is the main method for delivery of newly synthesized proteins and lipids to other sites in the cell.

In the endocytic pathway, proteins and lipids are internalized from the plasma membrane (discussed in further detail below) and are transported to early endosomes. Proteins then proceed from early endosomes to late endosomes and/or multivesicular bodies (MVBs), which are generated by inward budding of endosomal membranes to form internal vesicles. Subsequently, these compartments fuse with or mature into lysosomes, which are acidified compartments containing hydrolytic enzymes for protein and lipid degradation (Futter et al., 1996). At numerous stages of the endocytic pathway, there are sorting mechanisms for recycling back to the plasma membrane or to the *trans*-Golgi network, which can divert proteins away from lysosomal degradation. Importantly, actin is required at numerous stages of the endocytic pathway, and disruption of actin dynamics severely impairs endocytic events (Merrifield et al., 2002; Yarar et al., 2005). Together, the exocytic and endocytic pathways play critical roles in biosynthetic and degradative processes.

Vesicular transport processes employ common mechanisms

In general, vesicular trafficking between compartments follows a common order of events: protein and lipid sorting, vesicle budding and scission, transport along the cytoskeleton, tethering to and finally fusion with the target compartment (Figure 2). For proteins to be incorporated into vesicles, they must first be sorted and segregated into membrane subdomains. While this process may involve passive diffusion and/or active sequestration, protein sorting has the dual effect of concentrating cargo into eventual sites of budding and restricting or reducing incorporation of non-cargo proteins into vesicles. Alternatively, bulk flow of proteins and membranes may occur, which allows non-specific transport between compartments. Subsequently, resident proteins that have escaped the initial compartment can be sorted and retrieved. For example, soluble ER proteins containing a C-terminal KDEL sequence are retrieved from post-ER structures and recycled to the ER by the KDEL receptor (Pelham, 1988; Semenza et al., 1990).

At sites of cargo sequestration and/or vesicle budding, cargo molecules recruit coat proteins, either directly or via interaction with adaptor proteins, to drive or stabilize regions of high membrane curvature necessary for vesicle budding (Bonifacino and Glick, 2004). To date, three major coat protein complexes have been identified in the secretory pathway, each of which appears function at discrete transport steps. The COPII complex, consisting of the small GTPase Sar1 and the coat proteins Sec23/Sec24 and Sec13/Sec31 (Barlowe et al., 1994), is involved in budding of vesicles from the ER. These vesicles then fuse with the ERGIC compartment, also known as vesicular-tubular clusters (VTCs). Secondly, COPI, or coatomer, is a heptameric complex that regulates anterograde transport from ERGIC to *cis*-Golgi and between Golgi cisternae, as well as

Figure 2: Vesicle budding and fusion. Prior to transport, soluble or membrane-associated cargo molecules must be sorted into budding vesicles either through active or passive mechanisms. At sites of cargo concentration, coat proteins and their adaptors are recruited, and interaction with cargo and/or membranes drives curvature of the budding vesicle. Once high-curvature membrane domains are generated, a scission event occurs to separate the nascent vesicle from the donor compartment. Subsequently, vesicles are transported along the cytoskeleton, and uncoating takes place. Prior to fusion, vesicles tether to the acceptor compartment, possibly through Rab GTPases and tethering complexes. Vesicle docking and fusion can then occur through SNARE proteins, and the contents of the vesicle are released into the acceptor compartment. Reprinted from Bonifacino and Glick (2004) *Cell* 116: 153-166, with permission from Elsevier.

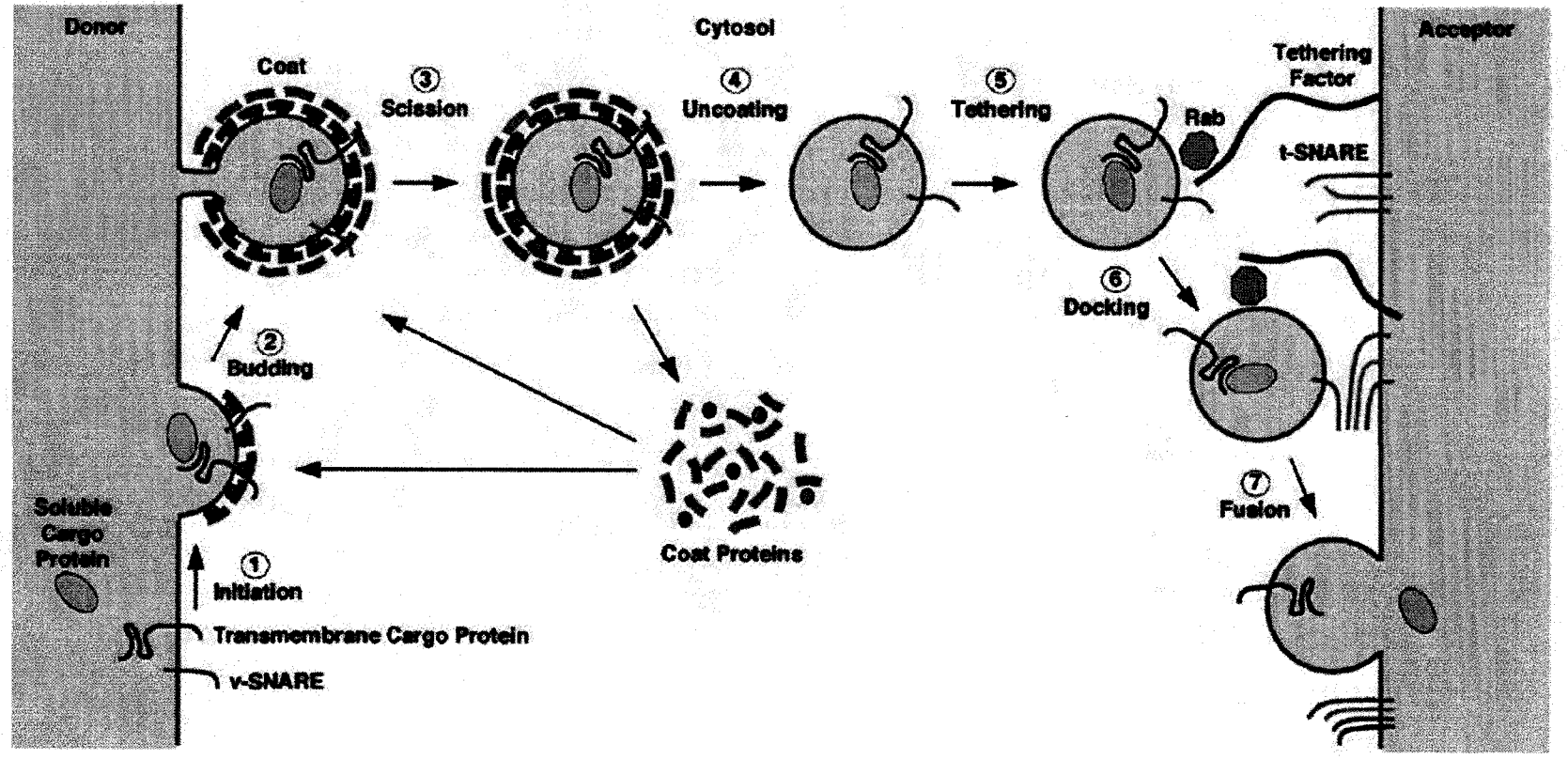
Donor
Cytosol
Acceptor
Coat
③
Scission
④
Uncoating
⑤
Tethering
Tethering
Factor
Rab
t-SNARE
⑥
Docking
②
Budding
Soluble
Cargo
Protein
①
Initiation
Transmembrane Cargo Protein
v-SNARE
Coat Proteins
⑦
Fusion

retrograde Golgi-to-ER retrieval (Lee et al., 2004; Waters et al., 1991). Finally, transport from the TGN to the plasma membrane and some forms of endocytosis are mediated by adaptor proteins and the clathrin coat (Bonifacino and Glick, 2004). Vesicles are pinched from the donor compartment, either by proteins such as the GTPase dynamin, which promotes constriction of the neck of a budding vesicle (Roux et al., 2006), or through other mechanisms that may require actin (Merrifield et al., 2002; Sever et al., 1999). Newly formed vesicles are then uncoated, and are transported along the cytoskeleton by motor proteins such as dynein and kinesin for microtubule-based transport, or myosin (possibly through the class VI myosins involved in retrograde movement along actin cables) for actin-based transport (Buss et al., 2001). Actin polymerization can also propel endocytic vesicles by forming comet tails that generate compressive force, causing 'rocketing' of vesicles through the cytosol (Benesch et al., 2002; Kovacs et al., 2006).

To ensure that vesicles have reached the appropriate compartment, proteins such as the Rab family of Ras-like small GTPases interact with tethering complexes on the acceptor compartment (Cai et al., 2007). There are over 60 mammalian Rab isoforms identified which have differential localizations and interactions with other proteins to regulate specific transport steps (Zerial and McBride, 2001). The large number of Rab GTPases underscores the complexity of target specificity, which is essential to prevent cargo delivery to inappropriate compartments. Finally, fusion is mediated by the soluble N-ethylmaleimide-sensitive factor attachment protein receptor (SNARE) proteins (Söllner et al., 1993). For synaptic vesicles, there is one SNARE protein on the vesicle, termed vesicle-associated membrane protein 2 (VAMP2), and two SNAREs on the target membrane, Syntaxin 1 and SNAP-25 (synaptosome-associated protein of 25 kDa). Each

protein is membrane-associated and contains at least one α-helical motif that interacts with other SNAREs. SNARE proteins on the vesicle and target membranes (v- and t-SNAREs, respectively) interact to form a parallel four-helix bundle, with one helix contributed by VAMP2 and Syntaxin 1, and two from SNAP-25 (Söllner et al., 1993; Sutton et al., 1998). Other donor and acceptor combinations use different SNARE proteins, thereby adding a further level of refinement to the specificity of fusion (Pevsner et al., 1994). Overall, the transport and fusion processes involve complex co-ordination of multiple events to ensure appropriate cargo incorporation and target specificity.

Vesicular trafficking within the endocytic pathway

Protein sorting in the endocytic pathway

The endocytic pathway is an important process for nutrient uptake, but is also critically important for turnover of proteins and lipids as well as for regulation of extracellular signals. Ligand-receptor interactions at the plasma membrane often result in receptor internalization, and the endocytic pathway is critical for regulation of signal termination through protein degradation. Alternatively, recycling back to the plasma membrane can allow further rounds of signaling to occur, thereby amplifying a signal or extending its duration. For recycling to occur, receptors must be diverted away from the lysosomal pathway to recycling endosomes or to the *trans*-Golgi network for subsequent return to the plasma membrane. Alternatively, proteins may be actively sorted for lysosomal degradation. The presence of consensus sequences within the cytoplasmic portion of many receptors, such as tyrosine-containing (YXXΦ, where X is any amino acid and Φ is a bulky, hydrophobic amino acid) or di-leucine (DXXLL or

[D/E]XXXL[L/I]) motifs, mediates recruitment of adaptor and coat proteins involved in sorting (Bonifacino and Traub, 2003). Additionally, ubiquitination of receptors recruits sorting proteins such as the hepatocyte growth factor-regulated tyrosine kinase substrate (Hrs) and members of the endosomal sorting complex required for transport (ESCRT-I) to promote incorporation into MVBs and delivery to lysosomes (Bache et al., 2003; Katzmann et al., 2001; Raiborg et al., 2002). Sorting is also dependent on the lipid composition of endosomal membranes. Endocytic compartments are enriched in specific subpopulations of phosphoinositides (PIs); for example, sites of clathrin-mediated endocytosis at the plasma membrane contain high levels of $PI(4,5)P_2$ (phosphatidylinositol-4,5-bisphosphate), while early and late endosomes are enriched in PI(3)P (phosphatidylinositol-3-phosphate) and $PI(3,5)P_2$ (phosphatidylinositol-3,5-bisphosphate), respectively (Roth, 2004). Many proteins involved in endocytosis and receptor sorting contain domains that recognize specific PI species, and are thus recruited to compartments enriched in these lipids (Lemmon, 2008).

Sorting nexins are phosphoinositide-binding proteins involved in receptor sorting

Sorting nexins (SNXs) are a recently identified family of approximately 30 proteins involved in sorting and trafficking events at multiple steps within the endocytic pathway. All SNXs contain a Phox homology (PX) domain that shares homology with the $p40^{phox}$ and $p47^{phox}$ subunits of NADPH oxidase, and inserts into the membrane via a hydrophobic lipid-binding pocket lined with basic residues that recognize the negatively-charged PI headgroup (Bravo et al., 2001; Hiroaki et al., 2001). SNX isoforms show preference for specific PIs, and binding specificity is thought to be important for cellular

function through recruitment to appropriate membrane domains (Worby and Dixon, 2002). For example, while SNX1 and SNX2 bind preferentially to PI(3)P and PI(3,5)P_2, SNX9 interacts broadly with PIs containing two or three phosphate groups (Carlton et al., 2005; Cozier et al., 2002; Lundmark and Carlsson, 2003; Yarar et al., 2007). The majority of SNXs contain additional domains that are required for function. Many of these, including Bin/amphiphysin/Rvs (BAR), regulator of G-protein signaling (RGS) and Src homology 3 (SH3) domains, are common in proteins involved in cell signaling and/or endocytosis, suggesting potential roles for SNXs in these processes (Cullen, 2008; Worby and Dixon, 2002).

In addition to PX domain-mediated recruitment to endosomal membranes, SNXs also interact with internalized receptors to direct recycling or delivery to lysosomes. Initially, SNX1 was identified as a protein that could interact with the lysosomal targeting motif of the epidermal growth factor receptor (EGFR), and overexpression of SNX1 promoted EGFR degradation (Kurten et al., 1996). Although these results identified a role for SNX1 in lysosomal delivery of EGFR, a later study suggested that the observed effects were due to protein overexpression, since knockdown of SNX1 or the closely related SNX2 did not affect receptor turnover (Gullapalli et al., 2004). Since the initial characterization of SNX1, many studies have identified interactions of other SNXs with numerous cell-surface or lysosomal sorting receptors (Haft et al., 1998; Worby and Dixon, 2002). These interactions can promote delivery to lysosomes, as is the case for SNX1 and the protease-activated receptor PAR1 (Gullapalli et al., 2006). Alternatively, SNXs may direct recycling back to the cell surface as seen for SNX4 and the transferrin receptor or Grd19p/Snx3p and the yeast iron transporters Ftr1p and Fet3p (Strochlic et

al., 2007; Traer et al., 2007), or endosome-to-TGN retrieval of the cation-independent mannose 6-phosphate receptor by SNX1, SNX2, SNX5 and SNX6 (Rojas et al., 2007; Wassmer et al., 2007). Although SNX proteins appear to play diverse roles in receptor sorting, the mechanisms by which this function is achieved are not yet clear.

Retromer is an SNX-containing complex involved in endosome-to-TGN retrieval

Initial genetic screens in the yeast *Saccharomyces cerevisiae* identified more than 40 genes that played a role in sorting of the hydrolytic enzyme carboxypeptidase Y (CPY) to the vacuole, which is the yeast equivalent of mammalian lysosomes (Bankaitis et al., 1986; Banta et al., 1988; Robinson et al., 1988; Rothman et al., 1989; Rothman and Stevens, 1986). Among the products of these genes, five proteins (Vps5p, Vps17p, Vps26p, Vps29p and Vps35p) were found to be necessary for endosome-to-Golgi retrieval of Vps10p, a receptor required for lysosomal delivery of CPY (Horazdovsky et al., 1997; Seaman et al., 1997; Seaman et al., 1998). These proteins form a pentameric sorting complex, termed retromer (Seaman et al., 1998). Retromer is composed of two distinct subcomplexes in yeast, with Vps26p, Vps29p and Vps35p forming a cargo-selective subcomplex, and a Vps5p/Vps17p heterodimer acting as an additional structural subcomplex (Figure 3). While Vps35p interacts directly with cargo proteins (Nothwehr et al., 1999; Nothwehr et al., 2000), Vps26p and Vps29p stabilize membrane association and mediate interaction with Vps5p/Vps17p (Gokool et al., 2007; Reddy and Seaman, 2001). Vps5p and Vps17p are PX and BAR domain-containing proteins that dimerize via the BAR domain, which is proposed to drive membrane tubulation as described in further detail below (Horazdovsky et al., 1997; Seaman and Williams, 2002).

Figure 3: The retromer complex. Retromer is a pentameric endocytic sorting complex that consists of two distinct subcomplexes. The cargo-recognition subcomplex consists of Vps35, the cargo-interacting subunit, as well as Vps26 and Vps29, which facilitate membrane association and interaction with the structural subcomplex. In yeast, the structural subcomplex consists of Vps5p and Vps17p, which are believed to drive membrane tubulation. In mammals, homo- and heterodimers of SNX proteins appear to fulfill the structural subcomplex roles.

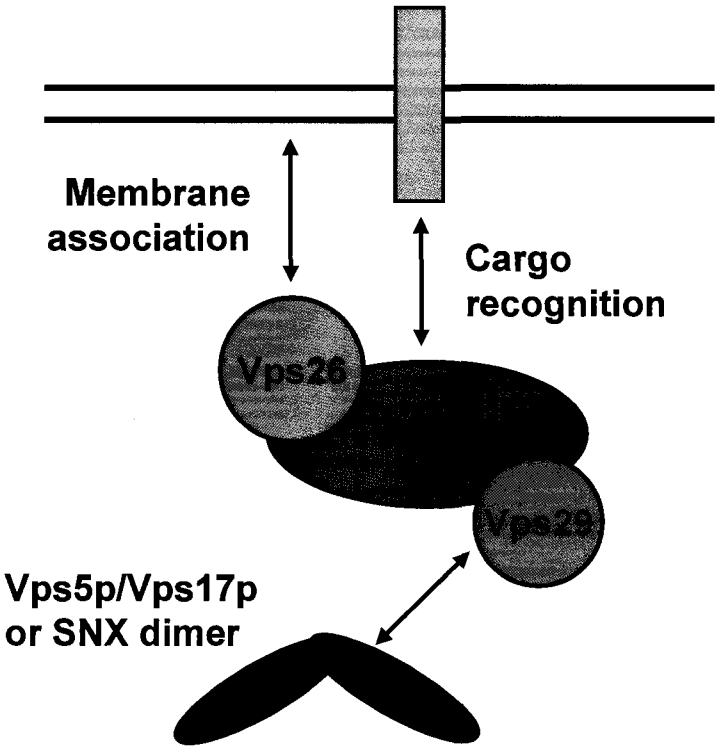
Membrane
association
Cargo
recognition
Vps26
Vps29
Vps5p/Vps17p
or SNX dimer

With the exception of Vps17p, mammalian orthologues of all subunits of the yeast retromer complex have been identified, and are known to form the same cargo recognition and structural complexes (Edgar and Polak, 2000; Haft et al., 2000; Nothwehr and Hindes, 1997). Remarkably, the mammalian retromer complex is required for endosome-to-TGN retrieval of the cation-independent mannose 6-phosphate receptor, the mammalian orthologue of the yeast Vps10p (Arighi et al., 2004). Thus, retromer function appears to have been conserved through evolution. Loss of retromer function by homozygous deletion of Vps26 in mice resulted in embryonic lethality, further demonstrating the importance of retromer activity in development (Radice et al., 1991). Notably, SNX1 and SNX2, which share greater than 60% sequence identity (Figure 4), were identified as the mammalian orthologues of Vps5p. In addition, SNX5 and SNX6 have been identified as potential members of retromer (Wassmer et al., 2007), while SNX3 may function as an adaptor for the complex (Strochlic et al., 2007). Thus, it is possible that additional SNX proteins in mammals could compensate for the lack of a Vps17 orthologue, and different combinations of retromer-associated SNXs could confer receptor or targeting specificity.

Although SNX1 and SNX2 are the most extensively studied members of the SNX family, their cellular functions are not well understood. While retromer-dependent functions of SNX1 and SNX2 are well established, a recent study reported a retromer-independent role for SNX1 in promoting degradation of the protease-activated receptor PAR1 (Gullapalli et al., 2006). In addition, depletion of Vps35 in *Drosophila melanogaster* S2 cells promotes aberrant signaling and actin polymerization events (Korolchuk et al., 2007). These findings suggest that SNX1, SNX2 and Vps35 may

Figure 4: Sequence alignment of human SNX1 and SNX2. Alignments were performed with ClustalW version 2.0.8, with identities indicated by asterisks and similarities depicted by points and colons. Blue and red bars correspond to the PX and BAR domains, respectively. Red amino acid residues in SNX2 were mutated to alanines for generation of the PX or BAR mutants.

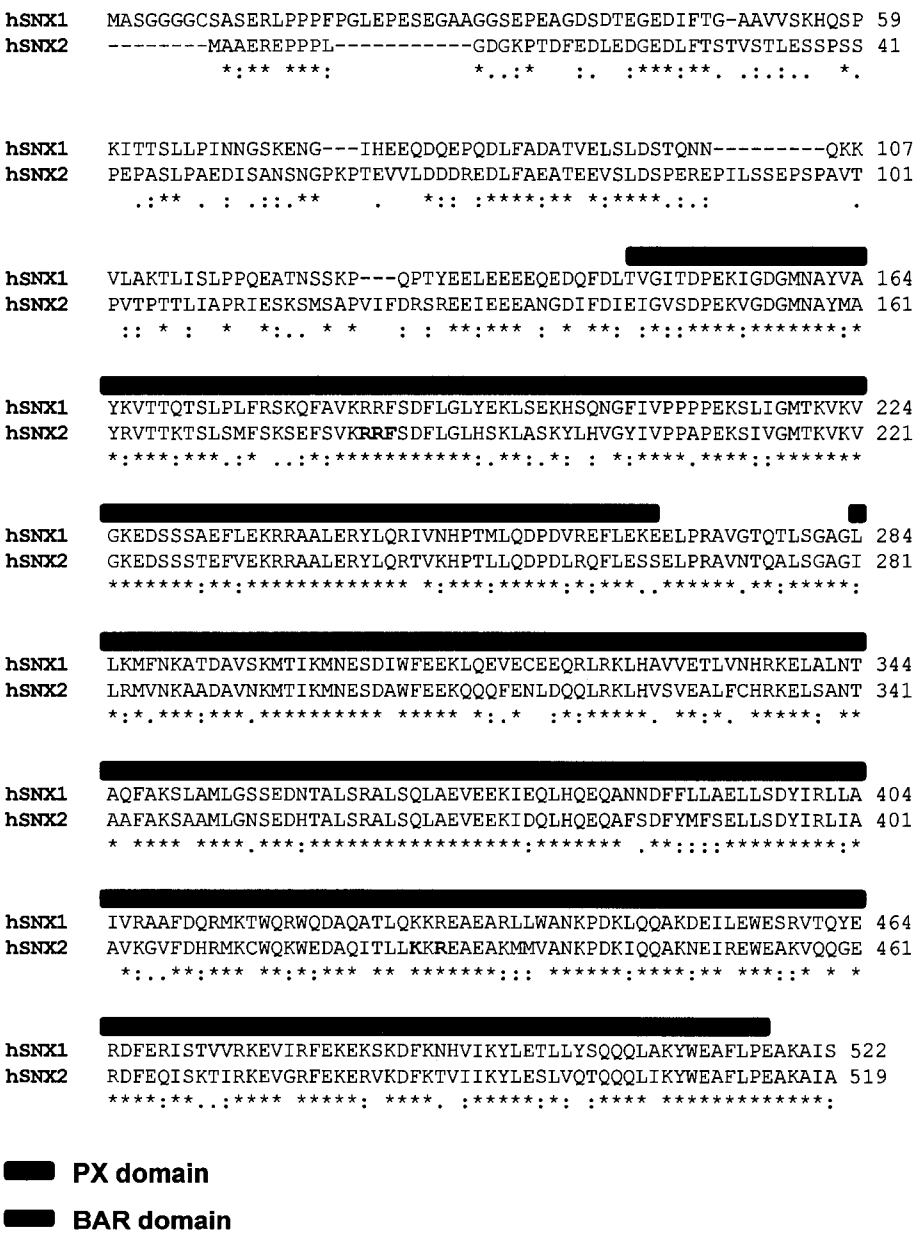
hSNX1 MASGGGGCSASERLPPPFPGLEPESEGAAGGSEPEAGDSDTEGEDIFTG-AAVVSKHQSP 59
hSNX2 --------MAAEREPPPL----------GDGKPTDFEDLEDGEDLFTSTVSTLESSPSS 41
hSNX1 KITTSLLPINNGSKENG---IHEEQDQEPQDLFADATVELSLDSTQNN---------QKK 107
hSNX2 PEPASLPAEDISANSNGPKPTEVVLDDDREDLFAEATEEVSLDSPEREPILSSEPSPAVT 101
hSNX1 VLAKTLISLPPQEATNSSKP---QPTYEELEEEEQEDQFDLTVGITDPEKIGDGMNAYVA 164
hSNX2 PVTPTTLIAPRIESKSMSAPVIFDRSREEIEEEANGDIFDIEIGVSDPEKVGDGMNAYMA 161
hSNX1 YKVTTQTSLPLFRSKQFAVKRRFSDFLGLYEKLSEKHSQNGFIVPPPPEKSLIGMTKVKV 224
hSNX2 YRVTTKTSLSMFSKSEFSVKRRFSDFLGLHSKLASKYLHVGYIVPPAPEKSIVGMTKVKV 221
hSNX1 GKEDSSSAEFLEKRRAALERYLQRIVNHPTMLQDPDVREFLEKEELPRAVGTQTLSGAGL 284
hSNX2 GKEDSSSTEFVEKRRAALERYLQRTVKHPTLLQDPDLRQFLESSELPRAVNTQALSGAGI 281
hSNX1 LKMFNKATDAVSKMTIKMNESDIWFEEKLQEVECEEQRLRKLHAVVETLVNHRKELALNT 344
hSNX2 LRMVNKAADAVNKMTIKMNESDAWFEEKQQQFENLDQQLRKLHVSVEALFCHRKELSANT 341
hSNX1 AQFAKSLAMLGSSEDNTALSRALSQLAEVEEKIEQLHQEQANNDFFLLAELLSDYIRLLA 404
hSNX2 AAFAKSAAMLGNSEDHTALSRALSQLAEVEEKIDQLHQEQAFSDFYMFSELLSDYIRLIA 401
hSNX1 IVRAAFDQRMKTWQRWQDAQATLQKKREAEARLLWANKPDKLQQAKDEILEWESRVTQYE 464
hSNX2 AVKGVFDHRMKCWQKWEDAQITLLKKREAEAKMMVANKPDKIQQAKNEIREWEAKVQQGE 461
hSNX1 RDFERISTVVRKEVIRFEKEKSKDFKNHVIKYLETLLYSQQQLAKYWEAFLPEAKAIS 522
hSNX2 RDFEQISKTIRKEVGRFEKERVKDFKTVIIKYLESLVQTQQQLIKYWEAFLPEAKAIA 519
PX domain
BAR domain

interact with other proteins and have cellular functions that are independent of the retromer complex or, alternatively, that the retromer complex could also be involved in processes other than endocytic sorting.

Retromer may constitute a membrane-deforming coat complex

Recent studies have solved the crystal structures of all three members of the cargo-selective subcomplex of retromer. The first structure reported was that of Vps26, which forms a β-sandwich fold that is highly reminiscent of the β-arrestin family of proteins involved in G protein-coupled receptor signaling (Collins et al., 2008; Shi et al., 2006). Although this similarity indicates an evolutionary relationship between Vps26 and β-arrestins, residues involved in β-arrestin function are not conserved, suggesting that Vps26 is unlikely to have arrestin-like activities. Subsequently, Vps29 was found to share structural similarity with a number of phosphodiesterases and protein phosphatases (Wang et al., 2005). Vps29 also possesses a negatively-charged groove on its surface that is a putative metal-binding site required for phosphodiesterase activity; however, further studies have shown no enzymatic activity (Hierro et al., 2007). Although Vps26 and Vps29 do not appear to perform functions similar to structurally related genes, it remains possible that these activities have not yet been identified or that they act on different proteins or pathways. Finally, the structure of Vps35 in complex with Vps29 was recently solved. Vps35 is a largely α-helical protein that forms a superhelical α-solenoid structure, with Vps26 and Vps29 interacting at opposite ends (Hierro et al., 2007). In the same study, retromer was proposed to form a coat of alternating cargo-selective and structural subcomplexes on tubular endosomal membranes. Thus, retromer might act as a

novel coat complex for cargo sorting and budding of vesicles from endosomal compartments.

The BAR domain as a sensor or inducer of membrane curvature

Interestingly, all of the SNXs that have been identified as members of retromer possess a C-terminal BAR domain, and function of the PX and BAR domains appears to be critical for retromer activity (Carlton et al., 2004). To date, a BAR domain has been described in 12 members of the SNX family, and is invariably located directly downstream of the PX domain (Cullen, 2008; Seet and Hong, 2006). Initially identified as a conserved domain in bridging interactor 1 (BIN1), amphiphysin and the *S. cerevisiae* reduced viability upon starvation (Rvs) proteins Rvs161p and Rvs167p, BAR domains have since been reported in a large number of proteins that are generally targeted to the endocytic pathway (Habermann, 2004; Sivadon et al., 1995). BAR domain proteins have recently generated significant interest due to their ability to tubulate membranes *in vitro* and *in vivo* (Takei et al., 1999), since this property is thought to facilitate vesicle budding. The membrane-deforming activity of the BAR domain was first identified for the amphiphysin and endophilin families of proteins, which generated narrow-diameter tubules when incubated with liposomes *in vitro* (Farsad et al., 2001; Razzaq et al., 2001; Takei et al., 1999). A mechanism for BAR-mediated membrane tubulation was not proposed until the crystal structure of the amphiphysin BAR domain was solved, revealing the formation of a crescent-shaped dimer (Peter et al., 2004) (Figure 5). Each monomer contributes a coiled-coil of three antiparallel α-helices, with kinks in the helices contributing to the overall curvature of the dimer. Furthermore, the concave face

Figure 5: The Bin/amphiphysin/Rvs (BAR) domain family. BAR domains form a crescent-shaped dimer that is enriched in basic residues on the concave face, facilitating interaction with negatively-charged phospholipids. Based on the curvature of the BAR domain, curved membranes of 15-50 nm in diameter are preferentially recognized or can be generated from flat membranes. N-BAR proteins recognize similar curvatures, but possess an N-terminal amphipathic helix that inserts into the lipid bilayer to stabilize interaction or curvature. F-BAR proteins form a shallow crescent that senses or induces curvature of 40-200 nm in diameter, while I-BAR domains form a zeppelin-shaped dimer that induces opposite curvature to that of other BAR domains. Furthermore, some BAR and I-BAR proteins have been found to interact with small GTPases at the apex of the concave face (or the equivalent region of the I-BAR domain).

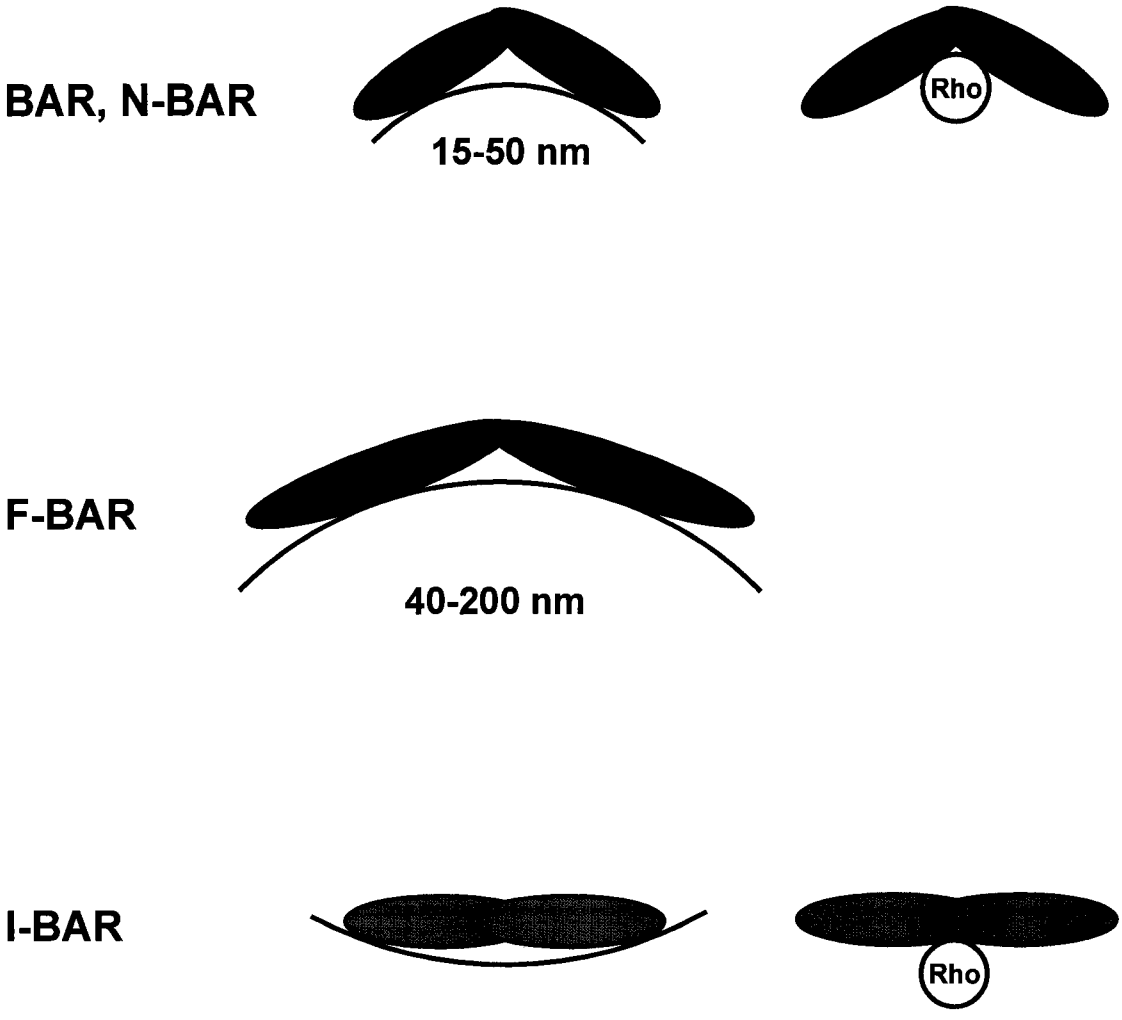
BAR, N-BAR
15-50 nm
Rho
F-BAR
40-200 nm
I-BAR
Rho

of the BAR dimer is enriched in basic, positively charged residues, which provide contact points for interaction with negatively charged phospholipid head groups on the surface of the membrane.

Although BAR domain proteins show very low sequence similarity, the crystal structures of Arfaptin 2, endophilin-B1, APPL1 and SNX9 are all strikingly similar to that of amphiphysin, forming crescent-shaped dimers with similar curvature (Gallop et al., 2006; Li et al., 2007; Pylypenko et al., 2007; Tarricone et al., 2001; Weissenhorn, 2005). Based on the structural features of the BAR domain, the concave surface could preferentially interact with curved membranes, or could induce curvature in a flat membrane sheet. In support of this model, numerous BAR domain-containing proteins, including amphiphysin, oligophrenin, centaurin, SNX1 and SNX2, show increased interaction with high-curvature liposomes and can generate high-curvature (15-50 nm) tubules *in vitro* (Carlton et al., 2004; Carlton et al., 2005; Peter et al., 2004). In addition, many BAR domain-containing proteins contain lipid-binding PX or PH domains. The combination of multiple lipid-interacting motifs could thus serve as a co-incidence detection module, such that the protein will be preferentially recruited to regions of appropriate membrane composition and curvature (Carlton et al., 2004; Yarar et al., 2008).

BAR domain proteins belong to a larger family of membrane-deforming proteins

A number of structures related to the BAR domain have recently been resolved, indicating that the BAR domain may belong to a larger family of proteins with membrane-deforming abilities (Figure 5). First, some proteins, including endophilin and

amphiphysin, contain a short amphipathic helix directly N-terminal to the BAR domain, and this grouping is referred to as N-BAR (Gallop et al., 2006; Peter et al., 2004). One face of the amphipathic helix is concentrated in hydrophobic residues, allowing it to partially insert into the membrane and thereby generate a wedge effect to enhance membrane deformation. Subsequently, a group of proteins containing an N-terminal FCH (Fes/CIP4 homology) domain followed by a coiled-coil motif were found to generate membrane tubules of greater diameter (40-200 nm), and the combination of FCH and coiled-coil was termed F-BAR (Itoh et al., 2005). The crystal structure of the F-BAR proteins CIP4, FBP17 and FCHo2 have been solved, and all of these also form a crescent-shaped dimer (Henne et al., 2007; Shimada et al., 2007). The curvature of F-BAR is shallower than that of BAR, which could explain the increased tubule diameter. Importantly, F-BAR filaments can arrange end-to-end to form a spiral coat around a membrane, which could promote tubule extension (Frost et al., 2008; Shimada et al., 2007). Finally, a BAR-like domain has been identified in the Rac1-binding insulin receptor substrate of 53 kDa (IRSp53) and missing-in-metastasis B (MIM-B). Structurally, IRSp53 and MIM-B differ from other BAR-family proteins in that they form a zeppelin-shaped dimer instead of a crescent (Lee et al., 2007; Mattila et al., 2007; Millard et al., 2005; Suetsugu et al., 2006). This motif, which has been termed inverse BAR (I-BAR), appears to generate opposite curvature with respect to BAR and F-BAR proteins, causing outward protrusion of the plasma membrane. Thus, the BAR family of proteins appears to have evolved and adapted to generate a wide variety of membrane curvatures.

BAR domains can interact with small GTPases

In addition to their established role in sensing or inducing membrane curvature, BAR domains of several proteins have been shown to interact with small GTPases of the Rho and Arf families. Specifically, the BAR domain of Arfaptin 2 has been shown to interact directly with Rac1 and Arf6, and this interaction appears to promote formation of actin-dependent membrane ruffles (D'Souza-Schorey et al., 1997; Van Aelst et al., 1996). While the interaction is specific for the active, GTP-bound form of Arf6, conflicting results have been reported for Rac1, and Rac1 activity may not influence its ability to bind to Arfaptin 2 (Shin and Exton, 2001; Tarricone et al., 2001). Additionally, the BAR domain of Hob3p interacts with Cdc42 in *Schizosaccharomyces pombe*, and this interaction appears to be necessary for Cdc42 recruitment to sites of cell division (Coll et al., 2007). Finally, the I-BAR domain of IRSp53 and MIM-B interacts with Rac1, and this interaction is thought to play a role in membrane remodeling (Bompard et al., 2005; Miki et al., 2000). For Arfaptin 2, the interaction with Rac1 has been mapped to the concave face of the BAR domain, suggesting that GTPase binding and membrane curvature occur via the same site (Tarricone et al., 2001). However, it is not clear whether the curvature sensing and GTPase-interacting properties are sequential or mutually exclusive (Habermann, 2004). It is likely that both properties are important, since the actin cytoskeleton is required for BAR-mediated tubulation *in vivo* (Itoh et al., 2005).

Rho GTPases act as molecular switches

Rho GTPases belong to the Ras-like superfamily of small GTPases, which act as molecular switches to regulate various aspects of cellular function (Wennerberg et al.,

2005). As illustrated in Figure 6, Rho GTPases undergo cycles of activation and inactivation, with activity linked to the nucleotide binding state of the protein. In addition, Rho GTPases are prenylated at a C-terminal CAAX motif (A corresponds to an aliphatic amino acid and X is any amino acid), where a hydrophobic geranylgeranyl moiety is covalently linked to the cysteine residue to serve as a membrane anchor (Pechlivanis and Kuhlmann, 2006). Normally, inactive, GDP-bound Rho is sequestered in the cytosol by Rho GDP dissociation inhibitors (RhoGDIs) to prevent inappropriate activation (DerMardirossian and Bokoch, 2005). In response to certain stimuli such as receptor activation, Rho-GDP is inserted into a membrane compartment, where a guanine nucleotide exchange factor (GEF) stimulates release of GDP to allow binding of GTP and activation of the Rho. Once activated, Rho-GTP recruits a series of effector proteins to execute cellular functions. Subsequently, Rho-mediated signals are terminated by GTPase activating proteins (GAPs), which stimulate the intrinsic GTPase activity of the Rho GTPase, resulting in hydrolysis of GTP to GDP. The inactive Rho-GDP can then be extracted from the membrane by RhoGDI, allowing it to undergo further rounds of recruitment and activation. Because the interaction of GDP-bound Rho GTPases with RhoGDIs is of very high affinity (in the low nM range), Rho GDIs are likely to tightly regulate inactive Rho GTPases by preventing inappropriate membrane recruitment and activation. It has been proposed that proteins or lipids could act as GDI displacement factors (GDFs), which might be necessary to catalyze the dissociation of this complex (DerMardirossian and Bokoch, 2005). In addition to catalyzing GDI release, a GDF could prevent extraction of inactive Rho from the membrane by reducing the affinity of membrane-associated Rho-GDP for RhoGDI, thereby permitting further rounds of

Figure 6: The Rho GTPase cycle. In their inactive, GDP-bound state, Rho GTPases are sequestered in the cytoplasm via interaction with RhoGDI. During specific stimuli, an inactive Rho can be recruited to a membrane compartment, and this process might require its release from RhoGDI by a GDI displacement factor (GDF). Following membrane recruitment, a guanine nucleotide exchange factor (GEF) activates the Rho by promoting exchange of GDP for GTP. The activated Rho can then interact with and recruit effector proteins to exert cellular effects. Upon signal termination, a GTPase activating protein (GAP) stimulates the ability of Rho to hydrolyze GTP to GDP, resulting in inactivation of the Rho. At this point, RhoGDI can extract the Rho from the membrane to allow subsequent rounds of recruitment and activation. An alternative role for potential GDFs is to prevent extraction of inactive Rho from the membrane, which could allow re-activation without extraction from the membrane.

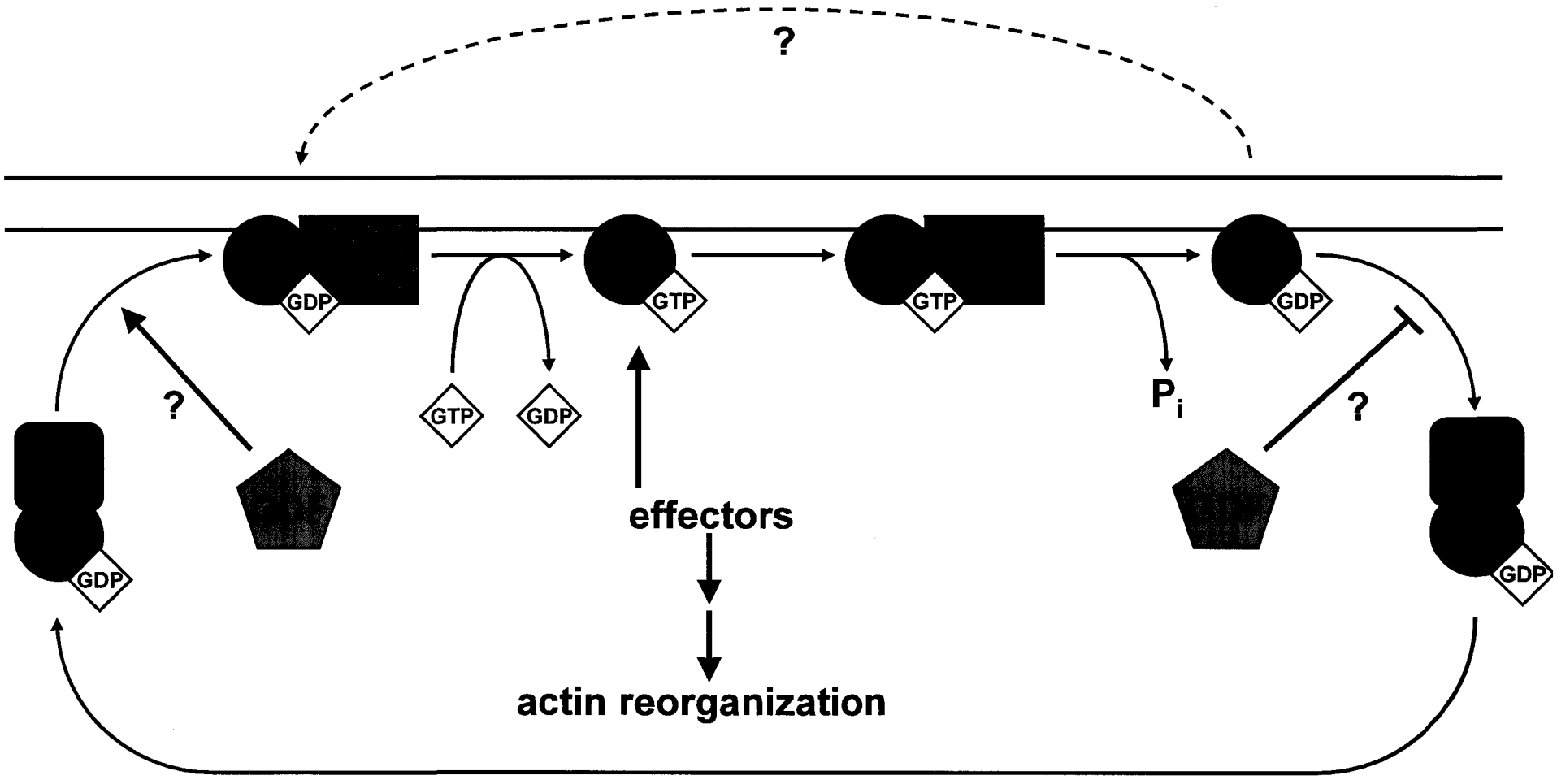
?
GDP
GTP
GTP
GDP
?
GTP
GDP
P_i
?
GDP
GDP
effectors
actin reorganization

activation without cycling through the cytosol. The ability of a GTPase to undergo rounds of activation, signaling and inactivation without membrane extraction and reinsertion would greatly enhance the speed of a given signaling system. Thus, GDF-mediated membrane retention of inactive GTPases could functionally amplify the downstream effects of a GTPase.

Rho GTPase activity regulates actin dynamics

Although 22 Rho isoforms have been identified to date, the majority of studies of this protein family have focused on three members, RhoA, Rac1 and Cdc42, each of which gives rise to specific actin-dependent structures when activated. Initial studies revealed that RhoA induces formation of contractile stress fibres, while Rac1 and Cdc42 stimulate extension of sheet-like protrusions and folds (termed lamellipodia and membrane ruffles) or finger-like projections (termed filopodia) from the cell periphery, respectively (Nobes and Hall, 1995; Ridley and Hall, 1992; Ridley et al., 1992). Since the initial characterization of these morphological structures, the signaling pathways leading from GEF-mediated activation to actin reorganization have been widely characterized. While these findings have been reviewed extensively (Burridge and Wennerberg, 2004; Jaffe and Hall, 2005; Ridley, 2006), there are several signaling events that are key to actin and membrane reorganization (Figure 7). For induction of stress fibres, RhoA activates the ROCK family of Rho kinases (Riento and Ridley, 2003). Subsequently, ROCKs phosphorylate the light chain (MLC) of myosin II and inhibit its dephosphorylation by MLC phosphatase. The increased pool of active, phosphorylated MLC is responsible for actin bundling and formation of stress fibres. Furthermore, RhoA

Figure 7: Rho GTPase signaling pathways. The GTPases RhoA, Rac1 and Cdc42 initiate stress fibres, lamellipodia and filopodia, respectively, through different signaling pathways. RhoA activates the Rho kinase ROCK, which potentiates phosphorylation and activation of myosin light chain (MLC) to promote actin bundling and contractility, resulting in stress fibres. RhoA can also promote actin polymerization through mDia, which also contributes to stress fibre formation. In contrast, Rac1 and Cdc42 interact with p21-activated kinase (PAK) to inhibit RhoA signaling. Active Rac1 can also interact with IRSp53 to stimulate actin nucleation through WAVE and the Arp2/3 complex, resulting in lamellipodia formation. Similarly, active Cdc42 promotes Arp2/3-mediated actin nucleation through N-WASP, and can additionally interact with Dia2 to enhance actin polymerization, leading to formation of filopodia. RhoG has been proposed to function as an upstream activator of Rac1 and Cdc42 through the ELMO/Dock180 GEF complex, but may also promote formation of lamellipodia independently of other GTPases through unknown mechanisms.

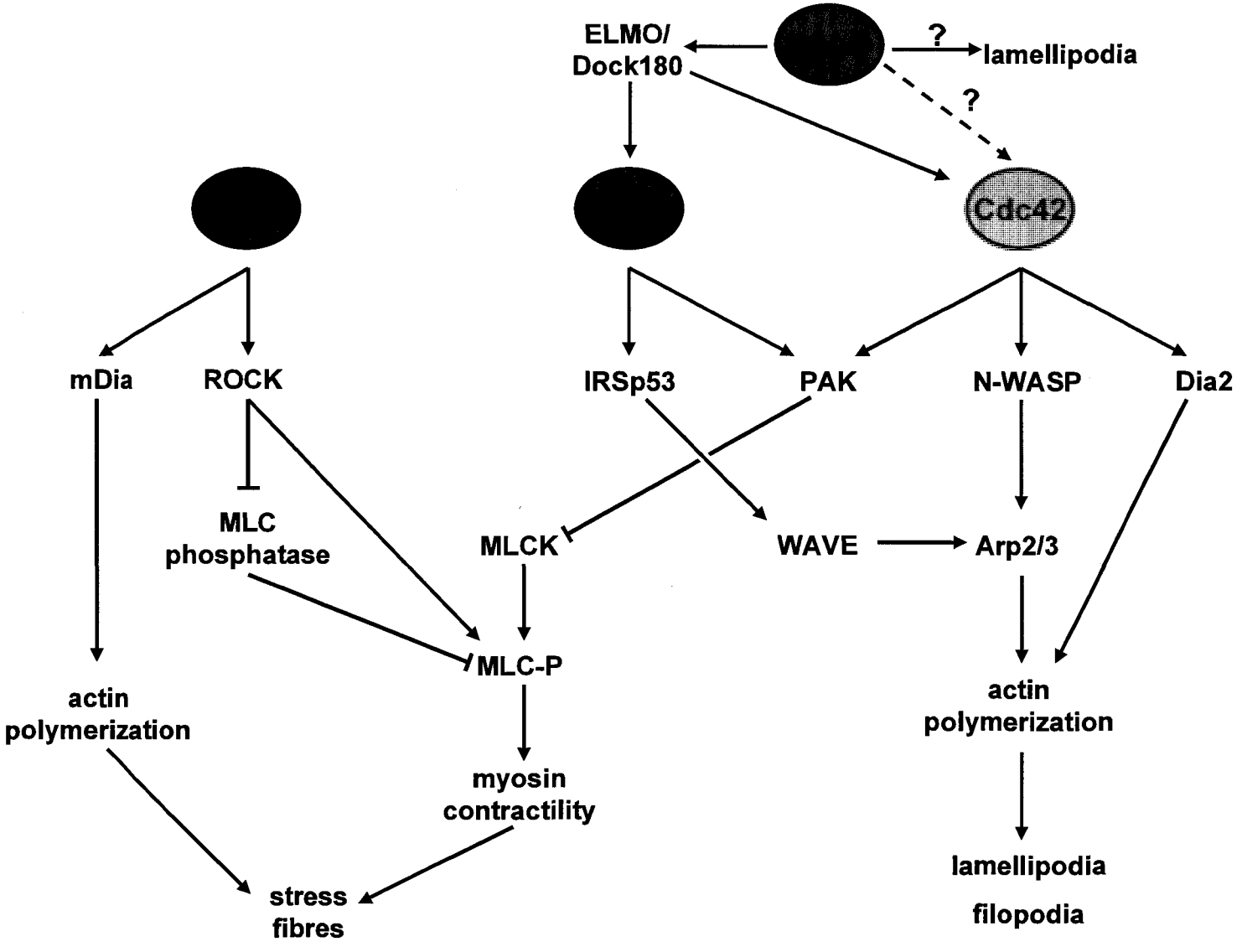
ELMO/
Dock180
?
lamellipodia
?
Cdc42
mDia
ROCK
IRSp53
PAK
N-WASP
Dia2
MLC
phosphatase
MLCK
WAVE
Arp2/3
MLC-P
actin
polymerization
myosin
contractility
actin
polymerization
stress
fibres
lamellipodia
filopodia

activates mammalian diaphanous (mDia), a formin-related protein involved in actin filament extension (Watanabe et al., 1997). In contrast, activation of Rac1 and Cdc42 leads to actin nucleation and polymerization through the actin-related Arp2/3 complex. Cdc42-GTP binds to the neural Wiscott-Aldrich syndrome protein (N-WASP) and relieves an autoinhibitory intramolecular interaction (Miki et al., 1998a). Activation of N-WASP results in conformational changes in the Arp2/3 complex to stimulate actin polymerization and/or branching. Rac1 promotes Arp2/3-mediated actin nucleation in a similar manner, but makes use of the WASP family verprolin-homologous (WAVE) proteins (Miki et al., 1998b). In contrast to Cdc42 and N-WASP, Rac1 cannot interact directly with WAVE, but instead interacts with the I-BAR protein IRSp53, which can then activate WAVE and regulate membrane protrusion (Miki et al., 2000). Alternatively, WAVE proteins are sequestered in an inhibitory complex that can be dissociated by active Rac1 to promote WAVE function (Eden et al., 2002). In addition to N-WASP, Cdc42 can also activate the mDia-related protein Dia2, suggesting multiple methods of promoting actin polymerization (Alberts et al., 1998; Peng et al., 2003). Thus, it is possible that the set of actin-polymerizing factors that are activated by specific Rho GTPases could dictate the resulting morphological effects.

In addition to activating WASP and WAVE proteins, Cdc42 and Rac1 also interact with the p21-activated kinase (PAK) to promote actin remodeling (Eby et al., 1998). Among its downstream targets, PAK phosphorylates MLC kinase, thereby inhibiting its activity. This has the effect of reducing levels of active, phosphorylated MLC, leading to a reduction in contractility and actin bundling necessary for stress fibre formation. Thus, Rac1 or Cdc42 activation can functionally antagonize RhoA signals.

Further complexity of Rho GTPase signals can occur through cross-talk between pathways, where many Rho GEFs can activate multiple GTPases, with broad signaling consequences. In other cases, activation of one Rho GTPase could in turn lead to activation of other Rho proteins, as seen for RhoG pathways that activate Rac1 and Cdc42 (Gauthier-Rouvière et al., 1998; Katoh and Negishi, 2003).

While the above morphological effects have been documented in fibroblasts, it should be noted that Rho family proteins are equally functional in other cell types as well, where they regulate actin-dependent processes. In neurons, for example, RhoA stimulates neurite retraction and growth cone collapse, while Cdc42, Rac1 and the related GTPase RhoG are important for neurite initiation and growth cone guidance events (Katoh et al., 2000; Kozma et al., 1997). Rho GTPases are also closely linked with endocytosis and vesicular transport. In particular, Rac1 and RhoG appear to be required for phagocytosis and macropinocytosis, where actin-dependent membrane protrusions are used to engulf extracellular objects (Cox et al., 1997; Ellerbroek et al., 2004; van Buul et al., 2007). Additionally, Rho GTPases are implicated in processes such as transcription and regulation of the cell cycle; however, these topics will not be discussed in further detail here.

Kalirin-7 is a brain-specific GEF for Rac1 and RhoG

To better understand the function of SNX2, a previous study in the laboratory used bacterial and yeast two-hybrid screens to identify potential interactors from a human brain cDNA library. In this study, SNX2 was found to interact with the RNA helicase Abstrakt to regulate its shuttling to the nucleus (Abdul-Ghani et al., 2005). This screen

also identified Kalirin-7 (Kal7), a brain-specific GEF for Rac1 and RhoG, as a potential binding partner for SNX2 (May et al., 2002; Penzes et al., 2000). Kal7 is a member of a family of multifunctional Rho GEFs that arise from a single gene by alternative splicing, and consists of a Sec14p-like lipid binding domain, nine spectrin repeats, a Dbl homology/Pleckstrin homology (DH/PH) motif responsible for GEF activity, and a C-terminal PSD-95/discs large/ZO1 (PDZ)-binding motif that targets it to the postsynaptic density (Johnson et al., 2000; Penzes et al., 2000). Other Kalirin isoforms include additional or alternate domains, including SH3 domains, an additional DH/PH motif that acts as a GEF for RhoA, and protein kinase-like domains (Johnson et al., 2000). Through its recruitment to the postsynaptic density and GEF activity, Kal7 is important for formation and maintenance of actin-rich dendritic spines in response to ephrin-B/EphB signals (Ma et al., 2003; Penzes et al., 2003; Penzes et al., 2001). An N-terminally truncated splice variant of Kal7 has also been implicated in signaling through the nerve growth factor (NGF) receptor TrkA to promote neurite outgrowth, suggesting that Kalirin isoforms are likely to regulate multiple processes through different receptors (Chakrabarti et al., 2005). Although the expression of Kalirin isoforms is largely restricted to the brain, the highly similar Rac1 and RhoG guanine nucleotide exchange factor Trio is broadly expressed in many tissues, and may perform similar functions in other cell types (Debant et al., 1996).

Human Kal7, also known as Duo, was initially identified as a Huntingtin-associated protein-1 (HAP1)-interacting protein (Colomer et al., 1997). Although HAP1 function is not fully understood, its role in endocytic trafficking has been well established (Kittler et al., 2004; Li et al., 2002; Rong et al., 2006). A truncated form of Kal7 was also

found to interact with the small GTPase Arf6 at the plasma membrane, and this process could be important for endocytic events (Koo et al., 2007). Potential interactions of Kal7 with HAP1, Arf6 or SNX2 could thus implicate Kal7 in transport through the endocytic pathway. Alternatively, interaction of SNX2 with Kal7 might suggest a novel role for SNX2 in modulation of the actin cytoskeleton. Thus, characterization of the potential roles of SNX and Kal7 in actin modulation and/or retromer activity is one of the main objectives of this study.

Vesicular trafficking within the exocytic pathway

Membrane-associated and secreted proteins are sorted in the ER

The ER is the principal site for synthesis of membrane-associated and secreted proteins. Following synthesis, proteins must be properly folded prior to export from ER exit sites, and specialized sorting mechanisms are necessary to ensure that improperly folded proteins do not aberrantly exit the ER. Misfolded proteins could adopt toxic functions or interactions with other proteins, thus failure of the sorting machinery could have very serious and possibly fatal consequences to a cell. Normally, ER-associated folding machinery and chaperone proteins interact with newly synthesized proteins to assist in this process. Once a protein adopts its native conformation, it can then diffuse through the ER membrane or lumen for incorporation into ER exit sites, where COPII-mediated vesicle budding occurs for subsequent transport to the ERGIC and Golgi compartments (Barlowe et al., 1994). Incorporation into ER exit sites can occur either through active sorting or by passive diffusion, and evidence exists to suggest that both mechanisms may be used. For example, membrane proteins containing a C-terminal di-

acidic DXE motif interact with the cargo-selective Sar1-Sec23/Sec24 subcomplex of the COPII coat, which can then recruit Sec13/Sec31 to drive vesicle budding (Miller et al., 2003a; Nishimura and Balch, 1997). Thus, the DXE motif acts as an export signal for selective incorporation into ER exit sites. In contrast, luminal ER-resident proteins containing a C-terminal KDEL or KKXX motif are able to transit out of the ER to ERGIC or Golgi compartments, where they are sorted for retrieval back to the ER by the KDEL receptor, as discussed above (Jackson et al., 1993; Pelham, 1988; Semenza et al., 1990). Since disruption of KDEL receptor function causes aberrant secretion of ER-resident proteins, KDEL-containing proteins are thought to exit the ER by passive mechanisms that require active retrieval.

Defects in protein sorting and exit cause ER stress

ER stress occurs when the protein folding machinery cannot sufficiently accommodate the load of nascent or unfolded proteins. Several cellular mechanisms exist to overcome ER stress, including inhibition of the translational machinery, upregulation of chaperone proteins, and degradation of unfolded or misfolded proteins (Zhao and Ackerman, 2006). Under stress conditions, increased levels of unfolded proteins bind to and sequester ER chaperone proteins such as BiP, a member of the heat-shock protein 70 chaperone family. Normally, free BiP can be found in an inhibitory complex with the protein kinase-like ER kinase PERK; however, titration of BiP levels during ER stress disrupts this complex. Activated PERK can then phosphorylate and inactivate eIF2α (eukaryotic initiation factor 2α), which is a part of the translation initiation machinery, to temporarily delay protein synthesis and allow chaperones to relieve the unfolded protein

load (Harding et al., 1999). In addition, excessive levels of unfolded proteins in the ER give rise to the unfolded protein response (UPR), which leads to upregulation of chaperone proteins via activation of the transcription factors ATF6 and XBP1 (Schröder and Kaufman, 2005). These transcription factors can also initiate transcription of genes involved in lipid synthesis to increase ER size, which may further serve to alleviate increased concentrations of unfolded proteins. The UPR is closely associated with the ER-associated degradation (ERAD) pathway, which is an additional compensatory mechanism leading to retrotranslocation of unfolded proteins from ER to the cytosol for degradation by the ubiquitin/proteasome system (Meusser et al., 2005). If these mechanisms are not sufficient to adequately relieve the load of unfolded proteins, prolonged ER stress eventually results in apoptotic cell death.

Structure and function of the ER is closely associated with the microtubule network

The characteristic reticular network of ER tubules that extends throughout the cell is generated by multiple interactions with the microtubule network. Among these, extension of ER tubules is mediated by interactions with motor proteins such as kinesin, which can pull ER membranes toward microtubule plus ends at the cell periphery (Feiguin et al., 1994; Lane and Allan, 1999). Furthermore, non-motor proteins are required to link the ER network to microtubules, thereby stabilizing ER tubules and preventing their collapse toward the perinuclear region. The first such protein identified was the 63 kDa cytoskeleton-linking membrane protein (CLIMP-63), an ER-localized transmembrane protein that binds directly to microtubules through its cytoplasmic tail (Klopfenstein et al., 1998). Consistent with the proposed function in linking ER and

microtubule networks, overexpression of CLIMP-63 causes rearrangement of the ER network and generation of thick, cable-like structures that co-localize extensively with microtubules. Interestingly, interaction of CLIMP-63 with microtubules appears to be cell cycle-dependent, where phosphorylation of CLIMP-63 disrupts this interaction during mitosis, leading to ER collapse (Vedrenne et al., 2005). A second ER-associated membrane protein, p180, was also found to interact directly with microtubules, and promoted bundling of tubulin filaments (Ogawa-Goto et al., 2007).

In addition to the structural link between ER and microtubule networks, there is a functional link that is important for regulation of protein diffusion, vesicle biogenesis and protein transport. Studies using the microtubule-depolymerizing drug Nocodazole have established a role for microtubules in generation of tubular ERGIC structures (Simpson et al., 2006). Furthermore, ER-to-Golgi trafficking is believed to be directed along stable microtubules (Mizuno and Singer, 1994). Additionally, Nocodazole treatment results in expansion of ER exit sites, suggesting a relationship between these structures and the microtubule network (Dukhovny et al., 2008). Overall, these studies suggest that an intact microtubule network is essential for normal ER function.

Membrane proteins diffuse laterally through the ER

Following synthesis and folding, membrane proteins must diffuse to ER exit sites for incorporation into transport vesicles. The presence of a transmembrane domain restricts the movement of a protein to two dimensions, meaning that proteins must diffuse laterally to sites of budding. Numerous computational studies on protein diffusion have been performed, and the proposed models regard the membrane as a lattice of unit cells,

where a diffusing protein can jump from one cell to the next at a given rate (Jacobson et al., 1987). Since the lipid bilayer has a fluid composition, proteins are generally thought to diffuse freely within the plane of the membrane in the absence of obstacles. However, several factors can restrict a protein's ability to move through the membrane, thereby decreasing its rate of diffusion. First, an increase in membrane viscosity can negatively affect diffusion by making it more difficult for the protein to move to adjacent spaces in the membrane (Saxton, 1987). In addition, the presence of other proteins can have potent effects on diffusion. When other proteins are also diffusing freely through the membrane, they have minimal effects on diffusion, since they do not permanently occupy membrane spaces (Kusumi et al., 2005; Saxton, 1987). However, at very high concentrations, freely diffusing proteins can reduce diffusion rates, presumably through an increase in membrane viscosity (Saxton, 1987). In contrast, when other proteins are immobile, they permanently occupy unit cells, thereby reducing the number of available spaces to which a mobile protein can move (Figure 8). Thus, as the concentration of immobile proteins or obstacles in a membrane increases, diffusion of free proteins drops sharply, since less space is available for movement of mobile proteins. At sufficiently high concentrations, immobile obstacles can create pockets of membrane that are inaccessible to mobile proteins, effectively preventing long-range diffusion (Saxton, 1987). Additional factors that could affect protein diffusion include interactions with other proteins or lipids, along with membrane microdomains that could retain or exclude a protein (Nicolau et al., 2007).

In order to create an immobile obstacle within a membrane, at least two anchor points are required to prevent its lateral movement. The first of these is generally a

Figure 8: Effect of immobile obstacles on lateral diffusion. At low concentrations (top), immobile obstacles in a lipid bilayer have no effect on the ability of a mobile protein to freely diffuse (from the green cell to the red cell in the right-hand panel of images, for example). However, at moderate concentrations (middle), immobile obstacles cause a decrease in the rate of diffusion by occupying a significant portion of the membrane, thereby reducing the fluid space available for mobile proteins to move laterally. At sufficiently high concentrations (bottom), immobile obstacles eventually generate pockets of membrane that are isolated from each other, and can effectively abolish long-range diffusion.

Immobile obstacle concentration

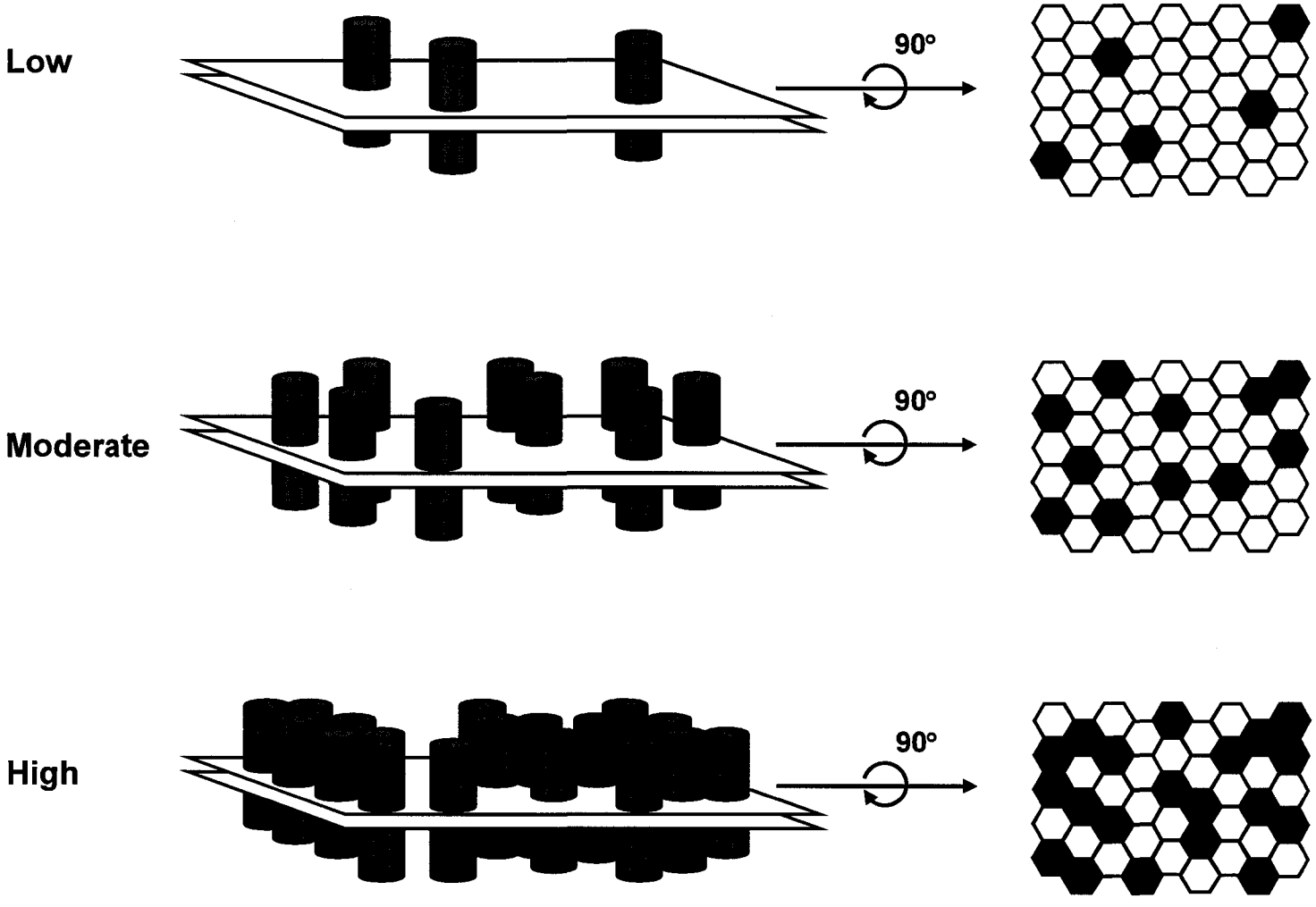

transmembrane domain, which anchors the protein in the lipid bilayer. The second anchor point can be achieved through interaction with another immobile obstacle. The cytoskeleton is thus an obvious structure onto which a membrane-associated protein can attach to become immobile (Saxton, 1987). Consequently, the ability of a protein to reversibly interact with the cytoskeleton could be used to regulate the ability of other proteins to diffuse through the membrane.

VAPs are ER-localized transmembrane proteins that associate with microtubules

In addition to CLIMP-63 and p180, a novel family of ER-resident proteins has been described that can also associate with microtubules. These proteins were initially discovered by virtue of their interaction with the v-SNARE VAMP2 (Skehel et al., 1995), and have thus been named VAMP-associated proteins (VAPs). Two highly similar isoforms, named VAPA and VAPB, have been identified to date (Figure 9), each of which has an N-terminal major-sperm protein (MSP) domain, a central coiled-coil region, and a C-terminal transmembrane domain (Nishimura et al., 1999). In addition, a splice variant of VAPB (termed VAPC) lacking the coiled-coil and transmembrane regions has been identified, although its function is not clear. The coiled-coil and transmembrane regions of VAPA and VAPB have a topology similar to a number of t-SNARE proteins, and VAPs were initially thought to have SNARE-related functions (Nishimura et al., 1999). However, studies have since shown that VAPs do not directly regulate the late secretory pathway and do not have SNARE-like activity, although they are capable of interaction with numerous SNARE proteins and could thereby regulate their sorting (Kagiwada et al., 1998; Soussan et al., 1999; Weir et al., 2001). Both VAPA and VAPB

Figure 9: Sequence alignment of human VAPA and VAPB. Alignments were performed with ClustalW version 2.0.8, with identities indicated by asterisks and similarities depicted by points and colons. Blue, red and green bars correspond to the major sperm protein (MSP), coiled-coil and transmembrane regions, respectively. The conserved proline residue at position 56, which is replaced by a serine residue in the ALS8-causing VAPB mutant, is indicated in red.

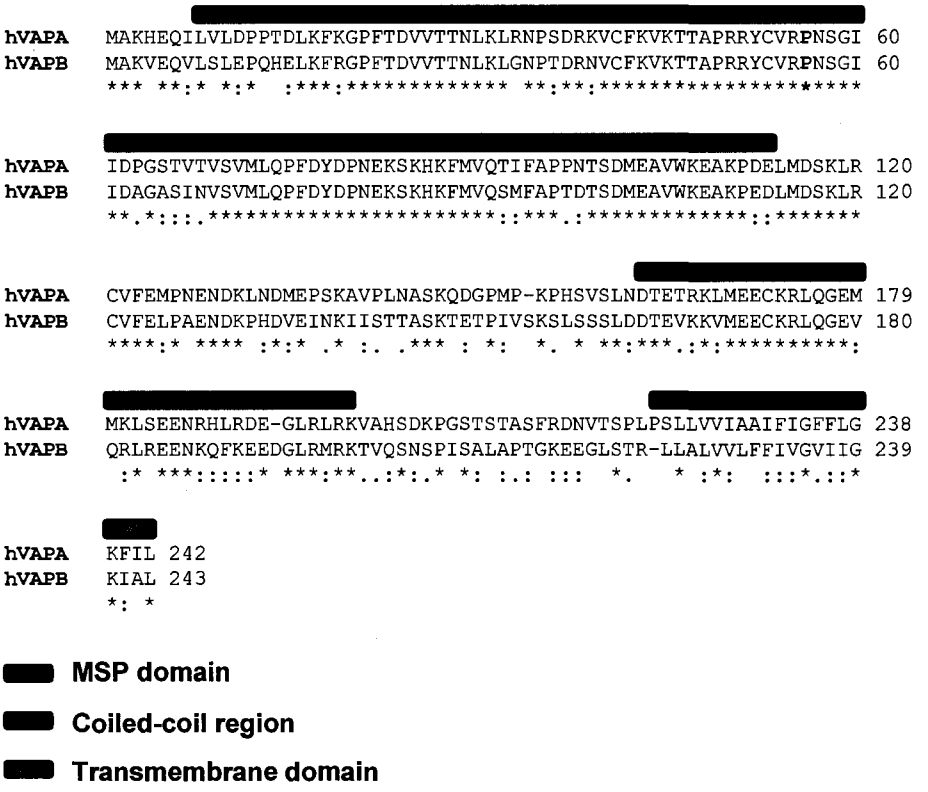
hVAPA MAKHEQILVLDPPTDLKFKGPFTDVVTTNLKLRNPSDRKVCFKVKTTAPRRYCVRPNSGI 60
hVAPB MAKVEQVLSLEPQHELKFRGPFTDVVTTNLKLGNPTDRNVCFKVKTTAPRRYCVRPNSGI 60
hVAPA IDPGSTVTVSVMLQPFDYDPNEKSKHKFMVQTIFAPPNTSDMEAVWKEAKPDELMDSKLR 120
hVAPB IDAGASINVSVMLQPFDYDPNEKSKHKFMVQSMFAPTDTSDMEAVWKEAKPEDLMDSKLR 120
hVAPA CVFEMPNENDKLNDMEPSKAVPLNASKQDGPMP-KPHSVSLNDTETRKLMEECKRLQGEM 179
hVAPB CVFELPAENDKPHDVEINKIISTTASKTETPIVSKSLSSSLDDTEVKKVMEECKRLQGEV 180
hVAPA MKLSEENRHLRDE-GLRLRKVAHSDKPGSTSTASFRDNVTSPLPSLLVVIAAIFIGFFLG 238
hVAPB QRLREENKQFKEEDGLRMRKTVQSNSPISALAPTGKEEGLSTR-LLALVVLFFIVGVIIG 239
hVAPA KFIL 242
hVAPB KIAL 243
MSP domain
Coiled-coil region
Transmembrane domain

are mainly ER-localized, but are also found in the ERGIC, suggesting that they function primarily within these compartments (Soussan et al., 1999; Weir et al., 2001). Thus, if VAPs play a role in early secretory events, it remains possible that they could indirectly exert effects on later steps as well by modulating the sorting or delivery of proteins involved in exocytosis.

Emerging evidence suggests that VAPs are indeed involved in protein transport. For example, VAPA is implicated in plasma membrane incorporation of the glucose transporter GLUT4, while VAPB appears to be involved in COPI-dependent vesicle transport (Foster et al., 2000; Soussan et al., 1999). Both VAPA and VAPB additionally form homo- and heterodimers which require the MSP and transmembrane domains, and this ability is thought to regulate their function (Amarilio et al., 2005; Nishimura et al., 1999; Weir et al., 2001). Furthermore, VAPs are known to interact with microtubules, although this association is believed to be indirect (Kaiser et al., 2005; Mitne-Neto et al., 2007; Skehel et al., 2000). Given the dual association of VAPs with the ER and with microtubules, it seems plausible that VAP may create immobile obstacles in the ER membrane, which could provide a mechanism for regulating vesicular transport.

A mutation in the MSP domain of VAPB is linked to amyotrophic lateral sclerosis

Recently, a mutation giving rise to a form of adult-onset, autosomal-dominant familial amyotrophic lateral sclerosis (ALS8) was mapped to the VAPB gene (Nishimura et al., 2005; Nishimura et al., 2004). ALS is a fatal neurodegenerative disorder that causes preferential loss of motor neurons, resulting in progressive symptoms including muscle weakness and paralysis, typically leading to death within 3-5 years of onset

(Boillée et al., 2006; Shaw, 2005). Although most cases of ALS are sporadic, approximately 10% are linked to mutations in a number of identified genes. In the case of ALS8, a missense P56S substitution within the MSP domain of VAPB has been identified, and gives rise to an ER aggregation phenotype (Kanekura et al., 2006; Nishimura et al., 2004; Teuling et al., 2007). Overexpression of wild-type VAPB enhances UPR-mediated responses to ER stress, while the P56S mutant blocks induction of UPR (Kanekura et al., 2006). These data suggest that VAPB might play a role in regulating levels of unfolded proteins in the ER, and that loss of motor neurons could result from an inability of these cells to adapt to ER stress. Further studies have shown that mutant VAPB recruits wild-type VAPA and VAPB into aggregates (Teuling et al., 2007; Tsuda et al., 2008), possibly through aggregation of the MSP domain or through transmembrane domain interactions. Although the mechanisms of mutant VAPB-mediated cell death are not clear, the propensity to form aggregates and segregate wild-type VAPs suggests that this mutation constitutes a toxic gain of function.

Notably, the most common genetic cause of ALS is mutation of the copper-zinc superoxide dismutase (SOD1), a protein involved in scavenging of reactive oxygen species (Tsuda et al., 1994). While SOD1 is broadly localized to numerous compartments and to the cytoplasm, numerous ALS-associated mutations have been identified that cause SOD1 aggregation. A mouse model of SOD1-dependent ALS has been generated, and analysis of VAP expression in this model has revealed that both VAPA and VAPB are downregulated in late stages of pathology (Teuling et al., 2007). Consequently, loss of VAP expression could be a contributing factor to multiple forms of ALS.

The major sperm protein of Ascaris suum *forms actin-like filaments*

Since the pathogenic mutation of VAPB is located in the MSP domain, understanding the function of this motif could provide insights into ALS8 disease progression. The MSP domain of VAPs was initially identified based on its homology to the major sperm protein of the nematodes *A. suum* and *Caenorhabditis elegans* (Skehel et al., 2000). The spermatozoa of nematodes utilize amoeboid movement rather than flagellar propulsion as observed for many other organisms. While these cells appear to lack the actin-based machinery required for locomotion, they instead form actin-like filaments consisting of polymerized major sperm protein, which appears to be sufficient to drive cell motility (Roberts and Stewart, 2000). The crystal structure of MSP has been solved, revealing an overall β-sandwich structure that forms a dimer as the minimal unit for polymerization (Baker et al., 2002; Bullock et al., 1996; Haaf et al., 1998). The residues required for dimerization and/or oligomerization of MSP are poorly conserved in VAPs, indicating that formation of filaments is unlikely to occur (Kaiser et al., 2005; Loewen and Levine, 2006; Skehel et al., 2000; Smith and Ward, 1998). The P56 residue of VAPB that is mutated in ALS8 is located to a kink within an extended β-sheet (Loewen and Levine, 2006). Mutation of this residue could thus alter the conformation of the β-sheet, which could lead to formation of aggregates and protein dysfunction.

The MSP domain of VAPs interacts with proteins involved in lipid synthesis and metabolism

Aside from their indirect association with microtubules, VAPs have been shown to interact with a number of other proteins. In terms of function, the largest group of

VAP-interacting proteins is involved in synthesis, transport or metabolism of lipids. These proteins include the ceramide transport protein CERT (Kawano et al., 2006), oxysterol-binding protein (OSBP) and the OSBP-related proteins or ORPs (Perry and Ridgway, 2006; Wyles et al., 2002; Wyles and Ridgway, 2004), and Nir/rdgB proteins linked with retinal degeneration (Amarilio et al., 2005). Scs2p, the yeast orthologue of VAP, interacts with Opi1p, a transcriptional repressor of genes involved in synthesis of phosphatidylinositol (Loewen et al., 2004). This interaction retains Opi1p in the cytoplasm under stress conditions such as during UPR, preventing its translocation to the nucleus and enhancing transcription of lipid-synthesizing genes (Brickner and Walter, 2004) Furthermore, Scs2p was identified as a suppressor of choline sensitivity and inositol auxotrophy in yeast, indicating a conserved role for VAPs in regulating lipid metabolism or transport (Kagiwada et al., 1998). In all of the cases above, interaction with VAP or Scs2p is sufficient for targeting of lipid-regulating proteins to the ER, and this activity could have the effect of promoting synthesis of new ER membranes or regulating the lipid composition or fluidity of the ER.

Interaction of VAPs with lipid-regulating proteins occurs through a conserved FFAT motif

Within the above listed lipid-regulating proteins, a short, highly conserved motif consisting of two phenylalanines in an acidic tract (FFAT) was identified as the minimal domain required for interaction with VAPs and Scs2p (Loewen et al., 2003). FFAT is a seven amino acid residue motif with the sequence EFFDAXE, and this peptide sequence interacts with and neutralizes a basic groove in the MSP domain of VAP (Kaiser et al.,

2005; Loewen and Levine, 2006). Similarly, mutation of either the phenylalanines or the acidic residues of FFAT blocks ER recruitment and interaction of the FFAT-containing protein with VAP, indicating that these residues are necessary for the observed interaction (Amarilio et al., 2005; Kawano et al., 2006; Wyles and Ridgway, 2004). Notably, expression of a K87D/M89D mutant VAPA that is unable to interact with FFAT causes expanded ER structures that are evenly distributed throughout the cell (Kaiser et al., 2005). Unlike the P56S mutation in VAPB, the FFAT-defective mutant remains monomeric, and likely constitutes a loss-of-function mutant rather than a toxic gain of function. One study (Teuling et al., 2007) has demonstrated that P56S mutant VAPB cannot interact with a green fluorescent protein (GFP)-tagged FFAT motif; however, it is possible that the observed loss of interaction is in fact due to aggregation of VAPB, which could reduce the accessibility of FFAT to its binding site. Additionally, exogenous expression of some FFAT motifs or FFAT-containing proteins, such as ORP3 and Nir2, causes formation of ER membrane stacks or whorls, while other FFAT proteins such as Nir3 cause rearrangement of ER and microtubule structures (Amarilio et al., 2005; Teuling et al., 2007). At this time, it is not clear whether the FFAT motif or other domains within the FFAT-containing proteins are responsible for the changes in ER structure. Although the mechanisms for these morphological changes remain unclear, it is possible that FFAT motif proteins can modulate interaction of VAPs with the microtubule network to promote rearrangement of the ER or facilitate anterograde transport. Consequently, a second objective of this study is the characterization of the effects of FFAT on VAP function.

Objectives and Hypotheses

The main objective of this study is to identify and characterize novel relationships between protein sorting and interaction with or regulation of the cytoskeleton. Given the complexity of cytoskeletal dynamics and protein transport in eukaryotic cells, two separate systems will be examined to address this issue using a combination of biochemical and cell biological approaches.

I. Novel functions for sorting nexins in modulating actin dynamics

While SNXs have a clearly established role in regulating protein sorting within the endocytic pathway, alternative functions remain largely uncharacterized. A previous laboratory screen identified the actin-modulating Rac1 and RhoG GEF Kalirin-7 as a potential interactor for SNX2. This interaction lends itself to two testable hypotheses:

(i) Interaction of SNX2 with Kal7 modulates Kal7 activity to regulate actin dynamics.

(ii) Recruitment of Kal7 to SNX-containing retromer complexes adds an actin component to retromer activity.

The results and discussion of this portion of the thesis will be presented in chapters I and III, respectively.

II. VAPs and FFAT regulate lateral diffusion and anterograde transport of ER cargo

Although VAPA and VAPB are known to interact with microtubules, the effects of this interaction on transport of proteins in the ER remains unclear. Furthermore, the interaction of FFAT proteins with VAPs can modulate ER architecture. Based on the dual

association of VAPs with the ER and microtubules, it is hypothesized that overexpression or aggregation of VAPs creates immobile obstacles that impede diffusion of membrane proteins, and that FFAT relieves immobile obstacles by releasing VAP from microtubules. The results and discussion of this portion of the thesis will be presented in chapters II and IV, respectively.

Materials and Methods

Materials

Unless otherwise stated, chemicals were obtained from Sigma, and restriction enzymes were purchased from Invitrogen.

Plasmid construction

cDNA coding for full-length human SNX1 or SNX2, as well as SNX2 truncations coding for amino acid residues 1-269 (N+PX) or 270-519 (BAR) were amplified by polymerase chain reaction (PCR) and cloned into the NotI and EcoRI sites of pFLAG-CMV2 (Sigma). SNX2 R182A/R183A/F184A (RRF) and K426A/R428A (KR/AA) mutants were generated by site-directed mutagenesis and cloned into pFLAG-CMV2 as above. Plasmids for purification of recombinant SNX1 or SNX2 from *Escherichia coli* were generated by PCR amplification and insertion of full-length Flag-SNX into the KpnI site of a modified pQE9 vector (Qiagen) containing a hemagglutinin (HA) tag (Abdul-Ghani et al., 2005).

His_6-myc-tagged wild-type and GEF-inactive N1415A/D1416A (ND/AA) mutant Kal7 cloned into pEAK10, as well as His_6-myc-Kal7 ΔCT cloned into psCEP were generous gifts from Dr. Betty A. Eipper (University of Connecticut).

Wild-type RhoA, Rac1 and Cdc42 in pRK5-myc were obtained from Dr. Alan Hall (University College London). cDNA for wild-type RhoG was inserted into the BamHI and EcoRI sites of pRK5-myc. Dominant-negative $RhoG^{T17N}$ was generated by site-directed mutagenesis, and was also inserted into pRK5-myc as above. Dominant-negative, HA-tagged $RhoA^{T19N}$, $Rac1^{T17N}$ and $Cdc42^{T17N}$ in pcDNA3.1(+) were obtained

from UMR cDNA Resource. For tandem affinity purification (TAP) of Rho GTPases, myc-tagged, wild-type RhoA, Rac1, Cdc42, and RhoG were inserted into the HindIII site of pBS1761 (EUROSCARF). The resulting N-terminally TAP-tagged cDNA was then PCR amplified and cloned into the KpnI and EcoRI sites of pYES2 (Invitrogen).

For all VAPA and VAPB experiments, cDNAs coding for wild-type human VAPA and VAPB were subcloned into pFLAG-CMV2 at the NotI and BamHI sites. The N-terminally truncated constructs lacking the MSP domain (ΔN) were also subcloned into the NotI and BamHI sites of pFLAG-CMV2 starting with amino acid residues 135 and 124 for VAPA and VAPB, respectively. The P56S mutation was generated by site-directed mutagenesis, and was subcloned into pFLAG-CMV2 at the NotI and EcoRI sites. The FFAT motif of rabbit OSBP (residues 347-468) was PCR amplified and inserted into the BamHI and EcoRI sites of pcDNA3.1(+)-myc.

Cell culture and transfection

All cells were maintained at 37°C in the presence of 5% CO_2 in medium supplemented with 100 units/ml penicillin and 100 μg/ml streptomycin (Invitrogen). Chinese hamster ovary (CHO) cells were grown in minimum essential medium α (Invitrogen) containing 5% fetal bovine serum (FBS), while HeLa cells were maintained in Dulbecco's modified Eagle's medium (DMEM, HyClone) containing 5% FBS. CHO and HeLa cells were transfected with LipofectAMINE reagent (Invitrogen) according to the manufacturer's instructions. 293TN cells (System Biosciences) were maintained in DMEM supplemented with 10% FBS and 500 μg/ml G418 (Invitrogen), and were

transfected with LipofectAMINE Plus (Invitrogen) according to the optimized procedure (System Biosciences) described for 293TN cells.

PC12 cells were grown in DMEM supplemented with 10% horse serum and 5% FBS, and were transfected with Effectene (Qiagen) according to manufacturer's instructions. For direct visualization, PC12 cells were co-transfected with a vector coding for monomeric red fluorescent protein (mRFP) in addition to Kal7 and/or SNX plasmids. 24 hours after transfection, cells were differentiated for 3 days in DMEM containing 10% horse serum in the presence of 10 ng/ml NGF-β. Alternatively, undifferentiated cells were grown for 3 days in DMEM containing 10% horse serum without NGF-β. Cells were then fixed as described below.

Immunocytochemistry and confocal microscopy

For visualization by confocal microscopy, cells were seeded onto 12 mm glass cover slips and transfected as above. 24-48 h after transfection, cells were fixed for 30 min with 4% paraformaldehyde in phosphate-buffered saline (PBS). Cover slips were then incubated with blocking buffer (1% bovine serum albumin, 2% normal goat serum, 0.6% saponin, and 0.01% NaN_3 in PBS) and stained with mouse or rabbit anti-Calreticulin (Stressgen), rabbit anti-EEA1 (Abcam), mouse anti-Flag (Applied Biological Materials), rabbit anti-Flag (Sigma), rabbit anti-Kalirin (Upstate), rabbit anti-Mannosidase II (a gift from Dr. Marilyn Farquhar, University of California, San Diego), mouse anti-myc (Sigma), rabbit anti-Sar1 (Upstate), 12G10 mouse anti-alpha tubulin (Drs. J. Frankel and E. M. Nelsen, University of Iowa Developmental Studies Hybridoma Bank) or mouse anti-Vps35 (Abnova) antibodies diluted in blocking buffer. Secondary

goat anti-mouse and goat anti-rabbit antibodies conjugated with Alexa 488 (Invitrogen) or Texas Red (Jackson Laboratories) were also diluted in blocking buffer, and cover slips were mounted in SlowFade Gold reagent (Invitrogen).

All images were captured on an Olympus IX70 inverted microscope equipped with an MRC1024 scanning confocal unit (BioRad) and a 60X, 1.4 numerical aperture oil-immersion objective. Images were acquired using LaserSharp software (BioRad), and further processing and measurements were performed with ImageJ version 1.37v (National Institutes of Health, Bethesda, MD).

Purification of His_6-SNX and TAP-Rho GTPases

Expression of recombinant His_6-HA-Flag-SNX proteins in mid-logarithmic phase *E. coli* was induced overnight with 1mM isopropyl-β-D-thiogalactoside (Roche). Cells were resuspended in PBS containing 10 mM imidazole, 2 mM β-mercaptoethanol (β-ME) and 2 mM phenylmethylsulfonyl fluoride (PMSF). Lysozyme was added to 20 mg/ml for 10 min, and cells were lysed by sonication in the presence of 1% Nonidet P-40 (NP-40). The lysate was then cleared by centrifugation at 30,000 x g, and the supernatant was added to nickel-nitrilotriacetic acid (Ni-NTA)-agarose beads (Qiagen) and allowed to bind for 4-8 h. Beads were then washed with 50 volumes of wash buffer 1 (0.1% NP-40, 10 mM imidazole and 2 mM β-ME in PBS) and 50 volumes of wash buffer 2 (10 mM imidazole and 2 mM β-ME in PBS), and eluted with 10 volumes of elution buffer (300 mM imidazole and 2 mM β-ME in PBS). All recombinant proteins were quantified by SDS-PAGE followed by staining with Coomassie Blue (BioRad) and densitometric analysis, using bovine serum albumin as a standard.

For purification of TAP-tagged Rho GTPases, pYES2 plasmids were transformed into the EUROSCARF yeast strain FY1679-08A (MATa; ura3-52; leu2Δ 1; trp1Δ63; his3Δ200; GAL2) using the LiCl method (Schiestl and Gietz, 1989) and grown in SC-ura medium. Protein expression in mid-logarithmic cells was induced overnight in SC-ura containing 2% galactose instead of glucose. Cells were disrupted by vortexing with 0.5 mm glass beads (Biospec) in 20 mM Tris-HCl pH 7.5, 150 mM NaCl, 5 mM EDTA, 2 mM PMSF. The lysate was solubilized with 1% NP-40 and cleared by centrifugation at 30,000 x g, and TAP-tagged Rho GTPases were immobilized on IgG Sepharose beads (GE Healthcare), which were then washed with 100 volumes of wash buffer 1 (20 mM Tris-HCl pH 7.5, 0.1% NP-40, 300 mM NaCl, 2 mM EDTA) and 200 volumes of wash buffer 2 (20 mM Tris-HCl pH 7.5, 50 mM NaCl, 2 mM $CaCl_2$) prior to storage at 4°C in wash buffer 2 containing 0.01% NaN_3.

Interaction of SNX1 and SNX2 with Kal7

To assess the interaction of SNX1 and 2 with Kal7, CHO cells were co-transfected with Flag-tagged SNX and either His_6-myc-Kal7 or empty vector. 48 h following transfection, cells were scraped in PBS and solubilized in 1% 3-(3-cholamidopropyl)diethylammonio-1-propanesulfonate (CHAPS, Bioshop), 20 mM imidazole and 20 mM β-ME in PBS containing a cocktail of protease inhibitors (4-[2-aminoethyl]benzenesulfonyl fluoride, Aprotinin, Bestatin hydrochloride, E-64, Leupeptin and Pepstatin A). The lysate was cleared by centrifugation at 5,000 x g, diluted to a final concentration of 0.1% CHAPS and incubated for 16 h at 4°C with Ni-NTA-agarose beads. Beads were then washed five times with 0.1% CHAPS, 20 mM imidazole and 20

mM β-ME in PBS, and eluted with 1X SDS sample buffer. Retained proteins were analyzed by Western immunoblot with mouse anti-Flag (Sigma) and mouse anti-myc antibodies.

Western immunoblot

For all immunoblot experiments, samples were resolved by SDS-PAGE on vertical slab gels. For domain-mapping experiments of SNX2 interaction with Kal7, resolution was performed on gradient gels of 7.5-15% polyacrylamide. Gels consisting of a single percentage of acrylamide within the range of 6% to 15% were used for all other studies as appropriate for protein size. Following SDS-PAGE, proteins were transferred to nitrocellulose membranes, and nonspecific binding sites were blocked with blocking buffer (Tris-buffered saline containing 0.05% Tween-20 and 5% skim milk powder). Blots were then incubated overnight with primary antibodies diluted in blocking buffer. Subsequently, blots were incubated for 1 h with Alexa 488-conjugated goat anti-mouse or anti-rabbit secondary antibodies diluted in blocking buffer. Following primary and secondary antibody incubations, blots were washed three times with Tris-buffered saline containing 0.05% Tween-20. All blots were visualized with a Typhoon 8600 variable mode imager (Molecular Dynamics). For quantitative immunoblots, densitometric analysis was performed using ImageQuant version 5.2 (Molecular Dynamics).

shRNA depletion of SNX1, SNX2 and Vps35

Lentiviral transduction was performed to deplete HeLa cells of SNX1, SNX2 or Vps35. Briefly, 293TN cells were transfected with pMD2.G and psPAX2 envelope and packaging plasmids (Addgene plasmids 12259 and 12260, Dr. Didier Trono, Ecole

Polytechnique Fédérale de Lausanne) as well as a mixture of five shRNA targets against SNX1, SNX2 or Vps35 in the pLKO.1 plasmid (GenBank accession numbers NM_003099, NM_003100 and NM_018206 from the RNAi consortium TRC-Hs1.0 library, Open Biosystems) according to supplier instructions. A GFP shRNA target in pLKO.1 (Addgene plasmid 12273, Dr. Robert Weinberg, Massachusetts Institute of Technology) was used for control infections. 48 h after transfection, lentivirus-containing medium was collected, filtered through a 0.45 μm cellulose acetate filter, and stored at 4°C.

For shRNA experiments, HeLa cells were seeded onto cover slips and transfected with His_6-myc-Kal7 ΔCT. 24 h after transfection, cells were infected with GFP, SNX1, SNX2 or Vps35 shRNA lentiviral particles in the presence of 5 μg/ml polybrene. Alternatively, cells were mock-infected with 5 μg/ml polybrene in the absence of pseudovirus, and were fixed and stained with anti-Kalirin antibodies 48 h after infection. To confirm protein depletion, infected 35 mm dishes of HeLa cells were solubilized in PBS containing 1% CHAPS and 2 mM PMSF. Following 5,000 x g centrifugation, protein concentration in the soluble fraction was determined using the D_C protein assay (BioRad) with bovine serum albumin as a standard, and equal amounts of protein were analyzed by Western immunoblot for all samples. Based on the supplier's estimated titer of 2 x 10^6 particles/ml, a multiplicity of infection of 20 gave optimal knockdown as determined by immunofluorescence and quantitative immunoblot with monoclonal anti-SNX1, anti-SNX2 (Stressgen) or anti-Vps35 antibodies. 12G10 mouse anti-tubulin antibody was used to confirm equal loading of samples.

Endogenous expression of RhoG mRNA in HeLa and CHO cells

HeLa and CHO cells were trypsinized and counted, and 5 x 10^6 cells were used for isolation of total RNA with an RNeasy mini kit (Qiagen) according to the manufacturer's instructions. Prior to reverse transcriptase-PCR (RT-PCR), any contaminating genomic DNA was eliminated by digestion with RNAse-free DNAse I (Fermentas) at 37°C for 30 min, and samples were heat killed at 95°C for 20 min. Subsequently, RT-PCR was performed using a OneStep RT-PCR kit (Qiagen) according to the manufacturer's instructions. For the RT-PCR reaction, RhoG and glyceraldehyde 3-phosphate dehydrogenase (GAPDH) primer pairs were selected using sequences within each gene that were identical for both hamster and human. The RhoG sequences used were: 5'-ATC TGT TTC TCC ATT GCC AGT-3' (sense strand) and 5'-CTT GGC CAG TGC CTG GCC CTG-3' (antisense strand), while the GAPDH sequences used were: 5'-GGC GCT GCC AAG GCT GTG GGC-3' (sense strand) and 5'-GTC ATA CCA GGA AAT GAG CTT-3' (antisense strand). For the PCR reaction, 30 cycles were performed with an annealing temperature of 47°C and an extension time of 1 min. In addition, control reactions were performed without RNA or without the reverse transcriptase reaction, where RNA was added to the reaction after heat-inactivation of the RT enzyme.

Interaction of SNX with Rho GTPases

Interaction of SNX2 with Rho GTPases was determined by transfection of CHO cells with myc-tagged RhoA, Rac1, Cdc42 or RhoG. 48 h after transfection, cells were harvested by scraping in PBS and solubilized with 0.5% CHAPS, 1 mM $MgCl_2$ and 10 mM β-ME in PBS containing protease inhibitors. The lysate was cleared by

centrifugation at 5,000 x g for 10 min, and diluted to a final concentration of 0.125% CHAPS. Cell extracts were then loaded with 200 μM guanosine 5'-(β-thio)diphosphate (GDPβS), 200 μM guanosine 5'-(γ-thio)triphosphate (GTPγS), or a combination of both nucleotide analogs (Sigma) at 200 μM each, for 10 min at 30°C. 100 pmol of recombinant His_6-HA-Flag-SNX2 was then added to the extracts, which were incubated for 16 h at 4°C in the presence of Ni-NTA-agarose beads that were blocked with 0.5% gelatin (BioRad). Beads were then washed five times with PBS containing 0.125% CHAPS, 150 mM NaCl, 1 mM mM $MgCl_2$, 10 mM β-ME and 20 mM imidazole, and proteins were eluted with SDS sample buffer prior to analysis by Western immunoblot.

For direct interaction studies, 45 pmol of recombinant TAP-myc-Rho GTPases immobilized on IgG-Sepharose beads were blocked with 0.5% gelatin in equilibration buffer (0.125% CHAPS and 1 mM $MgCl_2$ in PBS) prior to loading with 200 μM GDPβS in equilibration buffer for 10 min at 30°C. Beads were then incubated for 16 h with 45 pmol of recombinant His_6-HA-Flag-SNX1 or SNX2 at 4°C, and were washed five times with 0.125% CHAPS, 150 mM NaCl and 1 mM $MgCl_2$ in PBS prior to analysis by Western immunoblot.

Endoglycosidase H assay of VSVG transport from ER to Golgi

The effect of VAP overexpression on ER-to-Golgi transport of transmembrane cargo was analyzed by co-transfection of wild-type, truncated (ΔN) or P56S mutant VAPA or VAPB with $VSVG^{ts045}$-myc3 (kindly provided by Dr. Jesse C. Hay, University of Montana) using a modified assay for Endoglycosidase H (Endo H) sensitivity (Gabel and Bergmann, 1985). 16-18 hours after transfection, cells were shifted to 42°C for 6 h to

accumulate misfolded $VSVG^{ts045}$ in the ER. Cycloheximide was then added to 20 μg/ml for 10 min, and cells were rapidly shifted back to 37°C for 0, 30, 60 or 90 min to allow folding and exit of VSVG. At each of these chase times, cells were chilled on ice, washed with PBS and scraped with a rubber policeman. Cells were then resuspended in 20 mM Tris-HCl pH 7.5 supplemented with 2 mM PMSF and disrupted by sonication. Following low-speed centrifugation at 500 x g for 5 min, membranes were isolated at 100,000 x g for 1 h. The membrane fraction was then solubilized in 50 mM sodium citrate pH 5.5 containing 0.1% SDS, and proteins were heat inactivated by boiling for 10 min. Lysates were then diluted to a final concentration of 0.02% SDS in 50 mM sodium citrate pH 5.5, and glycoproteins were digested with 10 mU Endo H (Roche) in the presence of 1 mM PMSF for 17 h at 37°C. Samples were then precipitated with trichloroacetic acid and dissolved in SDS sample buffer. Proteins were subsequently resolved by SDS-PAGE and detected by Western immunoblot with anti-myc antibodies.

Time course of Chromogranin B-GFP^{S65T} transport

Transport of Chromogranin B from ER to Golgi was assessed by co-transfection of CHO cells with pCDM8/CgB-GFP^{S65T} (Wacker et al., 1997) and either empty vector, wild-type or P56S mutant VAPA or VAPB. Sixteen hours after transfection, cells were shifted to 15°C for 2 hours in medium buffered with 20 mM HEPES pH 7.4 (Invtrogen) to enhance GFP^{S65T} fluorescence and to prevent transport to the Golgi complex by trapping the cargo in the ER-Golgi intermediate compartment. Cycloheximide was then added to 20 μg/ml for 10 min before shifting cells back to 37°C. Cells were then chased

for 0 or 30 min, at which time cover slips were fixed as described above and stained with mouse anti-calreticulin antibodies.

Fluorescence recovery after photobleaching (FRAP)

CHO cells were seeded onto 0.17 mm glass-bottomed Delta T dishes (Bioptechs), and co-transfected with pCDM8.1/VSVG^{ts045}-GFP (a gift from Dr. Jennifer Lippincott-Schwartz, National Institutes of Health) and either empty vector, wild-type or P56S mutant VAPA or VAPB. To determine the effect of FFAT on lateral diffusion of VSVG^{ts045} in the ER membrane, cells were additionally co-transfected with myc-tagged OSBP-FFAT. VSVG^{ts045}-GFP was accumulated in the ER at 42°C for 5 h. For FRAP experiments examining the effect of microtubule depolymerization on lateral diffusion of VSVG^{ts045}-GFP, cells were treated with 33 μM Nocodazole (Sigma) during the 5 h incubation at 42°C. Prior to imaging, the media was buffered with 20 mM HEPES pH 7.4, and cycloheximide was added to a concentration of 20 μg/ml. Cells were imaged on a confocal microscope equipped with a Delta T stage adaptor (Bioptechs) maintained at a constant temperature of 32°C. A portion of the ER in the periphery of the cell was photobleached, and recovery was monitored by imaging every 20 seconds for 10 minutes. The extent of VSVG recovery into the photobleached area was determined using Medical Image Processing, Analysis and Visualization (MIPAV) software from the National Institutes of Health (McAuliffe et al., 2001). Values were expressed as a fraction of the pre-bleach fluorescence intensity, with any residual fluorescence signal immediately following photobleaching subtracted from all values as a background signal.

To estimate the recovery rate of VSVG^{ts045}, the corrected intensity values from all frames in the first two minutes following photobleaching were used, since these values

followed an approximately linear curve. A linear regression was applied to the values, and the slope of this regression was used as an indication of fluorescence recovery per unit of time.

Microtubule pulldown

CHO cells were transfected with wild-type or mutant VAPs as described above. 16-18 hours after transfection, cells were scraped in PBS, and homogenized by sonication in buffer H (5 mM HEPES-NaOH pH 7.4, 100 mM NaCl, 1X protease inhibitor cocktail). After clearing the lysate at 5,000 x g for 5 min, Triton X-100 was added to a final concentration of 0.25%, and insoluble proteins were removed by centrifugation at 130,000 x g for 20 min. Synthetic FFAT (DENEFFDAPE) or AAAT (DENEAADAPE) peptides (GL Biochem) in dimethyl sulfoxide (DMSO) were then added to equivalent amounts of supernatant to give final concentrations of 0, 62.5, 125, or 250 μM, and extracts were incubated on ice for 30 min.

During incubation of lysates with FFAT or AAAT peptide, bovine brain tubulin (Cytoskeleton) was pre-polymerized according to the manufacturer's instructions. Briefly, purified tubulin was reconstituted to 5 μg/μl in G-PEM buffer (80 mM 1,4-piperazinebis(ethanesulfonic acid) (PIPES) pH 6.9, 1 mM EGTA, 1 mM $MgCl_2$, and 1 mM GTP). To 15 μl of reconstituted tubulin, 1.875 μl of polymerization buffer (PEM containing 60% glycerol) was added, and polymerization was allowed to proceed at 37°C for 30 min. Subsequently, polymerized microtubules were stabilized with 135 μl of G-PEM buffer supplemented with 20 μM Taxol (G-PEM/Taxol) to give a final tubulin concentration of 0.5 μg/μl. To test for nonspecific pulldown of VAPs in the absence of

microtubules, a blank polymerization reaction was performed using G-PEM instead of tubulin.

To each sample, 7.5 μg of polymerized microtubules were added, and extracts were allowed to bind for 20 min at 25°C. The mixture was then diluted with an equal volume of G-PEM/Taxol and layered onto a cushion of 20% sucrose in 80 mM PIPES pH 6.9, 1 mM EGTA, 1 mM $MgCl_2$ and 10 μM Taxol. Polymerized microtubules were isolated by 100,000 x g centrifugation for 40 min at 25°C. The microtubule-containing high-speed pellet was washed once with G-PEM/Taxol and solubilized in SDS sample buffer. Proteins associated with the microtubule fraction were resolved by SDS-PAGE followed by Western immunoblot with mouse anti-Flag and 12G10 mouse anti-alpha tubulin antibodies.

Statistical analyses

Unless otherwise stated, an unpaired Student's t-test was performed to determine statistical significance of experimental results, and a p-value <0.05 was considered significant.

Chapter I: Novel functions for sorting nexins in modulating actin dynamics

Results

Kalirin-7 interacts with SNX1 and SNX2

To verify the interaction of SNX2 and Kal7 that was identified in the yeast two-hybrid screen, pulldown experiments were performed using N-terminally epitope-tagged His_6-myc-Kal7 and Flag-SNX2. Given the high degree of similarity between SNX1 and SNX2, Flag-SNX1 was also tested for interaction with Kal7. When co-transfected CHO extracts were incubated with Ni-NTA beads, both SNX1 and SNX2 specifically associated with Kal7, but could not be detected in the bead fraction in the absence of Kal7 (Figure 10A). In addition, the GEF-inactive Kal7 N1415A/D1416A (ND/AA) mutant could also interact with SNX1 and SNX2, suggesting that GEF activity of Kal7 is not required for its interaction with either SNX. It is worth noting that the cDNA isolated in the two-hybrid screen aligned within a region matching the second through the seventh spectrin repeats of Kal7. This region is also found in other Kalirin isoforms (Johnson et al., 2000), indicating that the Kal-SNX interaction may include isoforms other than Kal7. However, the ability of SNX1 or SNX2 to interact with other splice variants was not examined in this study.

To characterize the domains of SNX2 that are required for interaction with Kal7, truncated SNX2 fragments consisting of the N-terminus and PX domain (N+PX) or the BAR domain were generated (Figure 10B). Although both of these fragments were readily detected in CHO extracts, they failed to associate with Kal7, suggesting that the entire SNX2 protein is required for interaction (Figure 10A). Interaction of Kal7 with N-terminus, PX, or PX+BAR domain fragments of SNX2 was also tested; however, these

Figure 10: Interaction of Kal7 with SNX1 and SNX2. (A), Detergent-solubilized extracts from CHO cells co-expressing wild-type (WT) or GEF-inactive (ND/AA) His_6-myc-Kal7 and full-length or truncated Flag-SNX1 or SNX2 were subjected to pulldown with Ni-NTA beads. Retained proteins were analyzed by Western immunoblot with anti-Flag and anti-myc antibodies. The lower band present in all lanes corresponds to a non-specific product recognized by the mouse anti-Flag antibody. (B), Schematic of SNX1, SNX2 and Kal7 fragments used in this study.

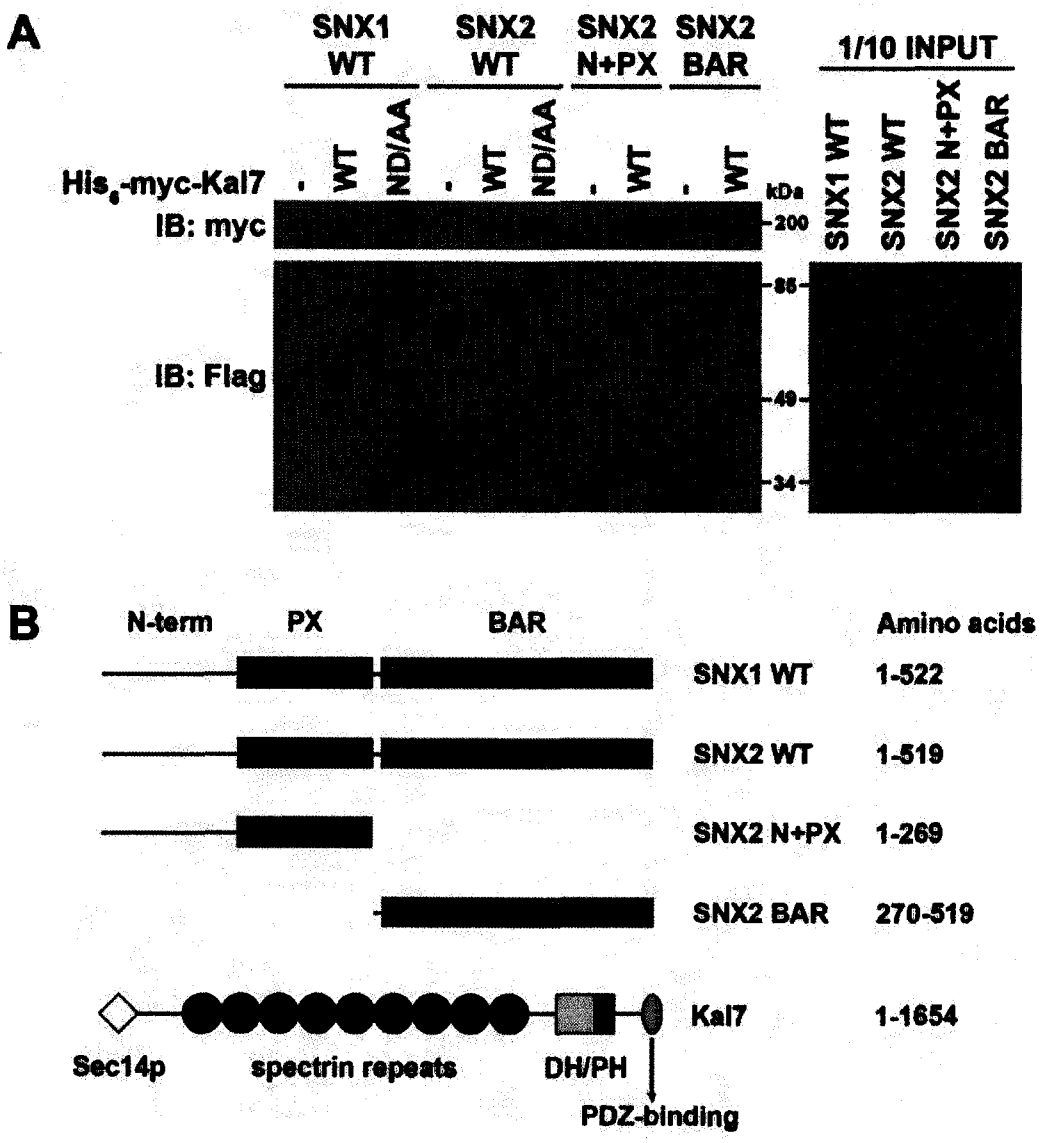
A
SNX1 WT
SNX2 WT
SNX2 N+PX
SNX2 BAR
1/10 INPUT
. WT ND/AA . WT ND/AA . WT . WT
SNX1 WT
SNX2 WT
SNX2 N+PX
SNX2 BAR
His6-myc-Kal7
IB: myc
IB: Flag
kDa
200
85
49
34
B
N-term
PX
BAR
Amino acids
SNX1 WT 1-522
SNX2 WT 1-519
SNX2 N+PX 1-269
SNX2 BAR 270-519
Kal7 1-1654
Sec14p
spectrin repeats
DH/PH
PDZ-binding

truncations did not express efficiently, and could not be used for interaction studies.

Co-expression of Kal7 and SNX potentiates lamellipodia formation

Next, the subcellular distribution of exogenous SNX1, SNX2 and Kal7 was determined in singly transfected CHO cells. As reported by others (Gullapalli et al., 2004; Zhong et al., 2002), Flag-SNX1 and SNX2 co-localized with the early endodomal antigen EEA1 (Figure 11A). Both wild-type and GEF-inactive myc-Kal7 also partially co-localized with EEA1, although the distribution of Kal7 appeared to be broader than that of SNX1 or SNX2. In co-transfected cells, both SNX1 and SNX2 partially co-localized with wild-type Kal7 (Figure 11B). Notably, co-transfected cells displayed dramatic lamellipodia and membrane ruffles (hereafter referred to only as lamellipodia), with SNX1 and SNX2 prominently redistributed to the leading edge of these structures. Within lamellipodial structures, Kal7 co-localized with SNX1 and SNX2 both on discrete patches at the cell surface and on vesicular structures within the cell (Figure 11B, inset). Both SNX1 and SNX2 co-localized extensively with F-actin in lamellipodia, as determined by staining with phalloidin (Figure 12). However, co-localization of Kal7 with F-actin at the leading edge was comparatively weak, and neither SNX1 nor SNX2 co-localized with F-actin in the absence of Kal7 or when co-expressed with GEF-inactive Kal7 ND/AA. In contrast to other studies showing that GEF activity of Kalirin is not required for lamellipodia (Schiller et al., 2005), expression of Kal7 ND/AA did not promote lamellipodia formation in a significant proportion of cells, either in the presence or absence of Flag-SNX. However, a second study reported that expression of Kal7 ND/AA was unable to induce lamellipodia in epithelial cells, but instead resulted in a

Figure 11: Subcellular localization of SNX1, SNX2 and Kal7. (A), CHO cells singly transfected with Flag-SNX1, Flag-SNX2, His_6-myc-Kal7 WT or His_6-myc-ND/AA (magenta) were stained with anti-EEA1 (green) and imaged by confocal microscopy. (B), Cells were co-transfected with Flag-SNX1 or SNX2 (magenta) and His_6-myc-Kal7 WT or ND/AA (green). Inset images were taken at higher magnification. Scale bar, 10 μm (inset scale bar = 5 μm).

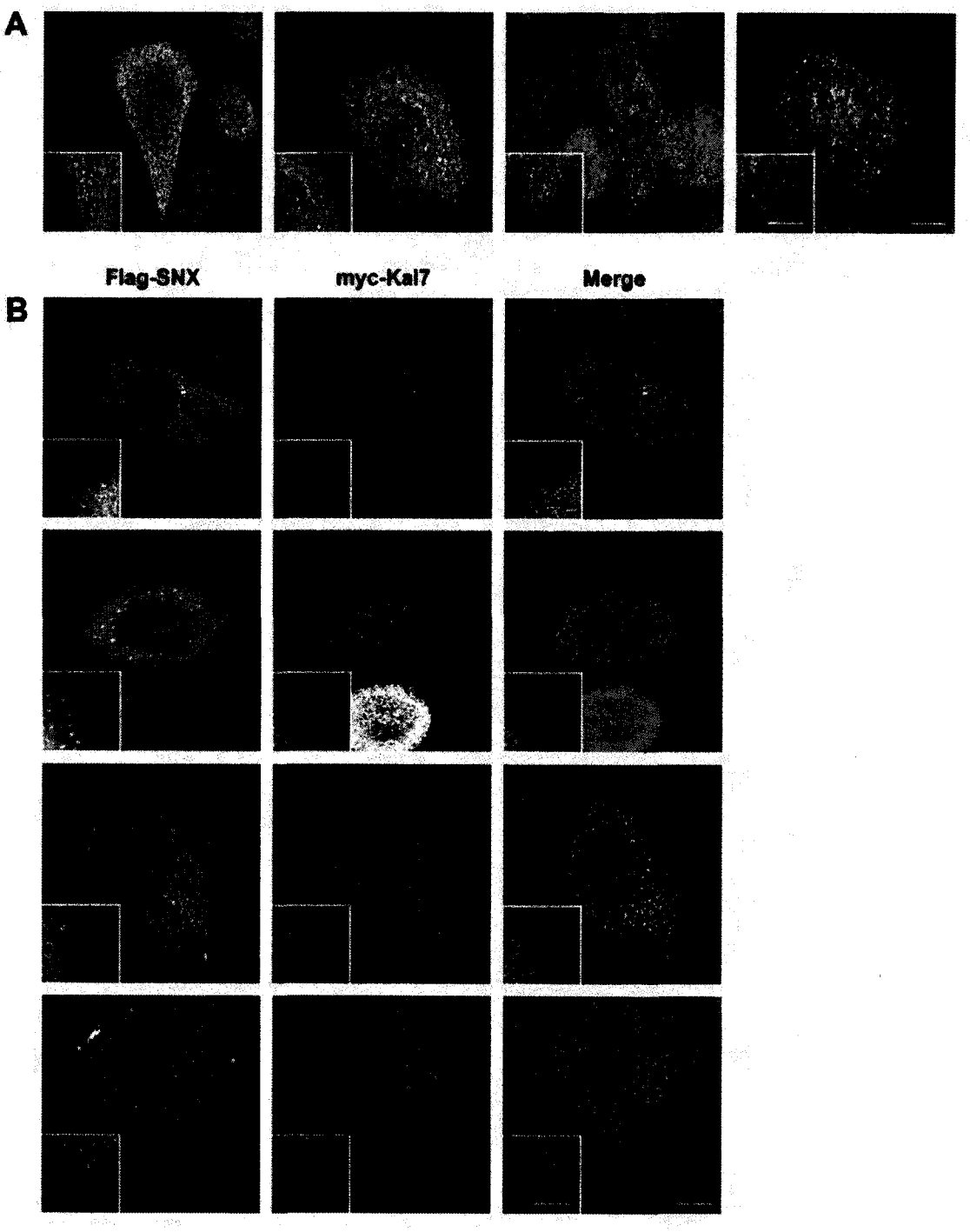
A
B
Flag-SNX
myc-Kal7
Merge

Figure 12: Co-localization of SNX1, SNX2 and Kal7 with F-actin. (A), CHO cells singly transfected with Flag-SNX1, Flag-SNX2, myc-Kal7 wild-type or ND/AA (green) were stained with phalloidin (magenta) to detect F-actin prior to visualization by confocal microscopy. (B), CHO cells co-expressing Flag-SNX1 or SNX2 with wild-type or GEF-inactive (ND/AA) myc-tagged Kal7 were fixed and stained with anti-Flag or anti-myc (green) and phalloidin (magenta) as indicated. Inset images were collected at higher magnification. Scale bars = 10 μm (inset scale bars = 5 μm).

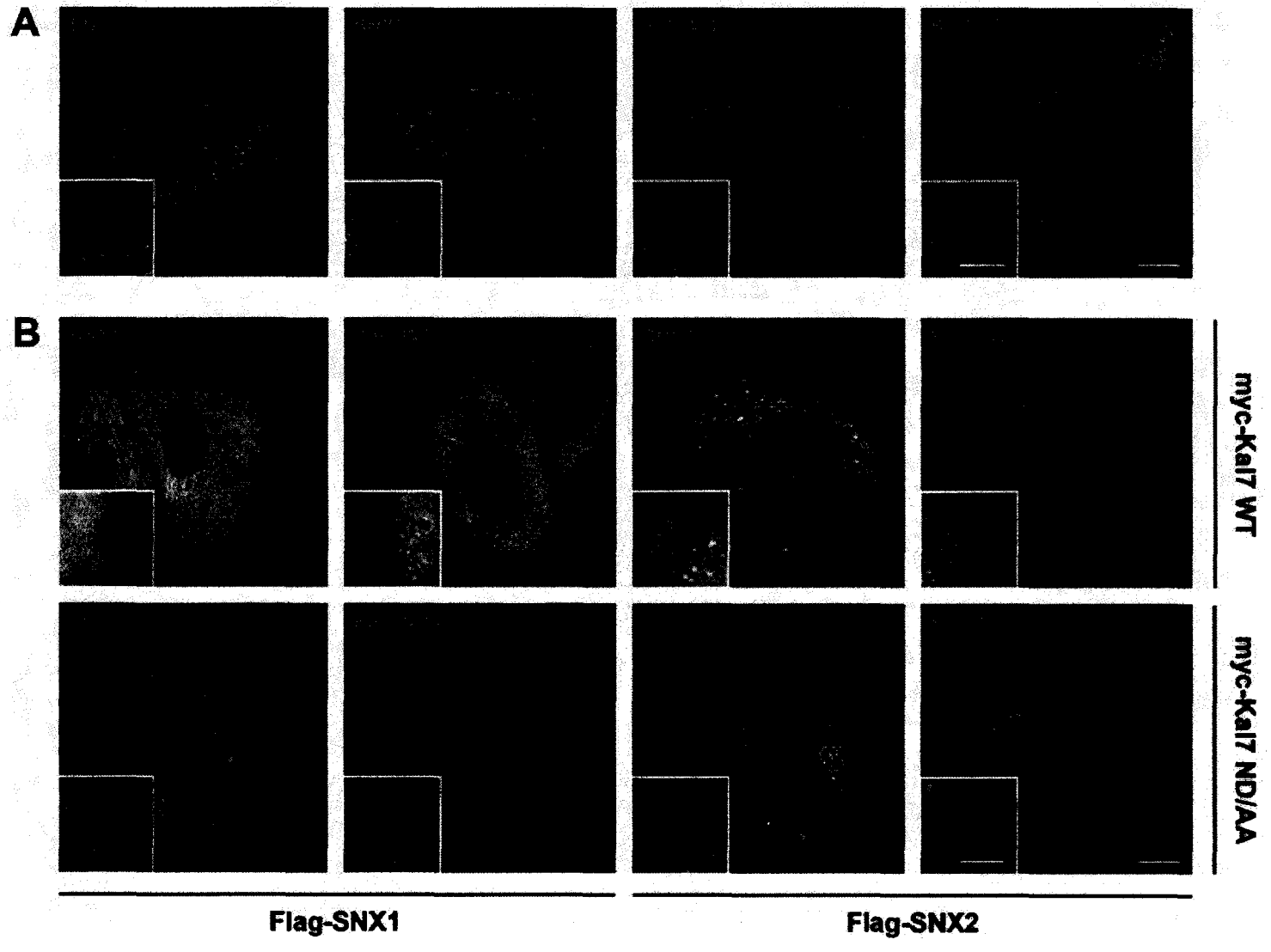
A
B
myc-Kal7 WT
myc-Kal7 ND/AA
Flag-SNX1
Flag-SNX2

rounded morphology with numerous membrane blebs (Schiller et al., 2008). Thus, the present study supports a role for Kal7 GEF activity in formation of lamellipodia.

To verify that lamellipodia formation is indeed due to co-expression of Kal7 and SNX, the proportion of transfected cells that displayed this phenotype were quantified. When transfected with an empty vector, only a small fraction of cells (1.5 ± 1.1%) formed lamellipodia (Figure 13A). Similarly, overexpression of Flag-SNX1 or SNX2 was unable to induce lamellipodia, where 6.7 ± 0.9% and 4.4 ± 1.3% of cells displayed phenotype, respectively ($p>0.05$). Although expression of wild-type Kal7 gave a small increase in the incidence of lamellipodia to 10.9 ± 0.7%, co-expression of Kal7 with SNX1 or SNX2 resulted in a striking increase in phenotype to 42.3 ± 1.7% and 55.3 ± 4.4% of cells, respectively. The requirement of Kal7 GEF activity for lamellipodia formation was also tested, and while 1.2 ± 0.4% of cells expressing Kal7 ND/AA developed lamellipodia, co-expression of SNX1 or SNX2 only modestly promoted lamellipodia formation (3.8 ± 0.6% and 10.2 ± 1.1% of cells, respectively). Taken together, these results suggest that co-expression of SNX1 or SNX2 with Kal7 can potentiate Kal7-dependent membrane remodeling, and that this phenotype is dependent on the GEF activity of Kal7.

Since truncated fragments of SNX2 did not interact with Kal7, the ability of SNX2 N+PX or BAR domain fragments to induce lamellipodia when co-expressed with Kal7 was also tested, with the expectation that these fragments would not promote lamellipodia formation. When expressed in the absence of Kal7, the N+PX and BAR fragments localized to punctate structures within the cell (Figure 14). Compared to wild-type SNX2 (Figure 11A), the truncated fragments showed reduced co-localization with

Figure 13: Quantification of lamellipodia phenotype. (A), CHO cells expressing empty vector (control), Kal7 WT or Kal7 ND/AA were co-transfected with an empty mRFP vector (black bars), Flag-SNX1 (grey bars) or Flag-SNX2 (white bars). Cells were fixed after 48 h, and mRFP- or Flag-positive cells were scored for lamellipodia. (B), CHO co-expressing wild-type Kal7 and either SNX2 wild-type, N+PX or BAR were scored for lamellipodia as in panel A. For all conditions, a minimum of 300 cells were counted per trial from blinded cover slips, and cells were scored as positive if lamellipodia were present on at least 10% of the cell periphery. Values are presented as mean ± SEM (n=4, $^{\#}$ $p<0.01$ compared to empty vector, *** $p<0.001$ compared to empty vector, Kal7 WT and the respective SNX alone for panel A, one-way ANOVA followed by Neuman-Keuls *post-hoc* test. ** $p<0.01$ compared to Kal7 WT + SNX2 WT for panel B).

A
Lamellipodia-positive cells (%)
0
10
20
30
40
50
60
Control
Kal7 WT
Kal7 (ND/AA)
***
***
#
B
Lamellipodia-positive cells (%)
0
10
20
30
40
50
60
WT
N+PX
BAR
**
**

Figure 14: Subcellular localization of SNX2 truncations and mutants. Shown are representative confocal images of CHO cells expressing low levels of Flag-tagged SNX2 N+PX and BAR truncations, or SNX2 RRF and KR/AA mutants stained with anti-Flag (magenta) and anti-EEA1 (green). Inset images were taken at higher magnification. Scale bar, 10 μm (inset scale bar = 5μm).

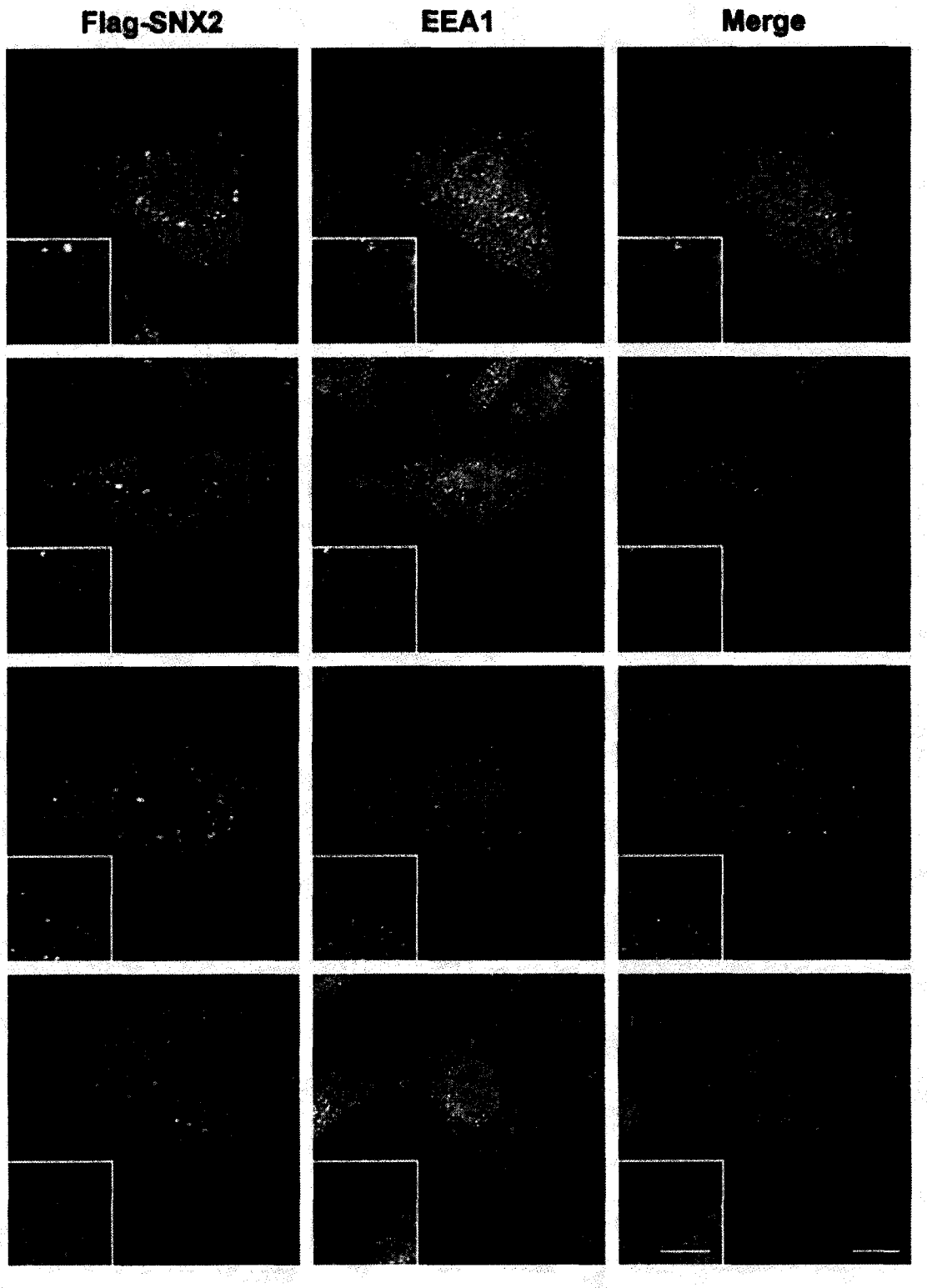
Flag-SNX2
EEA1
Merge

EEA1, suggesting that the PX and BAR domains are both involved in targeting to the correct compartment. When co-expressed with Kal7, the N+PX domain of SNX2 resulted in 31.9 ± 2.5% of cells with lamellipodia, while the BAR domain induced lamellipodia in 31.1 ± 2.1% of cells (Figure 13B). While these truncations are clearly not as effective as full-length SNX2, it is interesting to note that the observed values are greater than those seen for cells transfected with empty vector, Kal7 or SNX2 alone. It is possible, however, that either truncated fragment could interact with endogenous SNX proteins, since both the N-terminus and BAR domain of SNX1 and SNX2 have been implicated in dimerization (Zhong et al., 2002). Thus, it remains possible that overexpression of truncated SNX2 could promote Kal7-dependent lamellipodia by clustering endogenous proteins and facilitating their interaction with Kal7.

PX and BAR domain function of SNX is necessary for lamellipodia formation

Since truncated fragments of SNX2 were unable to interact with Kal7 and were less efficient in promoting Kal7-mediated lamellipodia, functionality of the PX and BAR domains might be important for the phenotypic effects observed upon co-expression of Kal7 with SNX2. To test this possibility, the R182A/R183A/F184A (RRF) mutant that has been previously shown to abolish phosphoinositide binding of the PX domain was generated (Gullapalli et al., 2004). In addition, a K426A/R428A (KR/AA) mutant of SNX2, which targets analogous basic amino acid residues known to affect tubulation or curvature-sensing properties of the SNX1 BAR domain, was also created (Carlton et al., 2004). Ni-NTA pulldown experiments with His_6-tagged Kal7 were then performed as above, and both SNX2 mutants retained their ability to interact with Kal7 (Figure 15A).

Figure 15: Effect of SNX2 PX and BAR domain mutation on interaction with Kal7 and lamellipodia formation. (A), Lysates from CHO expressing His_6-myc-Kal7 and either wild type, PX (RRF) or BAR (KR/AA) mutant Flag-SNX2 were subjected to pulldown with Ni-NTA beads. (B), CHO co-expressing wild-type Kal7 and either wild-type, RRF or KR/AA mutant Flag-SNX2 were scored for lamellipodia. For each trial, at least 300 cells were counted per condition from blinded cover slips (mean ± SEM; n=4, *** $p<0.001$).

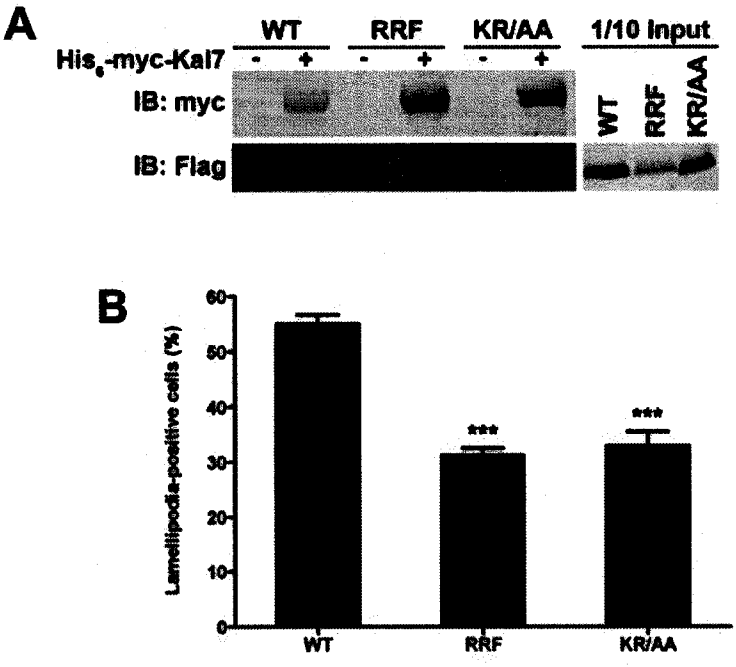
A
WT
RRF
KR/AA
1/10 Input
His6-myc-Kal7
- + - + - +
IB: myc
IB: Flag
WT
RRF
KR/AA
B
Lamellipodia-positive cells (%)
60
50
40
30
20
10
0
***
***
WT
RRF
KR/AA

However, when tested for the ability to form lamellipodia, co-expression of Kal7 with SNX2 RRF and KR/AA mutants was less effective (31.3 ± 1.3% and 32.9 ± 2.6% of cells, respectively) than co-expression with wild-type SNX2 (55.1 ± 1.7%, Figure 15B). As described for the SNX2 truncations, these values are higher than those seen for cells transfected with empty vector, Kal7 or SNX2 alone. Interestingly, mutation of either the PX or BAR domain did not prevent membrane recruitment of exogenous SNX2 at lower expression levels, although co-localization with EEA1 was reduced (Figure 14). However, at higher expression levels, SNX2 mutants mislocalized to the cytoplasm, as reported by others (Carlton et al., 2004; Gullapalli et al., 2004; Zhong et al., 2002). The observation that disruption of either PX or BAR domain function of SNX2 partially inhibits Kal7-mediated lamellipodia highlights the importance of these two domains in phenotypic expression.

Depletion of endogenous SNX1 or SNX2 inhibits Kal7-mediated lamellipodia formation

To rule out a possible non-specific effect of SNX overexpression, shRNA depletion was performed to determine if loss of endogenous SNX1 or SNX2 could attenuate Kal7-mediated lamellipodia formation. Since the sequences of hamster SNX1 and SNX2 are unavailable, HeLa cells were used for shRNA studies. The ability of HeLa cells to form lamellipodia when co-expressed with wild-type Kal7 and either SNX1 or SNX2 was comparable to the response seen for CHO cells, indicating that both cell lines elicit similar responses (Figure 16A). The above experiments showing that SNX1 and SNX2 promote lamellipodia formation when co-expressed with Kal7 were performed using wild-type Kal7 driven by the weaker mammalian EF1α promoter. Under these

Figure 16: Induction of lamellipodia in HeLa cells. (A) HeLa cells transfected with empty vector (control) or Kal7 WT were co-transfected with an empty mRFP vector (black bars), Flag-SNX1 (grey bars) or Flag-SNX2 (white bars). Cells were fixed after 48 h, and mRFP- or Flag-positive cells were scored for lamellipodia or dorsal ruffles. At least 50 cells were counted per trial for each condition (mean ± SEM; n=3, *** $p<0.001$). (B), Quantitative immunoblot of HeLa cells transfected with equivalent amounts of EF1α-driven Kal7 WT or CMV-driven Kal7 ΔCT to determine relative expression levels under the different promoters. Equal protein loading was confirmed by staining with anti-tubulin antibodies, while equivalent transfection efficiency was confirmed by co-transfection with EGFP. (C), Detergent-solubilized extracts from CHO cells co-expressing wild-type (WT) or ΔCT His_6-myc-Kal7 and Flag-SNX1 or SNX2 were subjected to pulldown with Ni-NTA beads. Retained proteins were detected with mouse anti-Flag and anti-myc antibodies. (D) HeLa cells expressing EF1α-driven Kal7 WT or CMV-driven Kal7 ΔCT were stained with anti-Kalirin antibodies, and the proportion of cells displaying lamellipodia or dorsal ruffles was determined (mean ± SEM; n=3, ** $p<0.01$).

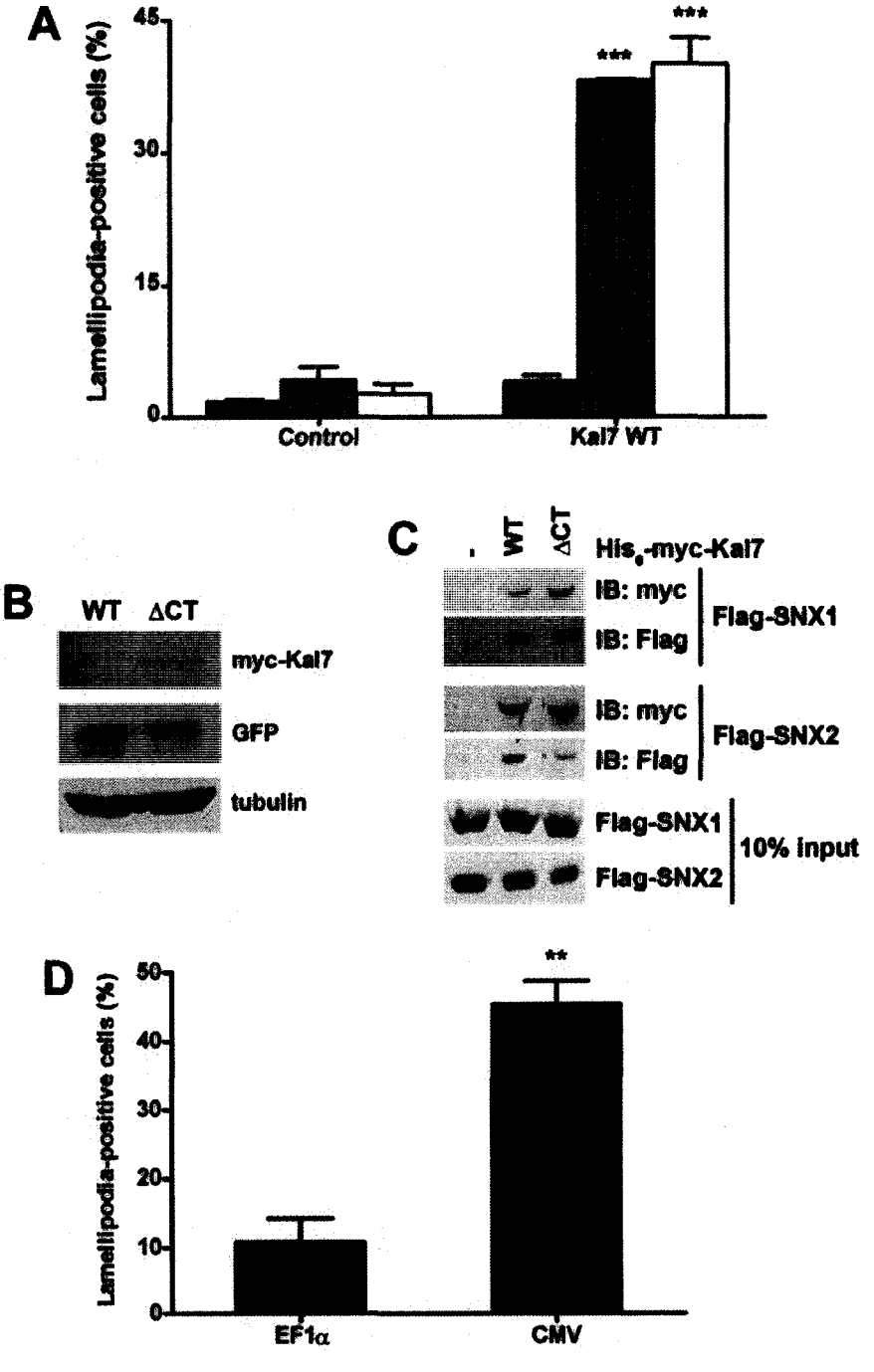
A
Lamellipodia-positive cells (%)
45
30
15
0
***
***
Control
Kal7 WT
B
WT
ΔCT
myc-Kal7
GFP
tubulin
C
.
WT
ΔCT
His6-myc-Kal7
IB: myc
IB: Flag
Flag-SNX1
IB: myc
IB: Flag
Flag-SNX2
Flag-SNX1
Flag-SNX2
10% input
D
Lamellipodia-positive cells (%)
50
40
30
20
10
0
**
EF1α
CMV

conditions, expression of Kal7 alone did not efficiently induce lamellipodia. Thus, overxpression of Kal7 under the stronger cytomegalovirus (CMV) promoter was used to determine if higher Kal7 protein levels could overcome the need for SNX overexpression. Compared to EF1α-driven Kal7 WT, cells transfected with CMV-driven Kal7 ΔCT, which lacks the C-terminal PDZ-binding motif, showed a 5- to 6-fold increase in Kal7 expression (Figure 16B). Importantly, Kal7 ΔCT still interacted efficiently with SNX1 and SNX2 when assessed by Ni-NTA pulldown (Figure 16C). At endogenous SNX levels, CMV-driven Kal7 ΔCT induced lamellipodia more efficiently than EF1α-driven Kal7 (45.4 ± 3.4% and 10.9 ± 3.4% of cells, respectively, Figure 16D). It is worth noting that deletion of the PDZ-binding motif of Kal7 does not affect GEF activity, indicating that spontaneous lamellipodia do not arise from loss of an autoinhibitory mechanism (Penzes et al., 2001). In addition, the observed phenotype indicates that subcellular targeting information provided by the PDZ-binding motif is not essential for induction of lamellipodia in epithelial cells.

Next, HeLa cells were infected with lentiviral shRNA targets directed against SNX1 or SNX2 to deplete endogenous proteins. shRNA infection caused a 50% decrease in SNX1 and SNX2 levels, without affecting expression of the cargo-selective retromer subunit Vps35 (Figure 17A). Interestingly, depletion of SNX1 resulted in a slight increase in expression of SNX2 and vice-versa, suggesting that loss of one protein may be compensated for by upregulation of the other. Co-infection with both lentiviral targets had a weaker effect than single infections, with a 27% and 38% reduction in SNX1 and SNX2 levels, respectively. Infection with a control shRNA target against GFP had no effect on expression of SNX1, SNX2 or Vps35. When examined for phenotypic changes,

Figure 17: Effect of SNX1 and SNX2 depletion on Kal7-mediated lamellipodia formation. (A), Confirmation of SNX1 or SNX2 depletion in HeLa cells 48 hours after infection with lentiviral shRNA targets. Mock- or GFP shRNA-infected cells were used as control. Quantification was performed by densitometric analysis, and values were corrected for equal loading based on tubulin levels. (B), Confocal images of lentivirus-infected HeLa cells expressing CMV-driven myc-Kal7 ΔCT and stained with anti-myc antibodies. (C), HeLa cells expressing Kal7 ΔCT were depleted of SNX1 or SNX2 for 48 hours prior to fixation and scoring for lamellipodia or dorsal ruffles. For each condition, a minimum of 50 cells were counted per trial from blinded cover slips (mean ± SEM; n=6, *** $p<0.001$ compared to mock or GFP infection).

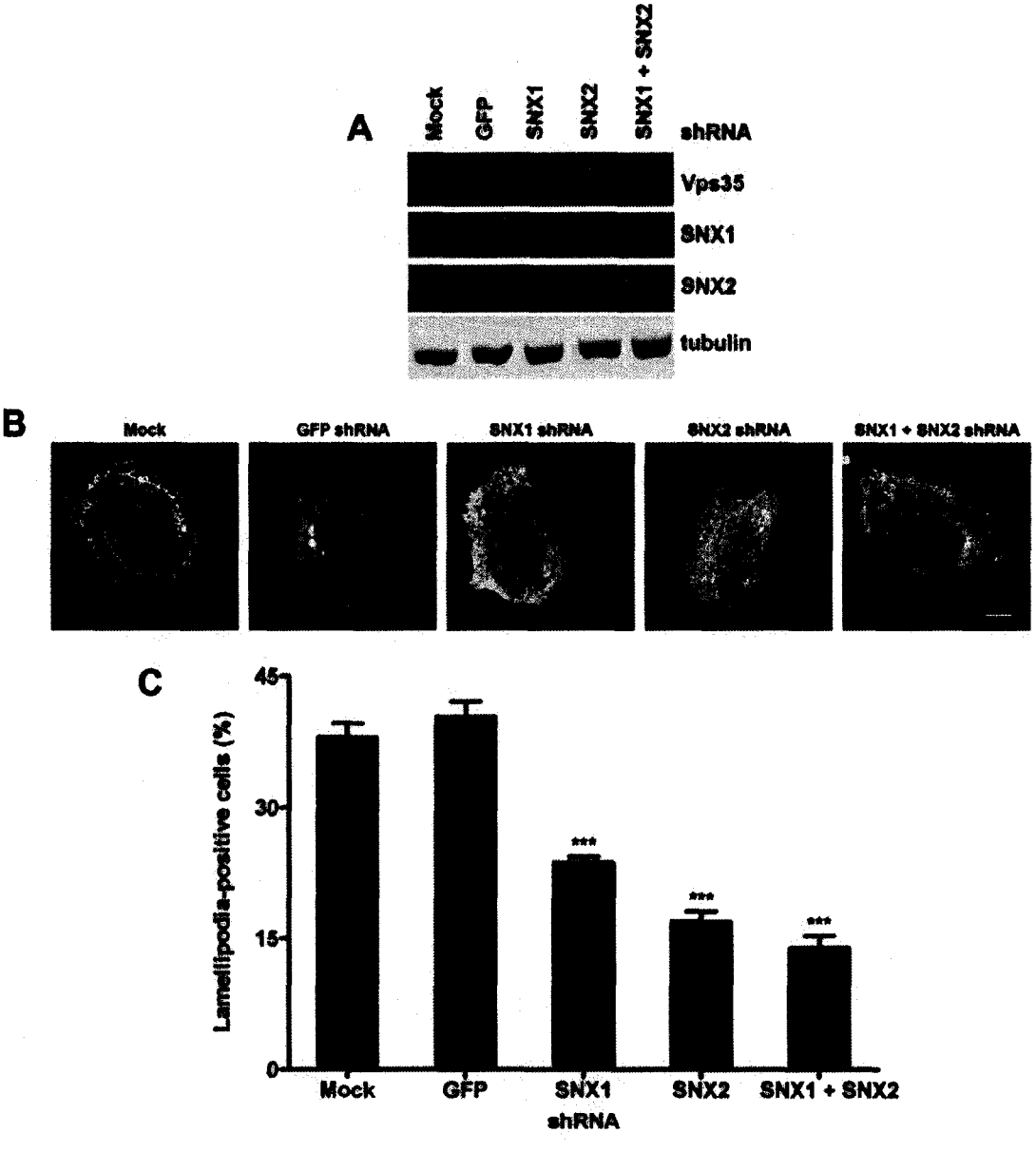
A
Mock
GFP
SNX1
SNX2
SNX1 + SNX2
shRNA
Vps35
SNX1
SNX2
tubulin
B
Mock
GFP shRNA
SNX1 shRNA
SNX2 shRNA
SNX1 + SNX2 shRNA
C
Lamellipodia-positive cells (%)
45
30
15
0
***
***
***
Mock
GFP
SNX1
SNX2
SNX1 + SNX2
shRNA

knockdown of SNX1 and/or SNX2 had no obvious effect on cell morphology in the absence of Kal7.

Subsequently, the phenotype of shRNA-infected HeLa cells expressing CMV-driven Kal7 ΔCT was examined. In many mock- or GFP-infected cells expressing CMV-driven Kal7 ΔCT, dorsal ruffles were observed in addition to lamellipodia (Figure 17B), and both phenotypes were included in the analysis since they reflect activation of Rac1 and RhoG (Ellerbroek et al., 2004; Ridley et al., 1992). Endogenous SNX1 and SNX2 partially redistributed to the leading edge of lamellipodia and to dorsal ruffles in Kal7 ΔCT-expressing HeLa cells (Figure 18, panels A and B), as was seen for epitope-tagged SNX1 and SNX2 in CHO cells. Furthermore, endogenous SNX1 and SNX2 co-localized with Kal7 ΔCT at the leading edge of these structures. The localization of endogenous SNX1 or SNX2 in CHO cells could not be assessed, since the SNX1 and SNX2 antibodies did not detect the hamster proteins. Infection with control GFP shRNA had no effect on induction of lamellipodia or dorsal ruffles compared to mock-infected cells (40.3 ± 1.8% and 38.0 ± 1.6% of cells, respectively, Figure 17C). However, depletion of SNX1 or SNX2 caused an approximate two-fold reduction in the proportion of cells displaying lamellipodia (to 23.7 ± 0.7% and 17.0 ± 1.2% of cells, respectively). Depletion of SNX1 and SNX2 in the same cells also reduced lamellipodia phenotype to 13.9 ± 1.5%. While the effect of SNX1 and SNX2 knockdown was significant compared to knockdown of SNX1 alone ($p<0.05$), it was statistically similar to knockdown of SNX2 alone ($p>0.4$). It is thus possible that SNX2 might play a more prominent role in lamellipodia formation than SNX1.

Figure 18: Co-localization of endogenous SNX1 and SNX2 with Kal7. (A), HeLa cells were fixed and stained with anti-SNX1 or anti-SNX2 to demonstrate localization of endogenous protein in the absence of Kal7. (B), HeLa cells transfected with CMV-driven myc-Kal7 ΔCT were stained with anti-Kalirin (magenta) and anti-SNX1 or SNX2 (green) antibodies. Arrows indicate regions of Kal7 and SNX overlap at the leading edge. Inset images were captured at higher magnification. Scale bars = 10 μm (inset scale bar = 5 μm).

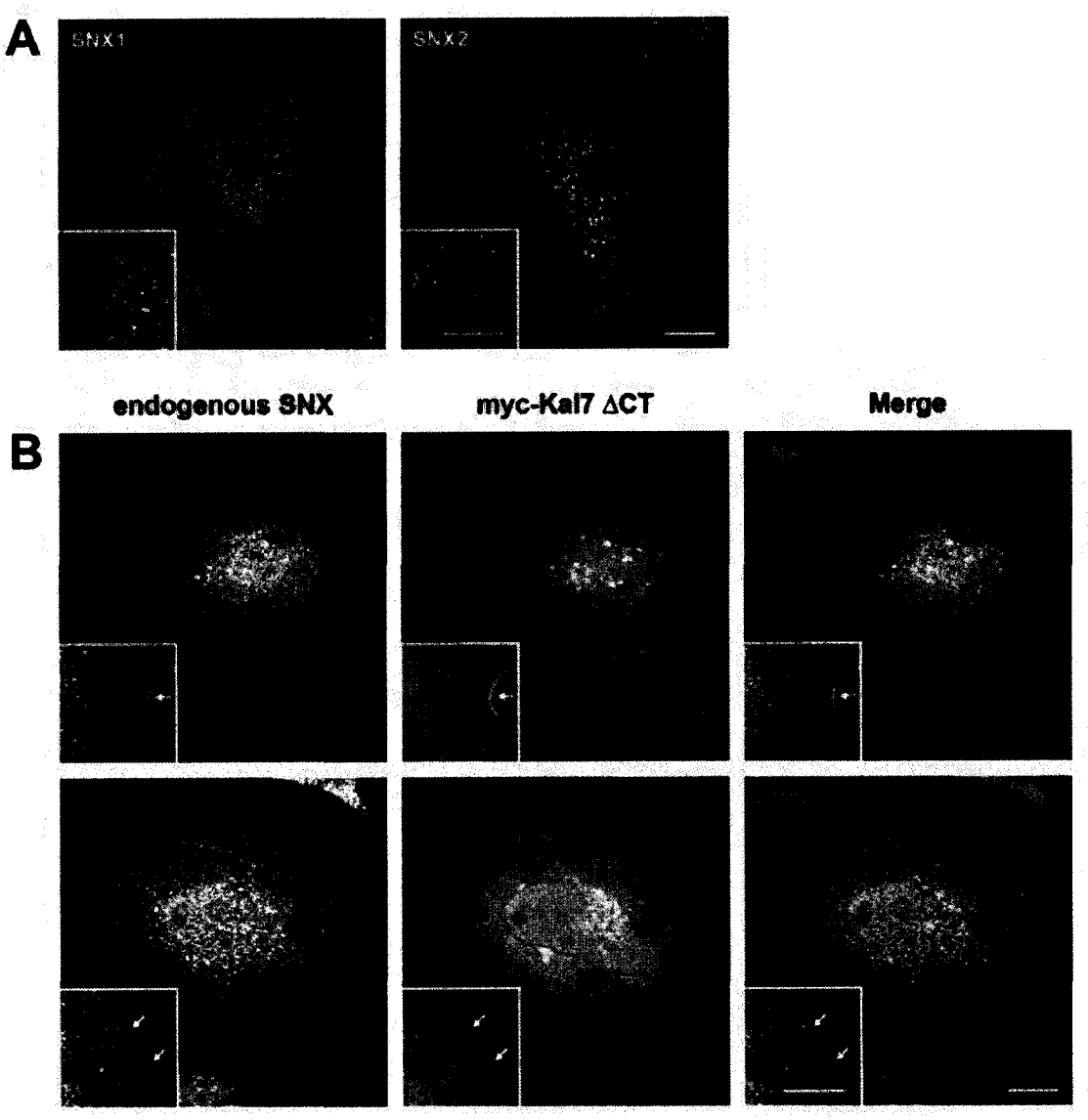
A
SNX1
SNX2
B
endogenous SNX
myc-Kal7 ΔCT
Merge

Induction of lamellipodia by Kal7 and SNX is a RhoG-dependent phenotype

Previous studies have shown that the DH/PH motif of Kal7 acts through both Rac1 and RhoG (May et al., 2002; Penzes et al., 2000). Since activation of either GTPase is known to promote formation of lamellipodia, the contribution of each GTPase to the phenotype observed upon co-expression of Kal7 and either SNX1 or SNX2 was determined. Wild-type Kal7 was co-expressed with SNX1 or SNX2 and either empty vector or dominant-negative $RhoA^{T19N}$, $Rac1^{T17N}$, $Cdc42^{T17N}$ or $RhoG^{T17N}$, and the effect of inactive GTPases on lamellipodia phenotype was assessed. In cells expressing Kal7 with either SNX1 or SNX2, co-expression of dominant-negative $RhoA^{T19N}$, $Rac1^{T17N}$ or $Cdc42^{T17N}$ had only a minor inhibitory effect on lamellipodia compared to empty vector (Figure 19 and Table I). Strikingly, co-expression of dominant-negative $RhoG^{T17N}$ inhibited lamellipodia in cells co-expressing Kal7 and either SNX1 or SNX2 by 7- to 8-fold. Thus, the lamellipodia phenotype induced by co-expression of Kal7 with SNX1 or SNX2 is likely to result from activation of RhoG, with only a minor, if any, contribution from Rac1 or other Rho GTPases.

CHO and HeLa cells express RhoG mRNA

While some studies have shown that RhoG is broadly expressed in tissues, others have suggested that it plays a particularly important role in cells from hematopoietic lineages and in neurons (May et al., 2002; Vigorito et al., 2004; Vincent et al., 1992). Although dominant-negative $RhoG^{T17N}$ was able to efficiently block Kal7- and SNX2-dependent lamellipodia formation, no information exists about the endogenous expression of RhoG in CHO cells. To confirm its expression, total RNA samples were

Figure 19: Effect of dominant-negative Rho GTPase expression on Kal7 and SNX-dependent lamellipodia formation. CHO cells were co-transfected with wild-type myc-Kal7, Flag-SNX1 or SNX2 and either empty vector (blue bars), $RhoA^{T19N}$ (red bars), $Rac1^{T17N}$ (green bars), $Cdc42^{T17N}$ (cyan bars) or $RhoG^{T17N}$ (purple bars). 48 hours later, Flag-SNX positive cells were scored for lamellipodia, with at least 300 cells counted per trial for each condition (mean ± SEM; n=4, *** $p<0.001$).

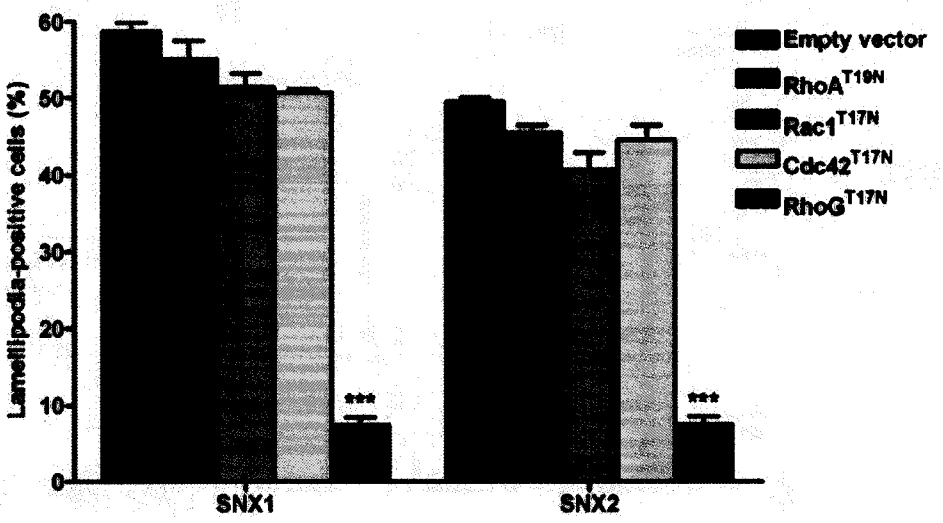
Lamellipodia-positive cells (%)
60
50
40
30
20
10
0
***
***
SNX1
SNX2
Empty vector
RhoA^{T19N}
Rac1^{T17N}
Cdc42^{T17N}
RhoG^{T17N}

Table I: Effect of dominant-negative Rho GTPases on lamellipodia induction in CHO cells co-expressing Kal7 and either SNX1 or SNX2[a]

	Kal7 + SNX1	Kal7 + SNX2
Empty vector	58.8 ± 1.1%	49.5 ± 0.5%
$RhoA^{T19N}$	55.1 ± 2.4%	45.5 ± 1.0%
$Rac1^{T17N}$	51.4 ± 1.8%	40.6 ± 2.3%
$Cdc42^{T17N}$	50.7 ± 0.5%	44.6 ± 1.9%
$RhoG^{T17N}$	7.4 ± 1.0% ***	7.5 ± 1.1% ***

[a] Values represent percentage of cells displaying lamellipodia (mean ± SEM; n=4)
*** $p<0.001$ compared to empty vector

purified from CHO and HeLa cells, and RhoG mRNA expression was confirmed by RT-PCR using primer pairs that recognize both hamster and human sequences for RhoG or GAPDH. Since the sequence of RhoG is similar to Rac1 and other Rac-related GTPases, primer sequences unique to RhoG were selected from the hypervariable region, which shows the weakest conservation among Ras family GTPases. Although the antisense primer selected for RhoG was highly similar to the related GTPase Rac2, the sense primer sequence was not conserved between these two GTPases, and only RhoG would be amplified by these primers in an RT-PCR reaction. BLAST searching of the primer sequences confirmed that the selected DNA sequences would not amplify other GTPases. For RT-PCR reactions, HeLa cells were used as a positive control, since they have previously been shown to express RhoG and because they were used in the above RNAi studies (van Buul et al., 2007; Yamaki et al., 2007). As shown in Figure 20, RhoG and GAPDH fragments were detectable in both CHO and HeLa cells, and amplified fragments corresponded well to the expected sizes of 204 bp and 311 bp, respectively. Furthermore, RhoG could not be amplified from control reactions lacking RNA or from samples that were not subjected to reverse transcription, confirming that amplification did not arise from contaminating genomic DNA. Thus, these data confirm that RhoG is indeed expressed at the mRNA level in CHO cells.

Lamellipodia formation does not require retromer function

Because of the well-documented role for SNX1 and SNX2 in retromer function, it is possible that Kal7-mediated lamellipodia formation depends on other components of the retromer complex. First, co-localization analysis was performed for Kal7, SNX1 and

Figure 20: Expression of RhoG mRNA in CHO and HeLa cells. Total RNA was isolated from CHO and HeLa cells and treated with DNAse I to remove contaminating genomic DNA. Samples were then subjected to RT-PCR with primer pairs that specifically recognize both hamster and human RhoG or GAPDH, and amplified products were resolved by electrophoresis. Control reactions in the absence of RNA (- RNA) or lacking the reverse transcriptase reaction (- RT) were performed to rule out sample contamination with exogenous RNA or genomic DNA.

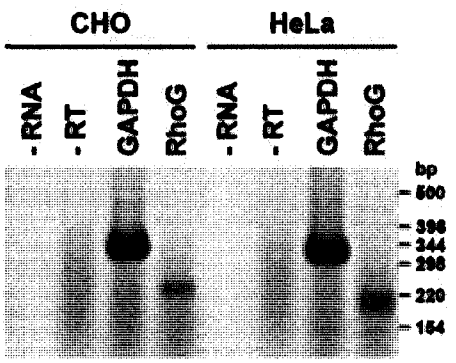
CHO
HeLa
- RNA
- RT
GAPDH
RhoG
- RNA
- RT
GAPDH
RhoG
bp
500
396
344
298
220
154

SNX2 with Vps35, the cargo-interacting subunit of retromer. In the absence of Kal7, Vps35 co-localized extensively with Flag-tagged SNX1 and SNX2 in CHO cells (Figure 21A). Conversely, myc-tagged Kal7 did not co-localize with Vps35. When wild-type Kal7 and either SNX1 or SNX2 were co-transfected in CHO cells, both SNX1 and SNX2 were still observed on Vps35-positive vesicular structures within the cell (Figure 21B). However, relocalization of either SNX to the plasma membrane in cells co-expressing Kal7 did not result in a concomitant redistribution of Vps35 to the plasma membrane. Thus, recruitment of SNX1 and SNX2 to the leading edge of lamellipodia is unlikely to require other subunits of retromer.

To further assess the potential role of retromer in Kal7 function, lentiviral shRNA infection was used to deplete HeLa cells of Vps35. In this way, it was possible to determine whether a loss of retromer function could impair lamellipodia formation by CMV-driven Kal7 ΔCT. Expression levels of the three members of the cargo-selective subcomplex of retromer have been closely associated, such that reducing levels of Vps26, Vps29 or Vps35 appears to de-stabilize other members of the subcomplex, without affecting expression of SNX proteins (Arighi et al., 2004; Vergés et al., 2004). Infection with a control GFP shRNA sequence had no effect on Vps35 expression, while infection with Vps35 shRNA targets caused a decrease in its expression by 80-90% without affecting levels of SNX1 or SNX2 (Figure 22A). When HeLa cells expressing CMV-driven Kal7 ΔCT were depleted of Vps35, 45.1 ± 2.1% of cells displayed lamellipodia or dorsal ruffles, which was statistically similar to mock- or GFP shRNA-infected cells (43.2 ± 1.8% and 42.9 ± 2.3%, respectively, $p>0.5$, Figure 22B), indicating that Kal7-mediated lamellipodia formation is likely retromer-independent.

Figure 21: Co-localization of SNX1 and SNX2 with Vps35. (A), CHO cells singly transfected with Flag-SNX1, Flag-SNX2 or wild-type myc-Kal7 (magenta) were stained with anti-Vps35 (green) prior to visualization by confocal microscopy. Arrows indicate regions of SNX1 or SNX2 co-localization with Vps35. (B), CHO cells co-expressing Flag-SNX1 or SNX2 and wild-type myc-Kal7 were stained with anti-Flag (magenta) and anti-Vps35 (green) antibodies. Scale bar = 10 μm (Inset scale bar = 5 μm).

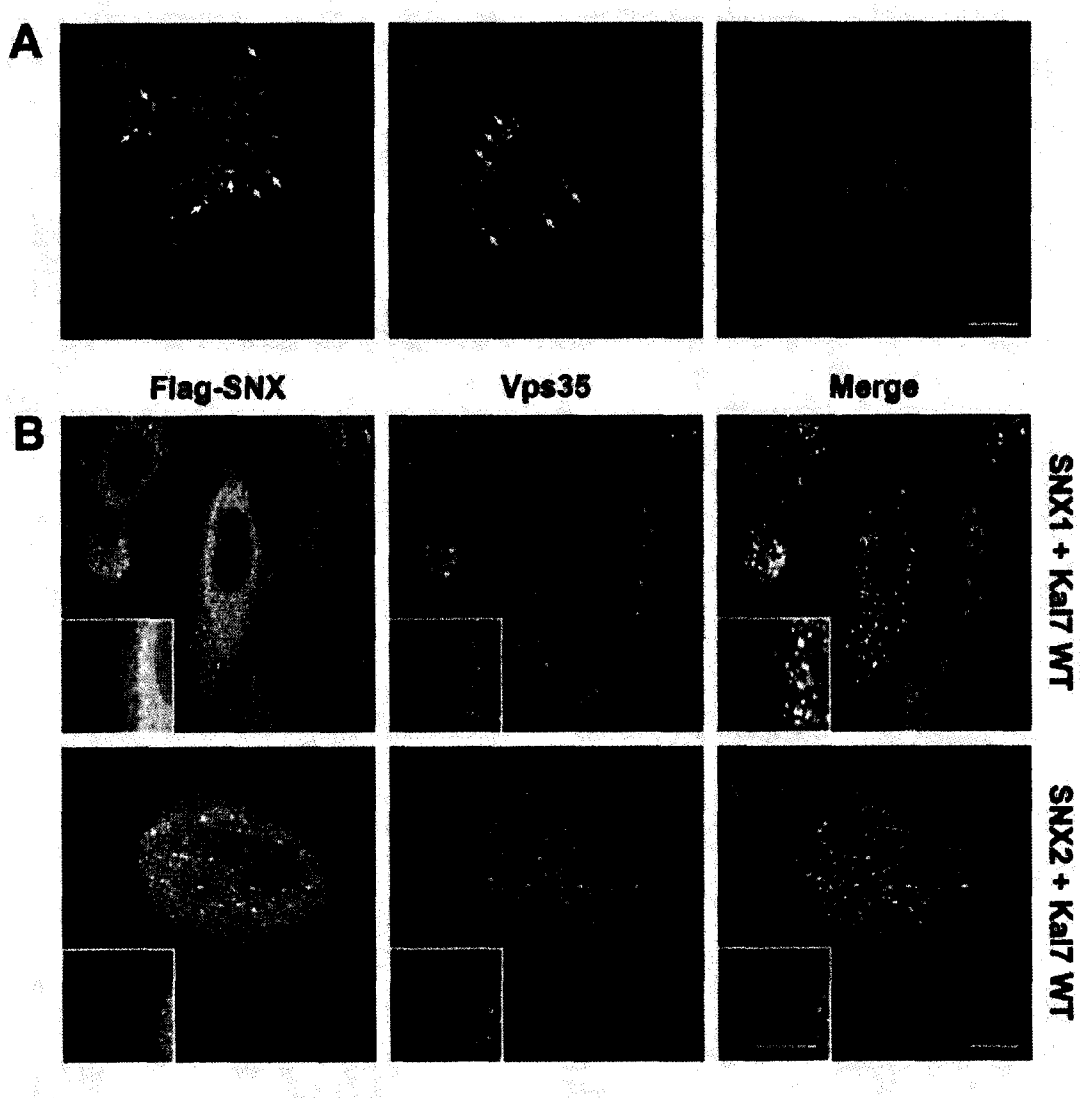
A
Flag-SNX
Vps35
Merge
B
SNX1 + Kal7 WT
SNX2 + Kal7 WT

Figure 22: Retromer independence of Kal7-dependent lamellipodia phenotype. (A), Confirmation of Vps35 depletion in HeLa cells 48 hours after infection. Equal sample loading was confirmed by detection with anti-tubulin antibodies, and quantification was performed by densitometric analysis. (B), HeLa cells expressing CMV-driven Kal7 ΔCT were depleted of Vps35 for 48 hours prior to fixation and scoring for lamellipodia or dorsal ruffles. For each condition, at least 50 cells were counted per trial (mean ± SEM; n=6).

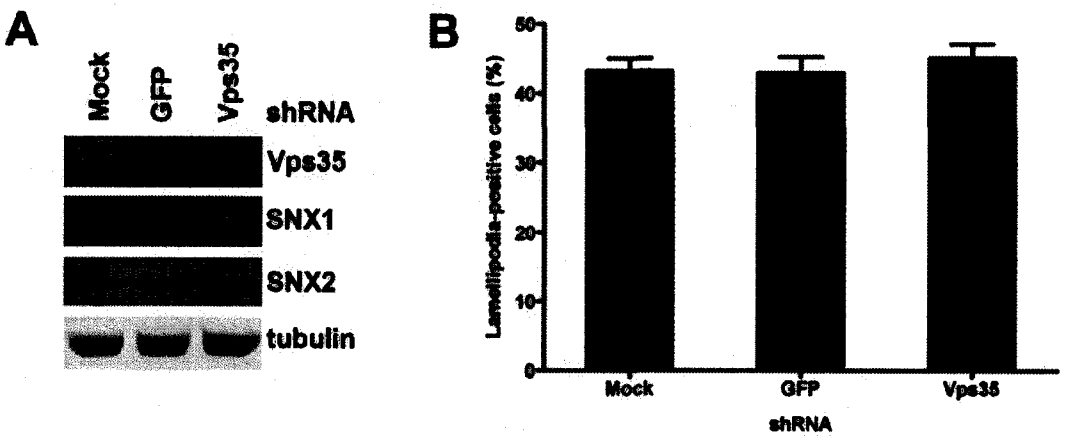
A
Mock
GFP
Vps35
shRNA
Vps35
SNX1
SNX2
tubulin
B
Lamellipodia-positive cells (%)
50
40
30
20
10
0
Mock
GFP
Vps35
shRNA

SNX1 and SNX2 interact specifically with inactive, GDP-bound RhoG

The BAR domains of Arfaptin-2 and Hob3p have previously been shown to interact with the small GTPases Rac1 and Cdc42, respectively (Coll et al., 2007; Shin and Exton, 2001; Tarricone et al., 2001). These findings raised the possibility that SNX1 or SNX2 could interact with Rho GTPases. For this purpose, recombinant, His_6-tagged SNX2 was used to pull down myc-tagged RhoA, Rac1, Cdc42 or RhoG from CHO cell extracts. Initially, the extracts were loaded with equal amounts the non-hydrolyzable guanine nucleotide analogs GDPβS and GTPγS to eliminate any potential bias toward inactive or active GTPase states. Under these conditions, RhoG specifically co-precipitated with SNX2, although a weak RhoG band could occasionally be seen in the absence of SNX2 (Figure 23A). Importantly, RhoA, Rac1 and Cdc42 did not associate with SNX2, and none of these Rho GTPases associated non-specifically with Ni-NTA beads, suggesting that this interaction is highly specific.

It is possible that the activation status of RhoG could influence its interaction with SNX2. For this purpose, identical myc-tagged RhoG cell extracts were loaded with either 200 μM GDPβS or 200 μM GTPγS to maintain the pool of RhoG in its inactive and active states, respectively. As determined by Ni-NTA pulldown, interaction of His_6-tagged SNX2 with RhoG strongly favored the inactive, GDP-bound state (Figure 23B). The preference for inactive RhoG was 8-fold greater than for activated RhoG, with 4.1 ± 1.0% of GDPβS-loaded RhoG and 0.5 ± 0.1% of GTPγS-loaded RhoG associated with SNX2 (Figure 23C).

To rule out a contribution of other cellular factors in the interaction of SNX2 with RhoG, direct interaction of recombinant SNX and Rho GTPases was tested using

Figure 23: Interaction of SNX1 and SNX2 with inactive, GDP-bound RhoG. (A), Detergent-solubilized extracts from CHO cells expressing myc-tagged Rho GTPases were loaded with 200 μM GDPβS and 200μM GTPγS. Lysates were then co-precipitated in the presence or absence of His_6-HA-Flag-SNX2 using Ni-NTA beads. (B), Extracts from CHO expressing myc-RhoG were subjected to co-precipitation with SNX2 as in panel *A*, but were loaded with either 200 μM GDPβS or 200μM GTPγS to determine the nucleotide preference of SNX2-RhoG interaction. Input lane (INP) corresponds to 10% of cell lysate used for pulldown. (C), Quantification of the preference of SNX2 for interaction with GDPβS-loaded RhoG. Band intensities were determined by densitometry, and the relative association with SNX2 was calculated as a percentage of input (mean ± SEM; n=3, * $p<0.05$). (D), Direct interaction of His_6-HA-Flag-SNX1 and SNX2 with TAP-myc-Rho GTPases was assayed using purified recombinant proteins. GDPβS-loaded Rho GTPases were immobilized on IgG-Sepharose beads for pulldown of SNX1 or SNX2, with empty IgG beads used as control. Input lane (INP) corresponds to 20% of total SNX used.

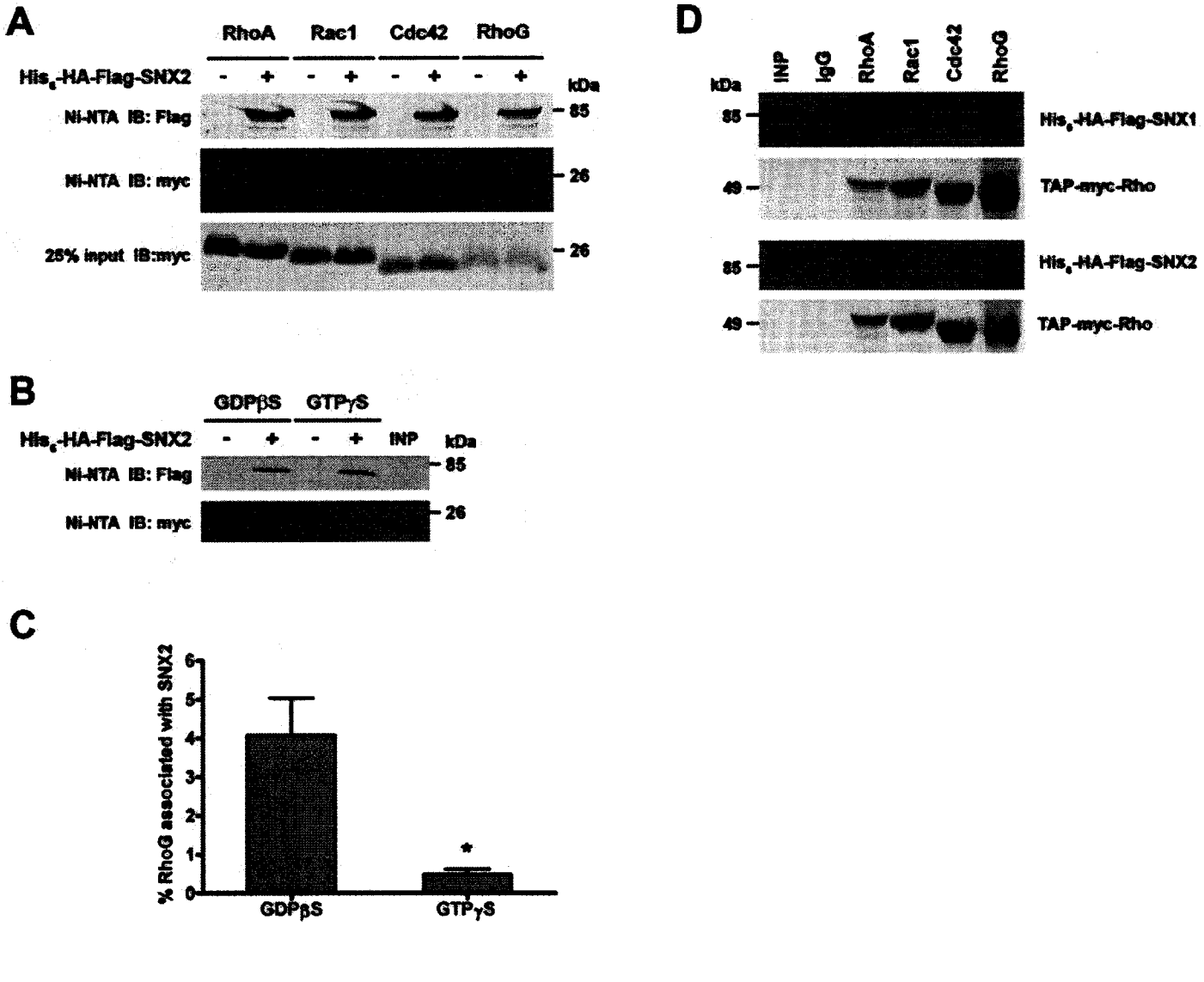
A
RhoA
Rac1
Cdc42
RhoG
His6-HA-Flag-SNX2
kDa
Ni-NTA IB: Flag
85
Ni-NTA IB: myc
26
25% input IB:myc
26
B
GDPβS
GTPγS
His6-HA-Flag-SNX2
INP
kDa
Ni-NTA IB: Flag
85
Ni-NTA IB: myc
26
C
% RhoG associated with SNX2
GDPβS
GTPγS
D
kDa
INP
IgG
RhoA
Rac1
Cdc42
RhoG
85
His6-HA-Flag-SNX1
49
TAP-myc-Rho
85
His6-HA-Flag-SNX2
49
TAP-myc-Rho

bacterially purified His_6-tagged SNX1 or SNX2 and prenylated, N-terminally TAP-tagged Rho GTPases isolated from yeast. The TAP tag consists of an IgG-binding protein A domain followed by a calmodulin-binding peptide, allowing for multiple steps of purification. When His_6-SNX1 or SNX2 were incubated with equimolar amounts of GDPβS-loaded RhoA, Rac1, Cdc42 or RhoG immobilized on IgG-Sepharose beads, both SNX1 and SNX2 were found to interact preferentially with RhoG compared to control IgG beads or other Rho GTPases (Figure 23D). Thus, both SNX1 and SNX2 can interact directly and specifically with inactive RhoG, and this interaction might occur *in vivo* as seen with pulldowns from cell extracts.

SNX2, but not SNX1, promotes Kal7-mediated neurite outgrowth in NGF-differentiated PC12 cells

Recent studies have reported a role for the Rac1- and RhoG-specific GEF domain of Kalirin and the closely related protein Trio in neurite outgrowth downstream of NGF and its receptor TrkA in PC12 cells (Chakrabarti et al., 2005; Estrach et al., 2002). Furthermore, overexpression of RhoG is known to bypass TrkA, and can promote neurite initiation in the absence of NGF (Katoh et al., 2000). Thus, interaction with Kal7 suggested a potential role for SNX1 and SNX2 in neurite initiation and outgrowth. To test this possibility, Kal7, SNX1 and SNX2 were overexpressed either alone or in combination in PC12 cells, and cells were differentiated for 72 hours in the presence of 10 ng/ml NGF-β, which is the biologically active subunit of NGF. Alternatively, undifferentiated cells were grown under the same conditions in the absence of NGF-β. Consistent with previous studies using Kalirin-5, a splice variant that generates an N-terminally truncated form of Kal7 (Chakrabarti et al., 2005; Johnson et al., 2000),

overexpression of wild-type Kal7 could not stimulate extension of neurites greater than one cell body in length in the absence of NGF. Furthermore, expression of either the GEF-inactive Kal7 ND/AA mutant, SNX1 or SNX2 was unable to stimulate extension of long neurites in the absence of NGF. The ability of transfected PC12 cells to form short cytoplasmic protrusions (less than one cell body in length) in the absence of NGF was assessed as a potential indicator of neurite initiation (Figure 24). In contrast to recently published findings (Xin et al., 2008), transfection of wild-type Kal7 did not enhance formation of cytoplasmic protrusions (33.0 ± 2.3% of cells) compared to monomeric red-fluorescent protein (mRFP)-transfected control cells (30.5 ± 0.5% of cells, Figure 25A), although short, filopodia-like extensions could occasionally be observed (Figure 24). Overexpression of SNX1 or SNX2 alone significantly increased the proportion of undifferentiated cells with cytoplasmic protrusions to 42.0 ± 2.0% and 43.9 ± 1.2%, respectively. Similarly, co-transfection of wild-type Kal7 with SNX1 and SNX2 resulted in an increase in the number of cells with short neurites (to 39.7 ± 1.4% and 42.2 ± 0.5%, respectively), which was significant compared to cells expressing Kal7 alone. Interestingly, expression of inactive Kal7 ND/AA alone did not affect spontaneous neurite formation (34.0 ± 1.8% of cells), while co-expression with SNX1 or SNX2 still gave an increase in cells with neurites, even though these values did not reach significance (39.5 ± 3.1% and 39.1 ± 2.6%, respectively, $p>0.1$ compared to Kal7 ND/AA alone). Overall, the incidence of spontaneous protrusions in SNX1- or SNX2-expressing cells was comparable when these cells were co-transfected with empty vector, wild-type or GEF-inactive Kal7. Given that exogenous Kal7 could not alter the effect of

Figure 24: Formation of cytoplasmic protrusions in SNX-overexpressing PC12 cells. PC12 cells were transfected with empty vector (control), myc-Kal7 wild-type (WT) or ND/AA, or Flag-SNX1 or SNX2. Additionally, cells were co-transfected with mRFP for visualization. Small, filopodia-like structures are indicated by asterisks, while cytoplasmic protrusions are indicated with arrows. Scale bar = 10 μm.

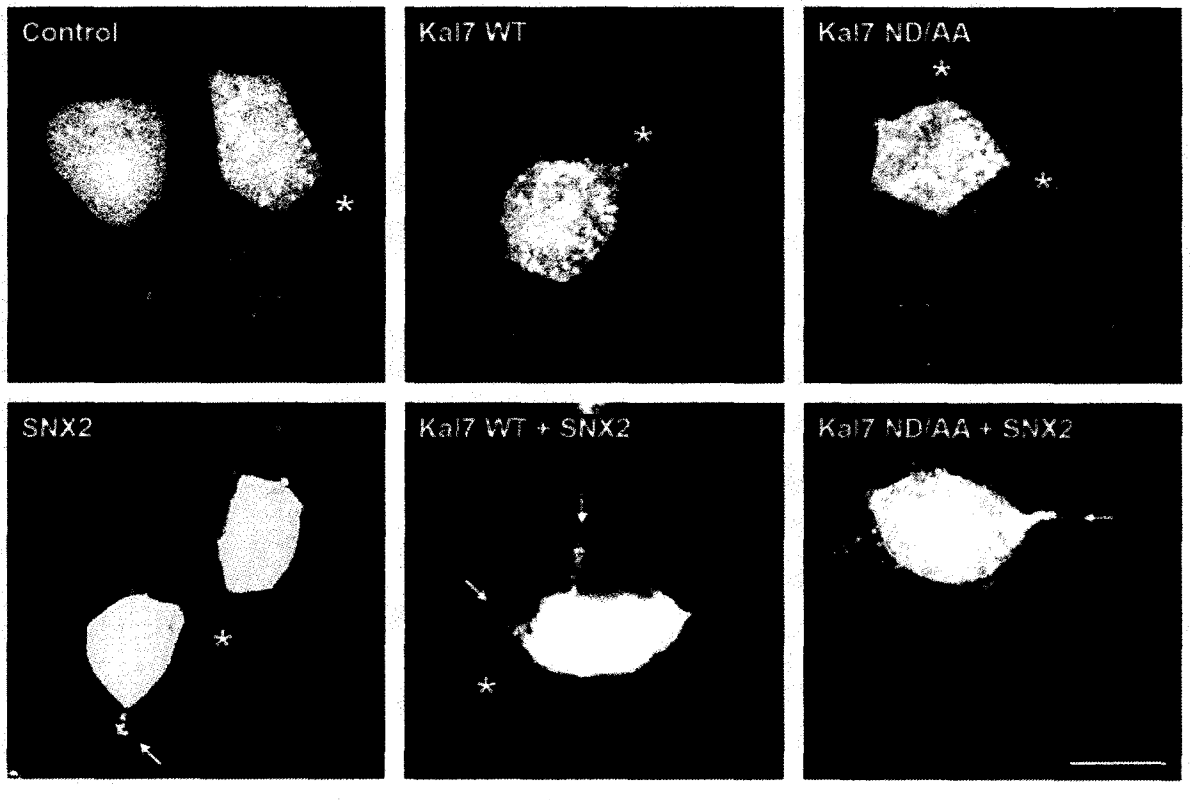
Control
Kal7 WT
Kal7 ND/AA
SNX2
Kal7 WT + SNX2
Kal7 ND/AA + SNX2

Figure 25: Effect of Kal7 and SNX overexpression on neurite initiation and outgrowth. PC12 cells expressing mRFP in the absence (control) or presence of Kal7 WT or Kal7 ND/AA were co-transfected with empty vector (black bars), SNX1 (grey bars) or SNX2 (white bars). Cells were differentiated for 3 days in the absence (panel *A*) or presence (panel *B*) of 10 ng/ml NGF-β. (A), At least 300 cells per condition were scored for the presence of neurites of any length as an indication of NGF-independent neurite initiation. (B), NGF-differentiated cells were scored for the presence of primary neurites greater than one cell body in length. For each trial, at least 100 cells were measured per condition from blinded samples (mean ± SEM; n=3, * $p<0.05$, ** $p<0.01$).

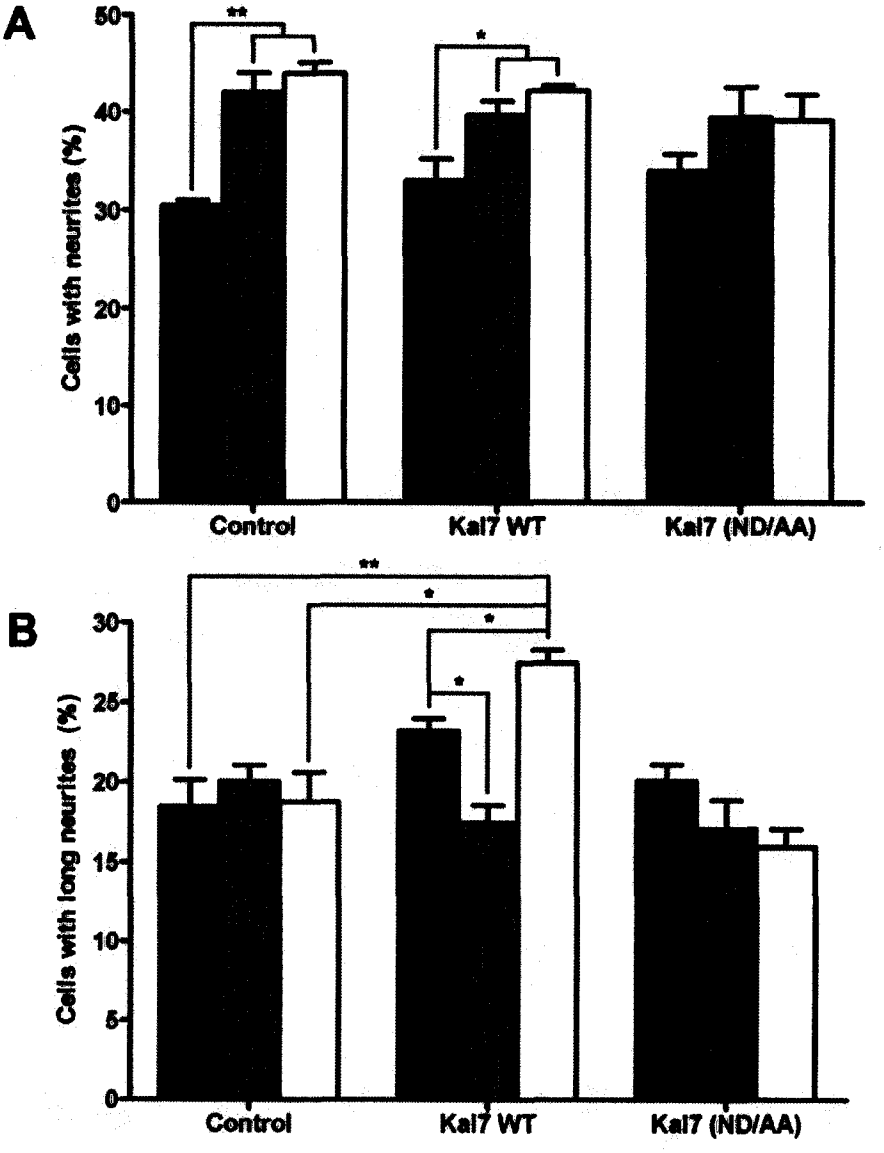
A
Cells with neurites (%)
50
40
30
20
10
0
**
*
Control
Kal7 WT
Kal7 (ND/AA)
B
Cells with long neurites (%)
30
25
20
15
10
5
0
**
*
*
*
Control
Kal7 WT
Kal7 (ND/AA)

SNX overexpression, these results suggest that the observed SNX effect in undifferentiated cells is independent of Kal7.

Next, the contribution of SNX1 and SNX2 to Kal7-mediated neurite extension in response to a low dose of NGF-β was examined. While 18.4 ± 1.7% of cells transfected with empty vector developed primary neurites greater than one cell body in length, transfection with Kal7 resulted in 23.2 ± 0.8% of cells with long neurites (Figure 25B). Although a previous study showed that overexpression of a truncated Kal7 fragment significantly increased the incidence of long neurites compared to control cells (Chakrabarti et al., 2005), the observed values in the present study were not statistically significant under the conditions used ($p>0.05$). Overexpression of SNX1 or SNX2 resulted in 20.0 ± 1.0% and 18.8 ± 1.8% of cells with long neurites, respectively, which was similar to values seen for empty vector cells. Notably, co-expression of wild-type Kal7 with SNX2 promoted extension of long neurites in 27.5 ± 0.8% of cells, which was significantly greater than values seen for cells transfected with empty vector, Kal7 or SNX2 alone. In contrast, co-expression of Kal7 with SNX1 resulted in 17.5 ± 1.1% of cells with long neurites. Although this value was similar to those seen for expression of empty vector or SNX1 alone, it corresponds to a significant decrease compared to expression of Kal7 alone. When cells were transfected with Kal7 ND/AA either alone or in combination with SNX1 or SNX2, the incidence of long neurites was similar to empty vector in all cases (20.1 ± 1.0%, 17.5 ± 1.1% and 15.9 ± 1.1% of cells, respectively). Taken together, these results suggest that overexpression of SNX1 or SNX2 can stimulate spontaneous formation of cytoplasmic protrusions, and that SNX2 enhances Kal7 GEF-dependent neurite extension in response to NGF.

Chapter II: VAPs and FFAT regulate lateral diffusion and anterograde transport of ER cargo

Results

FFAT rescues VAPB P56S-mediated ER aggregation

Because VAPA and VAPB are known to reside in the ER (Skehel et al., 2000; Soussan et al., 1999), co-localization analysis was performed to determine the effect of the P56S mutation on subcellular distribution of VAPs. Wild-type VAPA and VAPB both showed extensive co-localization with the ER marker calreticulin in CHO cells, consistent with the established distribution of these proteins (Figure 26). When P56S mutant VAPA and VAPB were expressed in CHO cells, both proteins retained ER localization. Expression of VAPB P56S resulted in formation of large intracellular aggregates, consistent with other studies (Kanekura et al., 2006; Nishimura et al., 2004; Teuling et al., 2007; Tsuda et al., 2008). However, in contrast to these studies, the VAP-containing aggregates were also immunoreactive for calreticulin, suggesting that these structures are part of the ER. Furthermore, VAPB P56S-expressing cells displayed a nearly complete collapse of calreticulin-containing reticular ER structures. Interestingly, the analogous P56S mutation in VAPA did not result in collapse of the ER or formation of aggregates, even though the MSP domains of VAPA and VAPB are highly similar.

To determine whether a FFAT sequence could alter the ER distribution VAPs, amino acid residues 347-468 of rabbit OSBP, which contains the MSP domain-interacting FFAT motif but lacks other functional domains, were co-expressed with Flag-tagged VAPs. Although myc-tagged FFAT did not noticeably affect ER structure or co-localization of calreticulin with VAPA WT, VAPA P56S or VAPB WT, its co-expression

Figure 26: ER localization of WT and P56S VAPA and VAPB. CHO cells were transfected with either Flag-tagged WT or P56S mutant VAPA or VAPB in the absence of FFAT (top row) or along with FFAT (bottom row). Proteins were detected with anti-Flag (magenta) and anti-Calreticulin (Calr, green) antibodies, and visualized by confocal microscopy. Scale bar, 10 μm.

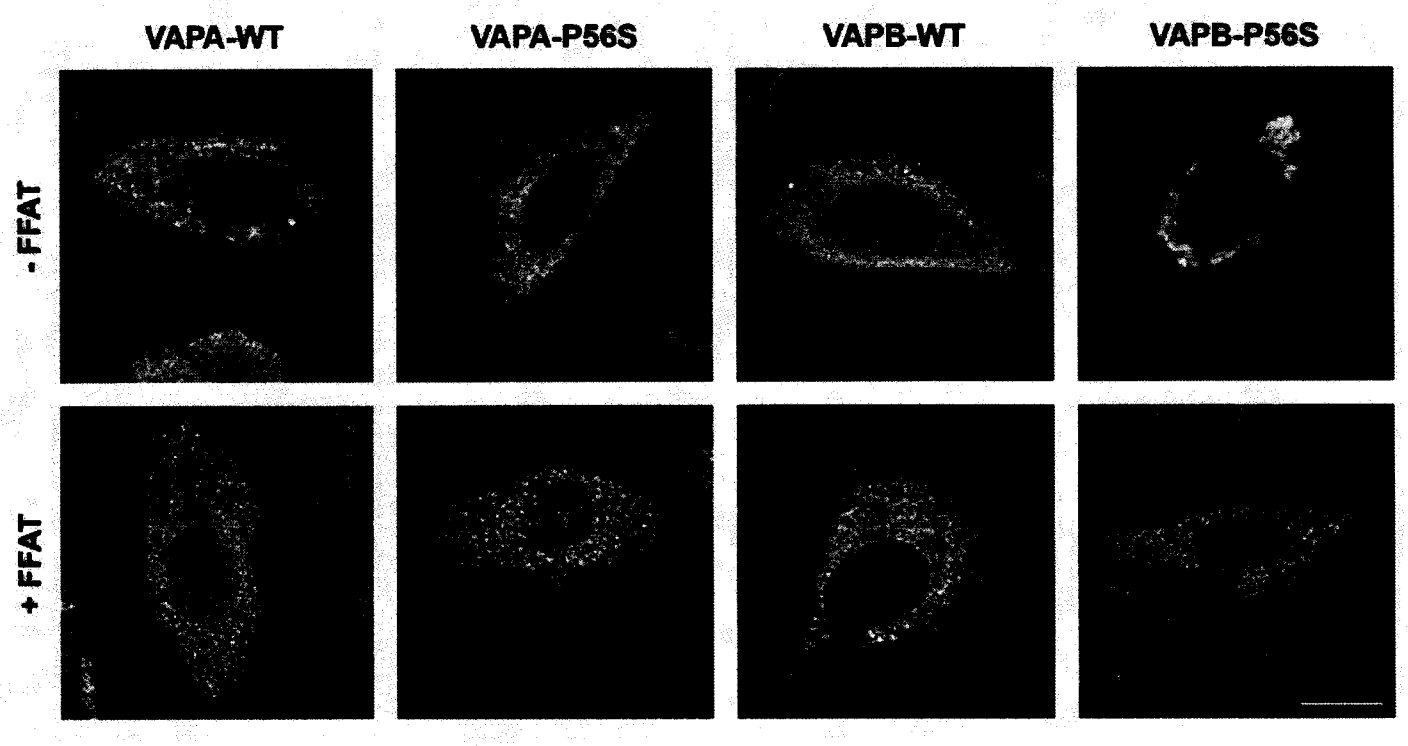
VAPA-WT
VAPA-P56S
VAPB-WT
VAPB-P56S
- FFAT
+ FFAT

with VAPB P56S caused a pronounced improvement in the ER aggregate phenotype (Figure 26, lower panel). While VAPB P56S retained co-localization with calreticulin when co-expressed with myc-FFAT, ER structures displayed a characteristic reticular pattern that was indistinguishable from untransfected cells. Thus, co-expression of FFAT appears to disperse VAPB P56S aggregates, or might prevent aggregation of mutant proteins.

In order to further characterize the ER localization of VAP isoforms, CHO cells expressing Flag-VAPA and VAPB were also stained with Sar1, a small GTPase required for COPII coat assembly and vesicle budding from ER exit sites (d'Enfert et al., 1991). As shown in Figure 27, Sar1 failed to co-localize with wild-type or mutant VAPA or VAPB, suggesting that VAPs are not enriched at ER exit sites. Interestingly, Sar1 was excluded from VAPB P56S-containing aggregates, suggesting that these structures might be deficient in ER-to-Golgi transport. When myc-FFAT was co-expressed, VAP failed to co-localize with Sar1, indicating that FFAT does not affect localization to ER exit sites.

A previous study showed that motor neurons expressing VAPB P56S developed a dispersed Golgi morphology, although epithelial cells retained an intact Golgi complex (Teuling et al., 2007). The above results (Figure 26) demonstrate that calreticulin-containing ER aggregates are often found in the perinuclear region. To rule out the possibility that these structures also contained Golgi markers or that Golgi morphology was altered, co-localization with the Golgi marker Mannosidase II (ManII) was assessed. Overexpression of wild-type or mutant VAPA or VAPB did not significantly alter Golgi morphology in CHO cells, either in the presence or absence of myc-FFAT (Figure 28).

Figure 27: Subcellular localization of WT and P56S VAPA and VAPB. CHO cells were transfected with either WT or P56S mutant Flag-VAP in the absence (top row) or presence (bottom row) of FFAT. Cells were stained with anti-Flag (magenta) to detect VAPs and anti-Sar1 (green) antibodies to detect ER exit sites, and were visualized by confocal microscopy. Scale bar, 10 μm.

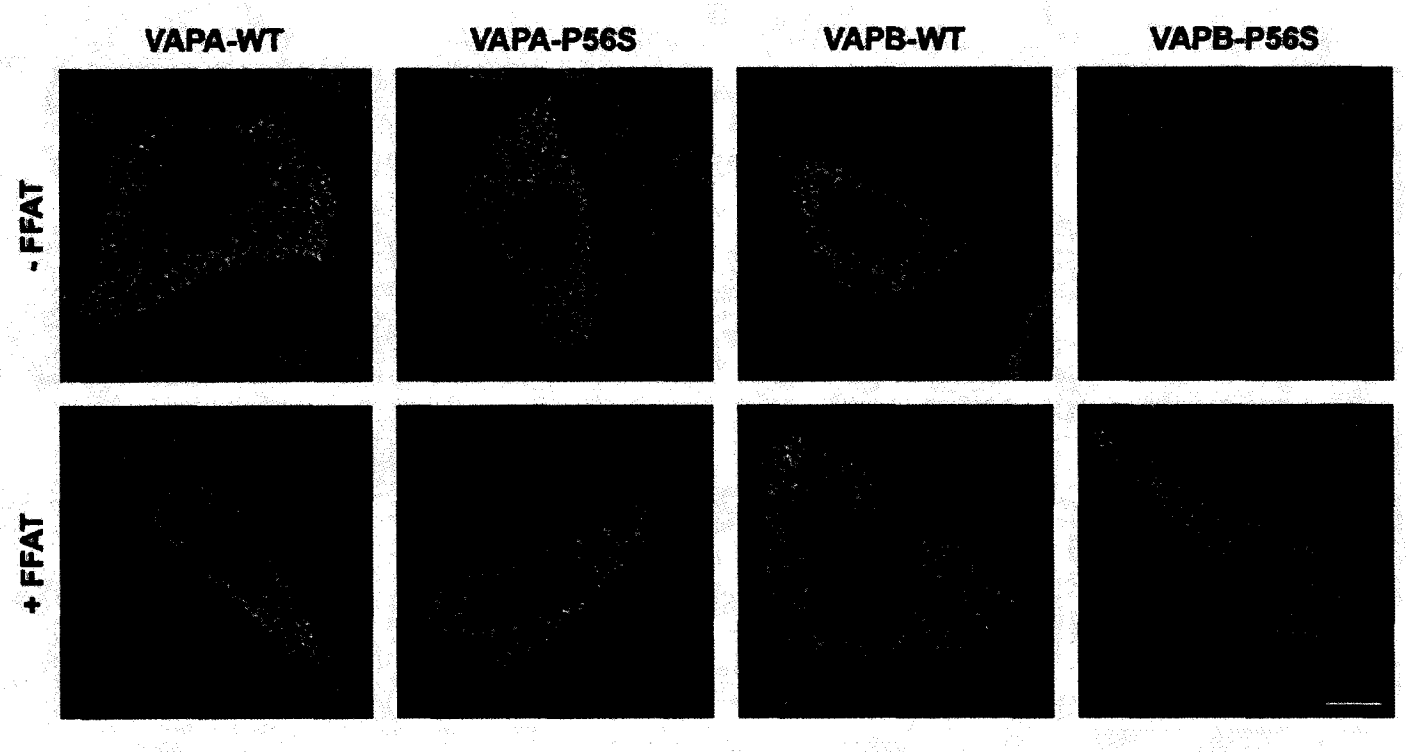
VAPA-WT
VAPA-P56S
VAPB-WT
VAPB-P56S
- FFAT
+ FFAT

Figure 28: Subcellular localization of WT and P56S VAPA and VAPB. CHO cells were transfected with either WT or P56S mutant Flag-VAP in the absence (top row) or presence (bottom row) of FFAT. Cells were then stained with anti-Flag (magenta) to detect VAPs and anti-Mannosidase II (ManII, green) to detect the Golgi complex, and were visualized by confocal microscopy. Scale bar, 10 μm.

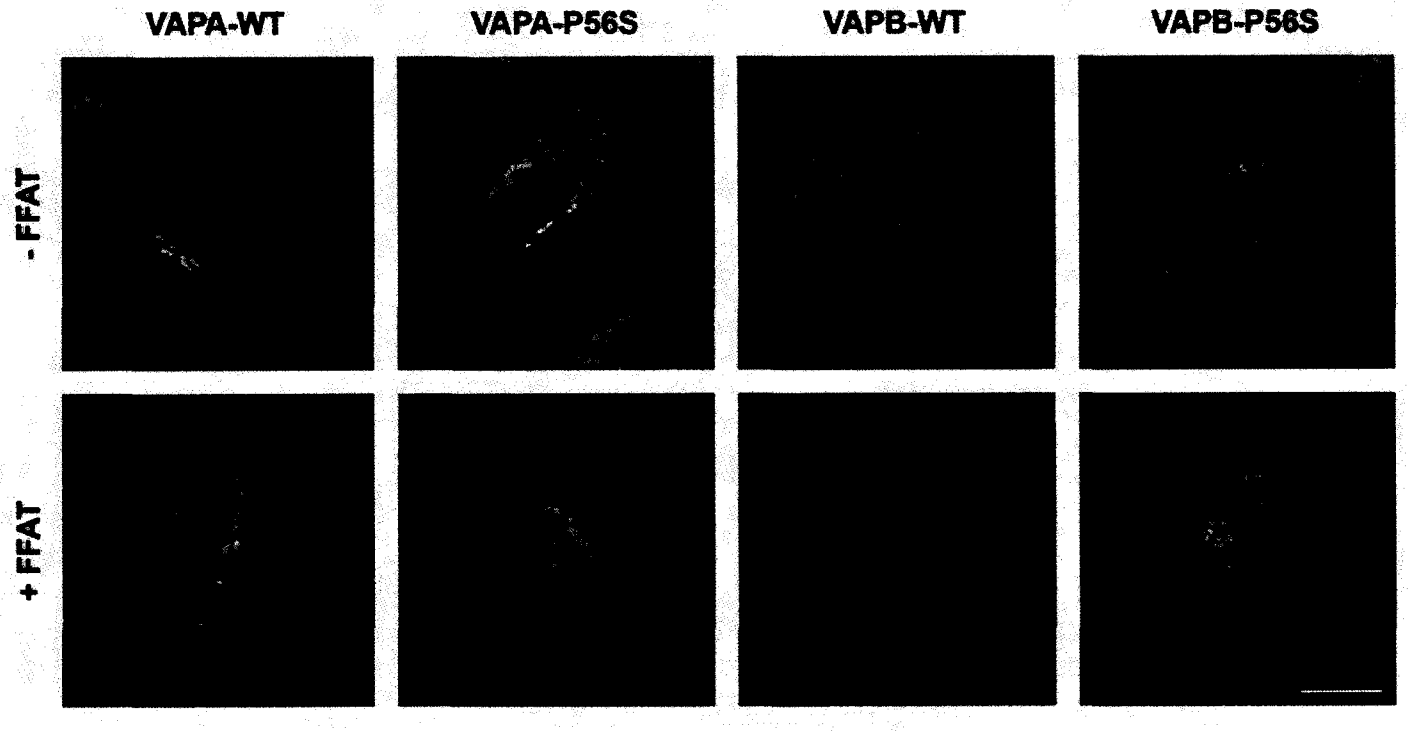
VAPA-WT
VAPA-P56S
VAPB-WT
VAPB-P56S
- FFAT
+ FFAT

Also, ManII failed to co-localize with wild-type and mutant VAPs, confirming that VAPB P56S-containing aggregates are distinct from the Golgi complex.

VAP overexpression does not affect microtubule organization or Golgi morphology

Overexpression of proteins involved in ER structure, such as the reticulon family, or in ER-microtubule interaction, such as CLIMP-63 and p180, often results in bundling and rearrangement of both ER and microtubule networks (Klopfenstein et al., 1998; Ogawa-Goto et al., 2007; Voeltz et al., 2006). Additionally, dVAP-33, the *Drosophila* orthologue of VAPA, has been shown to alter microtubule organization when overexpressed in neurons (Pennetta et al., 2002). To determine whether overexpression of VAPA or VAPB could alter the structure of the microtubule network in epithelial cells, CHO cells were transfected with Flag-VAP and co-stained with anti-tubulin antibodies. As shown in Figure 29, the microtubule network remained intact and showed no obvious signs of bundling or reorganization in cells expressing wild-type or P56S mutant VAPA or VAPB. Furthermore, co-expression of myc-FFAT had no effect on microtubule organization. VAP isoforms showed only partial co-localization with microtubules, as reported previously (Kaiser et al., 2005), although VAP-containing ER tubules could occasionally be seen in close proximity to microtubule structures.

Overexpression of VAPA, but not VAPB, delays ER-to-Golgi transport of VSVG^{ts045}

Transport of a temperature-sensitive mutant of the G glycoprotein of vesicular stomatitis virus (VSVG^{ts045}) was monitored to determine the effect of VAP overexpression on anterograde transport of membrane proteins from ER to Golgi. At

Figure 29: Subcellular localization of WT and P56S VAPA and VAPB. CHO cells were transfected with either WT or P56S mutant Flag-VAP in the absence (top row) or presence (bottom row) of FFAT. Cells were then stained with anti-Flag (magenta) to detect VAPs and anti-alpha tubulin (Tub, green) to detect microtubules, and were visualized by confocal microscopy. Scale bar, 10 μm.

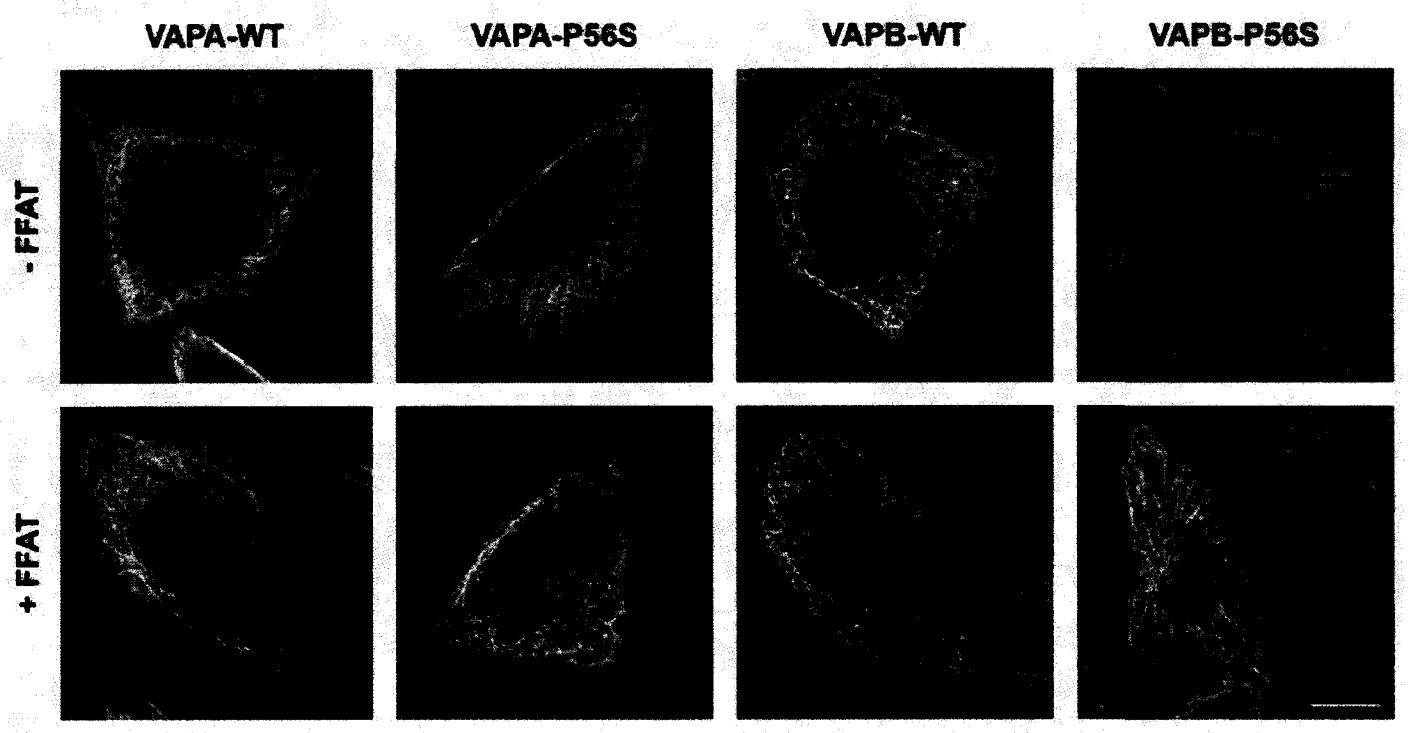
VAPA-WT
VAPA-P56S
VAPB-WT
VAPB-P56S
- FFAT
+ FFAT

temperatures of 37°C or lower, VSVG^{ts045} is synthesized at the ER, and is transported through the Golgi complex to the plasma membrane. However, when cells are incubated at 42°C, VSVG^{ts045} misfolds and remains in the ER, but can fold correctly and exit the ER upon shifting to the permissive temperature (Bergmann et al., 1981; Gallione and Rose, 1985). It is thus possible to accumulate VSVG^{ts045} in the ER and chase it through the secretory pathway. Furthermore, nascent VSVG acquires N-linked glycosylation in the ER, where high-mannose moieties are added to asparagine residues (Gabel and Bergmann, 1985). Once the protein reaches the Golgi complex, mannosidase enzymes trim mannose residues prior to addition of complex oligosaccharide chains. Once the mannose residues have been trimmed, the protein becomes resistant to cleavage with Endo H, which cleaves high-mannose but not complex oligosaccharide chains. Resistance to Endo H can be used to biochemically detect glycoproteins that have reached the Golgi complex, since proteins that are sensitive or resistant to Endo H digestion can be resolved by SDS-PAGE.

To examine the effect of VAP overexpression on ER-to-Golgi trafficking, CHO cells were co-transfected with myc-tagged VSVG^{ts045} and either wild-type or mutant VAPA or VAPB. VSVG was then accumulated in the ER at 42°C for 6 h, which was sufficient to allow clearance of previously synthesized protein (Gougeon et al., 2002). Cells were then rapidly shifted to 37°C and harvested at various times before digestion of solubilized proteins with Endo H. In control cells, VSVG rapidly acquired Endo H resistance within 30 min of shifting cells back to 37°C, indicating its transport to the Golgi (Figure 30). In sharp contrast, ER-to-Golgi transport was severely delayed in cells overexpressing wild-type or mutant VAPA, where VSVG remained Endo H-sensitive

Figure 30: Effect of VAP overexpression on transport of VSVG^{ts045} from ER to Golgi. CHO cells co-expressing VSVG^{ts045}-myc3 and either empty vector or wild-type, ΔN, or P56S VAPA or VAPB were incubated at 42°C to trap VSVG in the ER. Cycloheximide was added to cells, and the temperature was then shifted to 37°C for the indicated time (in minutes) before harvesting cells. Membranes were then solubilized, and samples were treated overnight in the absence (C) or presence of Endo H. Proteins were then resolved by SDS-PAGE and detected by Western immunoblot with anti-myc antibodies. The lower band corresponds to ER-localized, Endo H-sensitive VSVG (open arrowheads), while the upper band represents Golgi and/or post-Golgi, Endo H-resistant VSVG (closed arrowheads).

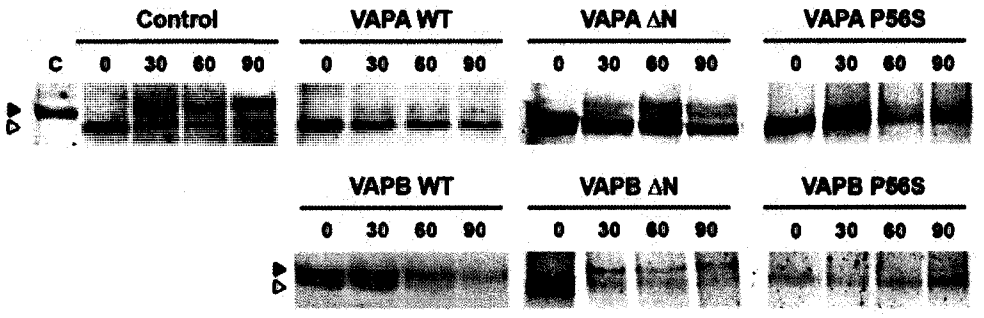
Control
VAPA WT
VAPA ΔN
VAPA P56S
C
0
30
60
90
VAPB WT
VAPB ΔN
VAPB P56S

over the 90 min time course. Deletion of the N-terminal MSP domain of VAPA (VAPA ΔN) was able to partially rescue ER-to-Golgi transport, suggesting that the MSP domain may play a role in regulating trafficking. Overexpression of wild-type or ΔN VAPB did not seem to have an effect on VSVG transport (Amarilio et al., 2005) (Figure 30, lower panel). Although a population of VSVG in VAPB WT experiments remained resistant to Endo H digestion immediately after shifting cells back to 37°C, the Endo H-sensitive fraction steadily decreased over the time course, indicating that the trapped protein could exit the ER. It is possible that the loss of Endo H-sensitive VSVG in VAPB-overexpressing cells was due to protein degradation. However, the persistence of detectable GFP- or YFP-tagged VSVG in post-ER structures at 90 min suggests that VSVG does indeed transit out of the ER (Amarilio et al., 2005; Prosser et al., 2008). When VAPB P56S was overexpressed, VSVG remained sensitive to EndoH, suggesting that protein transport out of aggregates is impaired. Taken together, these results suggest that VAPA and VAPB have differential effects on transport of membrane proteins from ER to Golgi, or that they might regulate transport of different cargoes.

Overexpression of VAPA inhibits lateral diffusion of membrane-associated ER cargo

Based on the known interaction of VAPs with microtubules and the presence of a transmembrane domain, VAPA could block VSVG transport by creating immobile obstacles within the ER membrane. Overexpression of VAPA would increase the level of microtubule-associated ER transmembrane protein, which might block lateral diffusion of cargo into ER exit sites and prevent their subsequent incorporation into COPII-coated vesicles. To test this possibility, fluorescence recovery after photobleaching (FRAP) of

cells expressing VSVG^{ts045}-GFP was used to monitor membrane cargo dynamics. After accumulation of VSVG in the ER at 42°C, a region of the ER in the cell periphery was photobleached, and recovery was monitored over a 10 minute time period. In control cells, VSVG^{ts045}-GFP recovered rapidly into the bleached area, approaching a plateau at approximately 70% of the pre-bleach intensity within 5-6 minutes (Figure 31, panels A and B). After 10 minutes at 32°C, VSVG fluorescence in the ER decreased rapidly, consistent with exit from the ER and accumulation within the Golgi complex by 15 min (Gougeon et al., 2002). Overexpression of wild-type or P56S mutant VAPA strongly inhibited recovery of VSVG into the bleached area compared to control cells by approximately 2- and 4-fold, respectively. Thus, these data are consistent with an inhibitory effect for VAPA overexpression on lateral diffusion of membrane cargo. Importantly, the block in VSVG transport due to VAPA overexpression was not a result of defective protein folding, since staining with a conformation-specific antibody showed that properly folded VSVG remained in the ER (Prosser et al., 2008). In agreement with previous studies showing that VAPB did not affect anterograde transport of VSVG (Amarilio et al., 2005), VSVG^{ts045}-GFP showed rapid recovery after photobleaching in cells overexpressing VAPB. The recovery curve of VSVG in VAPB-expressing cells was indistinguishable from recovery in control cells, with the total recovery reaching a plateau at ~70% of the pre-bleach signal within 5-6 minutes. Interestingly, these values are consistent with the total recovery reported for FRAP of VAPB-GFP (Teuling et al., 2007), suggesting that VAPB does not create immobile obstacles in the ER membrane. When VAPB P56S was expressed, it was not possible to perform FRAP of VSVG in reticular ER structures, since VSVG^{ts045} accumulated in perinuclear ER aggregates

Figure 31: Effect of VAP overexpression on FRAP of VSVG^{ts045}-GFP. Cells co-expressing VSVG^{ts045}-GFP and either empty vector, wild type or P56S mutant VAPA or VAPB were incubated at 42°C to trap VSVG in the ER. Cells were treated with cycloheximide before shifting to 32°C, and a portion of the peripheral ER was photobleached. Recovery was monitored every 20 s for 10 min. (A), Confocal images showing VSVG recovery over the first 5 min after photobleaching. Yellow boxes correspond to the bleached region. (B), FRAP recovery curves for cells transfected with control empty vector (blue ●), VAPA-WT (red ▼), VAPA-P56S (green ■), VAPB-WT (orange ▲) or VAPB-P56S (purple ♦). Values are presented as means ± SEM from at least three representative experiments (* $p<0,05$, ** $p<0.01$, *** $p<0.001$ for all time points compared to control).

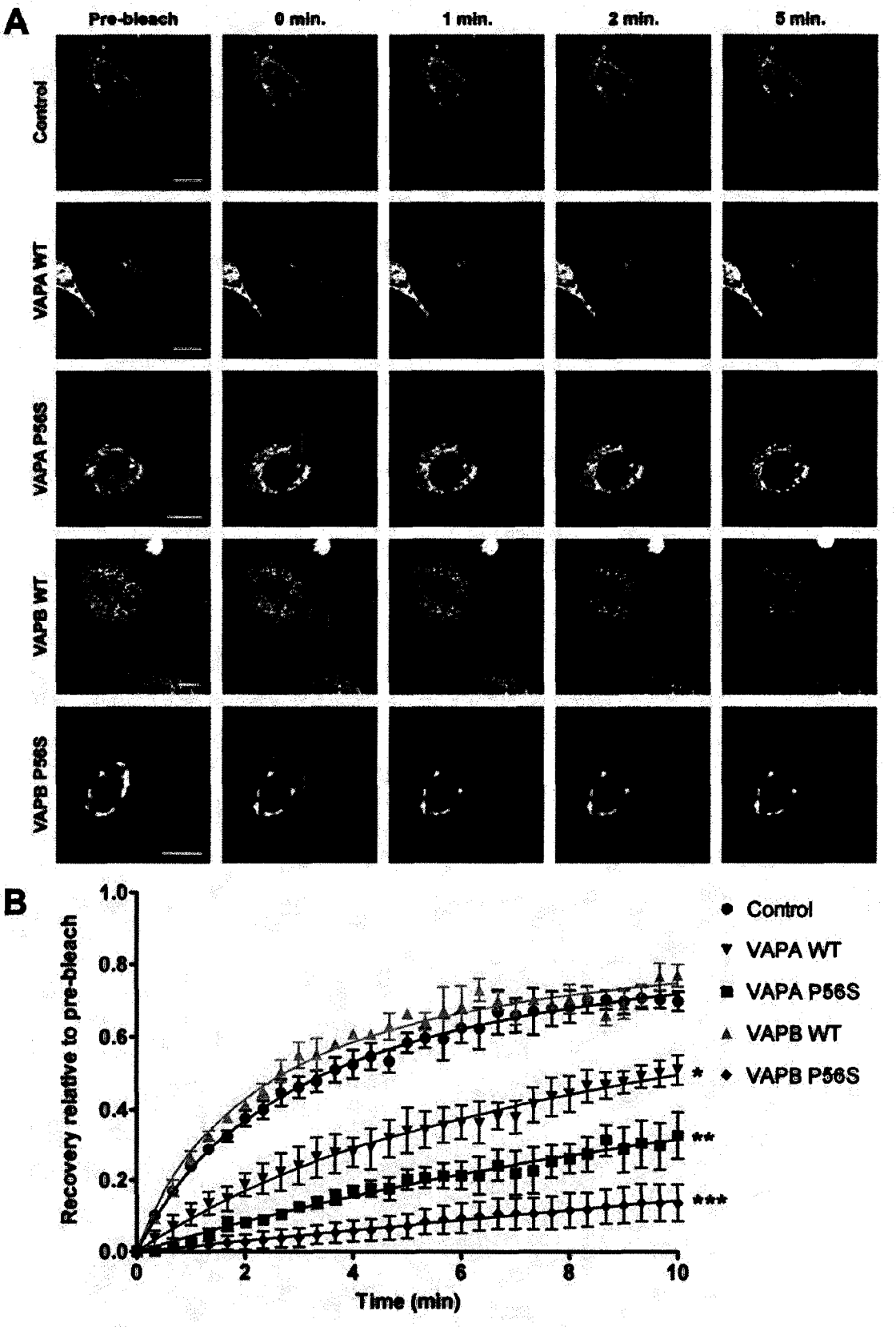
A
Pre-bleach
0 min.
1 min.
2 min.
5 min.
Control
VAPA WT
VAPA P56S
VAPB WT
VAPB P56S
B
Recovery relative to pre-bleach
1.0
0.8
0.6
0.4
0.2
0.0
0
2
4
6
8
10
Time (min)
Control
VAPA WT
VAPA P56S
VAPB WT
VAPB P56S
*
**
***

(Figure 31A). Instead, a portion of these aggregates was photobleached to determine whether VSVG could diffuse across aggregates. Within aggregates, lateral diffusion of $VSVG^{ts045}$-GFP was almost completely blocked, with less than 15% recovery relative to pre-bleach values (Figure 31B). Thus, the impaired VSVG transport observed in the Endo H assay is likely to arise from differential effects of VAPA and VAPB on lateral diffusion through the ER membrane.

FFAT rescues VAPA-mediated lateral diffusion defects

To determine whether co-expression of a FFAT motif could rescue the observed block in lateral diffusion resulting from VAPA overexpression, FRAP experiments were also conducted in which myc-FFAT was co-transfected. Under empty vector control conditions, $VSVG^{ts045}$-GFP recovery approached a plateau at approximately 60-65% of pre-bleach intensity, indicating that exogenous FFAT expression did not significantly alter the kinetics of VSVG lateral diffusion compared to experiments in the absence of FFAT (Figure 32, panels A and B). Co-expression of FFAT completely restored lateral diffusion of VSVG in cells overexpressing wild-type or P56S mutant VAPA, and recovery of VSVG was similar to control cells expressing myc-FFAT. Thus, FFAT might be able to relieve the formation of immobile obstacles. Given that wild-type VAPB did not adversely affect VSVG lateral diffusion in the absence of FFAT, co-expression of myc-FFAT was not expected to alter the ability of VSVG to diffuse through the ER membrane. Indeed, co-expression of FFAT with VAPB WT had no effect on recovery of VSVG, which was indistinguishable from empty vector in the presence of FFAT or from VAPB in the absence of FFAT. When FFAT was co-expressed with

Figure 32: Effect of VAP overexpression on FRAP of VSVG^{ts045}-GFP in the presence of FFAT. Cells co-expressing VSVG^{ts045}-GFP, myc-FFAT and either empty vector, wild type or P56S mutant VAPA or VAPB were incubated at 42°C to trap VSVG in the ER. Cells were treated with cycloheximide before shifting to 32°C, and a portion of the peripheral ER was photobleached. Recovery was monitored every 20 s for 10 min. (A), Confocal images showing VSVG recovery over the first 5 min after photobleaching. Yellow boxes correspond to the bleached region. (B), FRAP recovery curves for cells transfected with control vector (blue ●), VAPA-WT (red ▼), VAPA-P56S (green ■), VAPB-WT (orange ▲) or VAPB-P56S (purple ♦). Values are presented as mean ± SEM from at least three representative experiments.

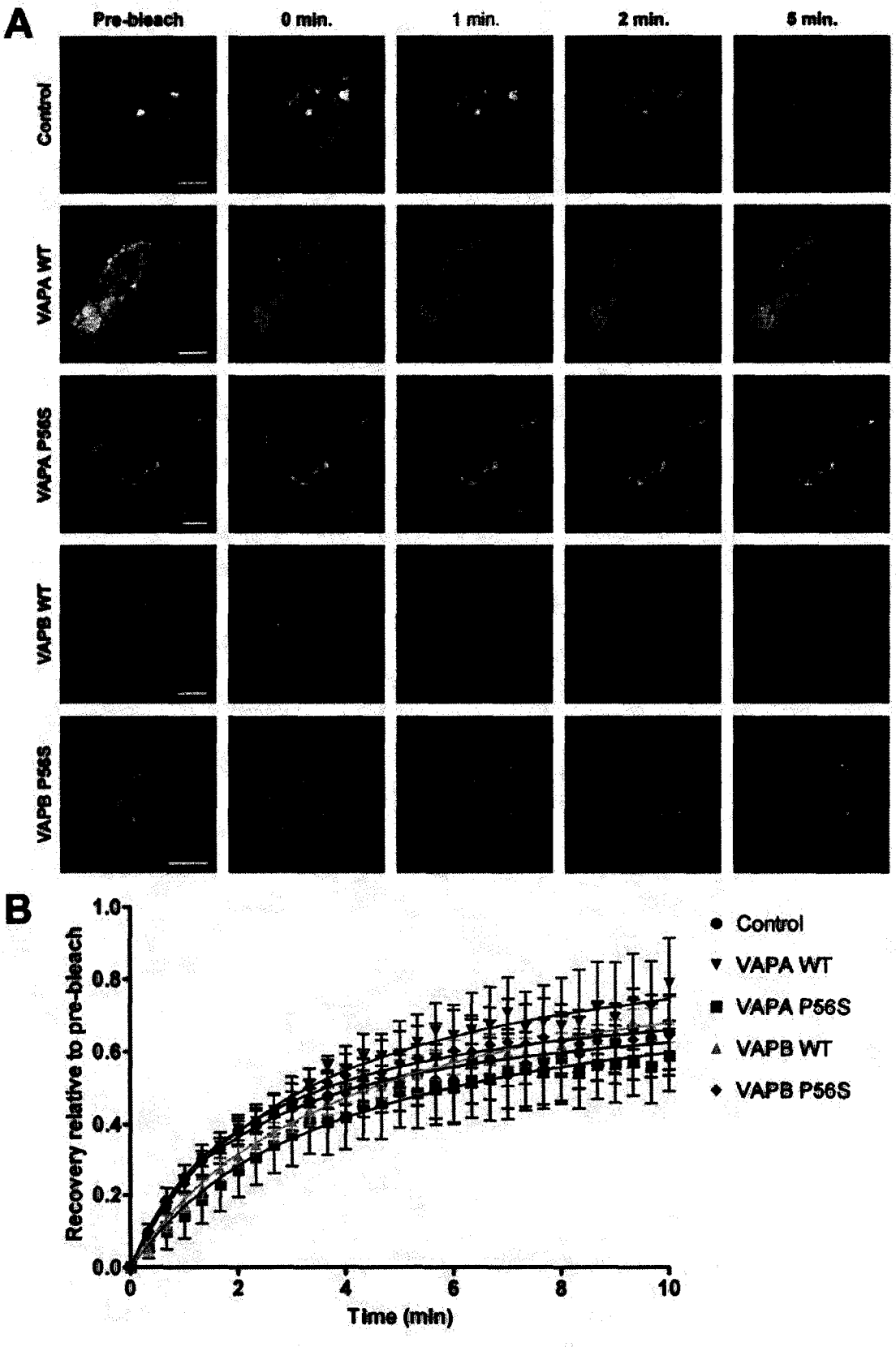
A
Pre-bleach
0 min.
1 min.
2 min.
5 min.
Control
VAPA WT
VAPA P56S
VAPB WT
VAPB P56S
B
Recovery relative to pre-bleach
1.0
0.8
0.6
0.4
0.2
0.0
0
2
4
6
8
10
Time (min)
Control
VAPA WT
VAPA P56S
VAPB WT
VAPB P56S

VAPB P56S, VSVG no longer accumulated in perinuclear aggregates, but was found in reticular ER structures throughout the cytoplasm (Figure 32A), consistent with the effect of FFAT on relieving VAPB P56S aggregates (Figure 26). Consequently, it was possible to assess VSVG lateral diffusion in reticular ER structures in VAPB P56S co-expressing FFAT. Under these conditions, VSVG recovery was similar to control cells, indicating that restoration of ER morphology could rescue VSVG trafficking.

To quantify the kinetics of FRAP recovery, the diffusion coefficient of the observed molecule is often used as a measure of distance diffused per unit of time (Reits and Neefjes, 2001). In order to accurately estimate the diffusion coefficient, maximal recovery of the photobleached protein, where the recovery curve reaches a plateau, must be obtained. However, for overexpression of wild-type or mutant VAPA, VSVG recovery did not reach a maximum over the course of the observation period (Figure 31B), which would make any estimation of diffusion coefficient inaccurate. Furthermore, it was not possible to extend the observation time past the 10 min period used because of overall signal loss due to photobleaching, and because of ER exit in control and VAPB conditions. Instead, the recovery rate of VSVG in the first 2 min following photobleaching was calculated. The initial 2 min period was selected because fluorescence recovery during this time was roughly linear, thus the slope of a linear regression could be used to estimate a rate constant. As shown in Figure 33 and Table II, the recovery rate of VSVG in CHO cells expressing wild-type or P56S mutant VAPA was 2- and 4-fold lower than for control cells, respectively. In contrast, the recovery rate for VAPB WT-expressing cells was similar to control. When FFAT was co-expressed with VAPA WT or P56S, the initial recovery rate was rescued to near control levels,

Figure 33: Initial recovery rate of VSVG^{ts045}-GFP from FRAP experiments in the presence or absence of FFAT. For all trials from Figures 31 (absence of FFAT, white bars) and 32 (presence of FFAT, black bars), fluorescence intensity values from all images taken in the first 2 min following VSVG photobleaching were subjected to linear regression. The slope of the regression curve was used to estimate an initial recovery rate constant in min^{-1}. Values are presented as mean ± SEM from at least three representative experiments. (** $p<0.01$ compared to control in the absence of FFAT; † $p<0.05$ compared to the respective condition in the absence of FFAT).

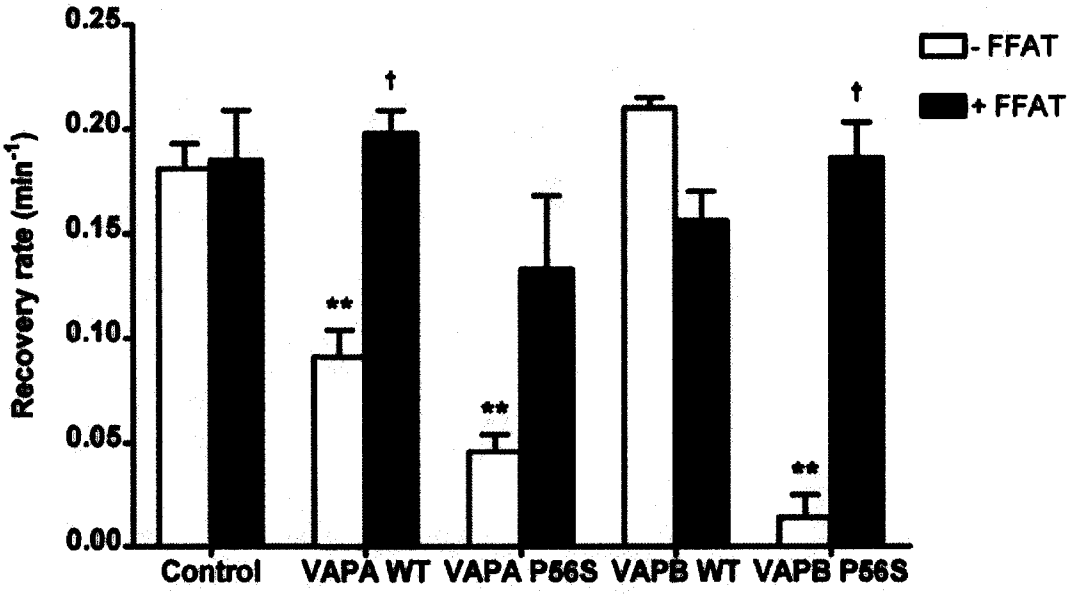
0.25
0.20
0.15
0.10
0.05
0.00
Recovery rate (min-1)
- FFAT
+ FFAT
**
**
**
†
†
Control
VAPA WT
VAPA P56S
VAPB WT
VAPB P56S

Table II: Effect of FFAT expression on fluorescence recovery rate. The recovery rate was calculated by linear regression from fluorescence values within the first two min of recovery (n≥3).

	Recovery Rate (min^{-1})
Control	0.181 ± 0.012
Control + FFAT	0.185 ± 0.024
VAPA WT	0.091 ± 0.013 **
VAPA WT + FFAT	0.198 ± 0.011 †
VAPA P56S	0.046 ± 0.008 **
VAPA P56S + FFAT	0.133 ± 0.035
VAPB WT	0.210 ± 0.005
VAPB WT + FFAT	0.156 ± 0.014
VAPB P56S	0.014 ± 0.011 **
VAPB P56S + FFAT	0.186 ± 0.017 †

† $p < 0.05$ compared to values in the absence of FFAT
** $p < 0.01$ compared to control

confirming that FFAT could relieve defects in lateral diffusion. Although the increased recovery rate was significant for VAPA WT compared to experiments in the absence of FFAT, the rescue in recovery rate seen for VAPA P56S failed to reach significance ($p>0.09$). For VAPB P56S, initial recovery was almost completely inhibited, while FFAT significantly rescued recovery to control levels. Overall, these data provide evidence that FFAT can relieve defects in lateral diffusion and protein aggregation caused by VAP overexpression, leading to a restoration of anterograde trafficking of membrane proteins.

Disruption of microtubules impairs lateral diffusion in the ER

If overexpression of VAPA creates immobile obstacles in the ER membrane through tethering to the microtubule network, one prediction of the model would be that disruption of microtubules would be sufficient to restore lateral mobility of cargo. To address this prediction, FRAP experiments were performed as described in previous sections, but cells were treated with Nocodazole during the 42°C incubation to disrupt the microtubule network. When cells were imaged, there was a noticeable change in ER morphology, such that tubular structures were often disrupted, and large, $VSVG^{ts045}$-containing punctae were often observed (Figure 34A). The appearance of these structures is consistent with the observed enlargement of ER exit sites in Nocodazole-treated cells (Dukhovny et al., 2008). When FRAP was performed on control cells treated with Nocodazole, total VSVG recovery was reduced by approximately 20%, indicating that disruption of the microtubule network inhibited lateral diffusion (compare control curves for Figures 31B and 34B). The reduced mobility of VSVG upon Nocodazole treatment in control cells is consistent with delayed recovery of an ER luminal dye in Nocodazole-

Figure 34: Effect of microtubule depolymerization on lateral diffusion of VSVG^{ts045}-GFP. Cells co-expressing VSVG^{ts045}-GFP and either empty vector or VAPA WT were incubated at 42°C in the presence of 33 μM Nocodazole (Noc) to trap VSVG in the ER and simultaneously depolymerize microtubules. FRAP was performed as described previously. (A), Confocal images showing VSVG recovery over the first 5 min after photobleaching. Yellow boxes correspond to the bleached region. (B), FRAP recovery curves for cells transfected with control vector (blue ■) or VAPA-WT (red ●). Values are presented as mean ± SD from two experiments.

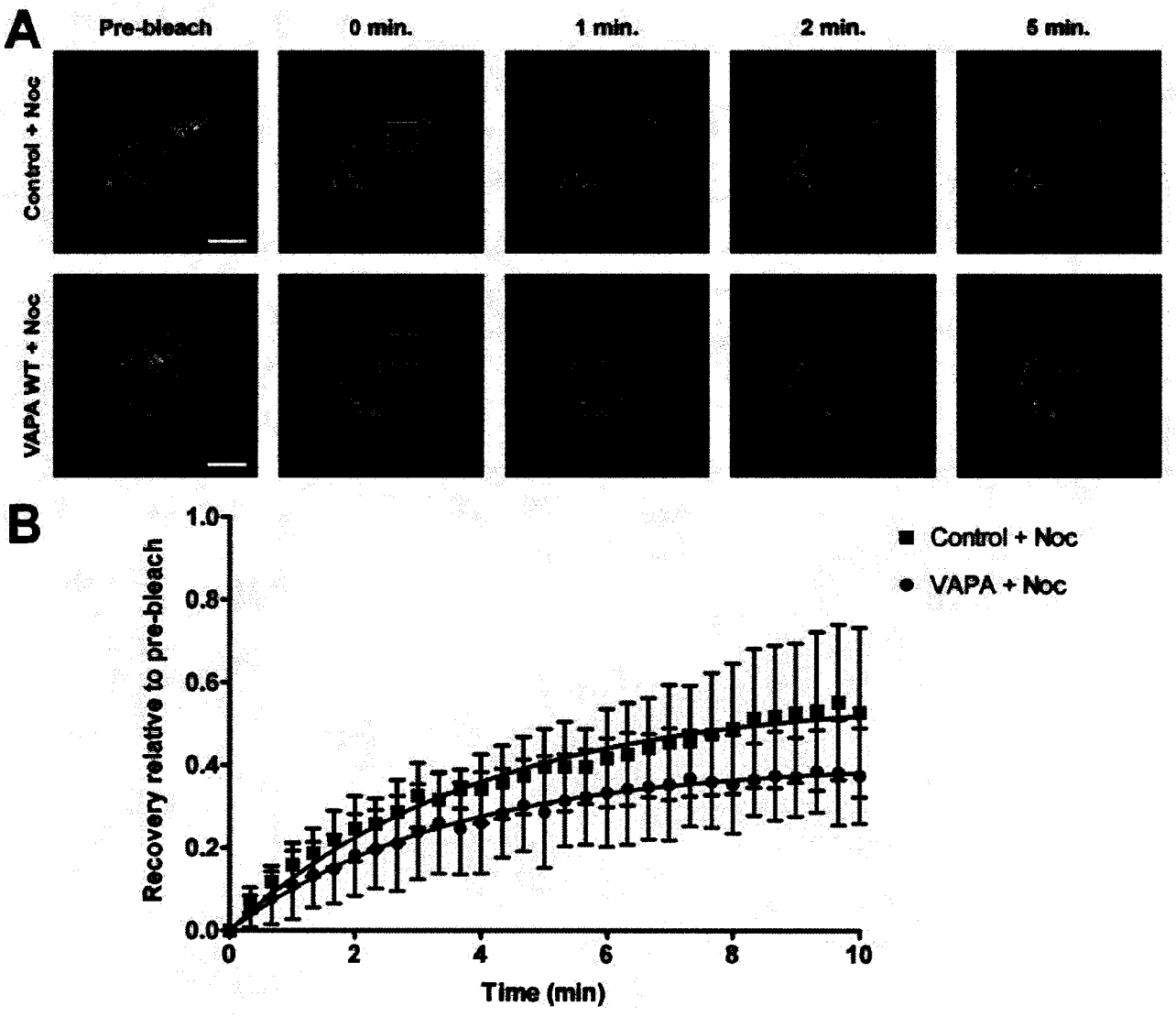
A
Pre-bleach
0 min.
1 min.
2 min.
5 min.
Control + Noc
VAPA WT + Noc
B
Recovery relative to pre-bleach
1.0
0.8
0.6
0.4
0.2
0.0
0
2
4
6
8
10
Time (min)
Control + Noc
VAPA + Noc

treated lacrimal acinar cells (Harmer et al., 2002). Overexpression of VAPA WT resulted in VSVG recovery that was similar to, but slightly less than, control cells treated with Nocodazole, and the total recovery was slightly less than in VAPA WT cells with an intact microtubule network. However, the general inhibitory effect of microtubule depolymerization on diffusion in the ER prevented an accurate assessment of whether Nocodazole could relieve VAPA-mediated immobile obstacles.

VAP overexpression does not affect transport of the luminal cargo chromogranin B

If VAPA creates immobile obstacles that impede lateral diffusion of transmembrane cargo, it is possible that soluble cargo could still diffuse freely through the ER lumen and reach exit sites for anterograde transport. As such, ER-to-Golgi transport of the soluble cargo protein chromogranin B (CgB) was assessed. For this purpose, CgB was fused to the temperature-sensitive GFP^{S65T} mutant, which is poorly fluorescent when synthesized at 37°C but fluoresces brightly when synthesized at temperatures below 25°C (Wacker et al., 1997). Cells were then incubated at 15°C to enhance GFP^{S65T} fluorescence and to simultaneously accumulate CgB in the ER-Golgi intermediate compartment (ERGIC), from which cargo cannot exit at this temperature (Saraste and Kuismanen, 1984). Subsequently, cells were rapidly shifted back to 37°C for 30 min to allow CgB transport to resume. Although this temperature block is at a post-ER stage, it was expected that if budding of soluble cargo from the ER were blocked, the CgB cargo would not be able to reach the ERGIC, and would remain trapped in the ER following temperature release. Conversely, if CgB exit from the ER is not impaired, the temperature block would not be sufficient to prevent trafficking to the ERGIC, and upon

release to the permissive temperature, CgB would transit to the Golgi complex. When cells co-expressing CgB-GFP^{S65T} and wild-type or P56S mutant VAPA or VAPB were incubated at 15°C, fluorescent cargo accumulated in the ER and/or ERGIC, as indicated by co-localization with calreticulin (Figure 35). Upon shifting the temperature to 37°C, CgB rapidly accumulated in the perinuclear Golgi compartment in all conditions, as well as in control cells transfected with an empty vector. Remarkably, CgB accumulated in ER aggregates in VAPB P56S-expressing cells, but was still able to transit to the Golgi, suggesting that soluble cargo is still able to exit from these structures. When transport of ER-trapped VSVG^{ts045}-GFP was monitored under identical treatment conditions, it remained in the ER in cells overexpressing wild-type VAPA, mutant VAPA or mutant VAPB, indicating that the 15°C temperature block did not allow exit of membrane proteins from the ER (D. Tran, unpublished results). Overall, these data suggest that defects in lateral diffusion are restricted to membrane-associated cargo, while soluble cargo is not affected by VAP overexpression. Furthermore, the ability of soluble cargo to exit the ER indicates that COPII-mediated budding from ER exit sites is not attenuated.

FFAT disrupts association of VAP isoforms with microtubules

VAPA and VAPB have both been shown to interact with microtubules, although this interaction is believed to be indirect (Kaiser et al., 2005; Mitne-Neto et al., 2007; Skehel et al., 2000). In order to characterize the interaction of VAP with microtubules, full-length VAPA and VAPB, as well as N-terminally truncated ΔN proteins lacking the MSP domain, were subjected to pulldown with pre-polymerized tubulin. When detergent-solubilized extracts from CHO cells expressing Flag-tagged VAPs were incubated with

Figure 35: Effect of VAP overexpression on transport of Chromogranin B. CHO cells were co-transfected with CgB-GFP^{S65T} and control or VAP vectors. The cells were incubated at 15°C for 2 h and rapidly shifted to 37°C for 30 min before fixation and staining with anti-calreticulin (Calr, magenta). Scale bar, 10 μm.

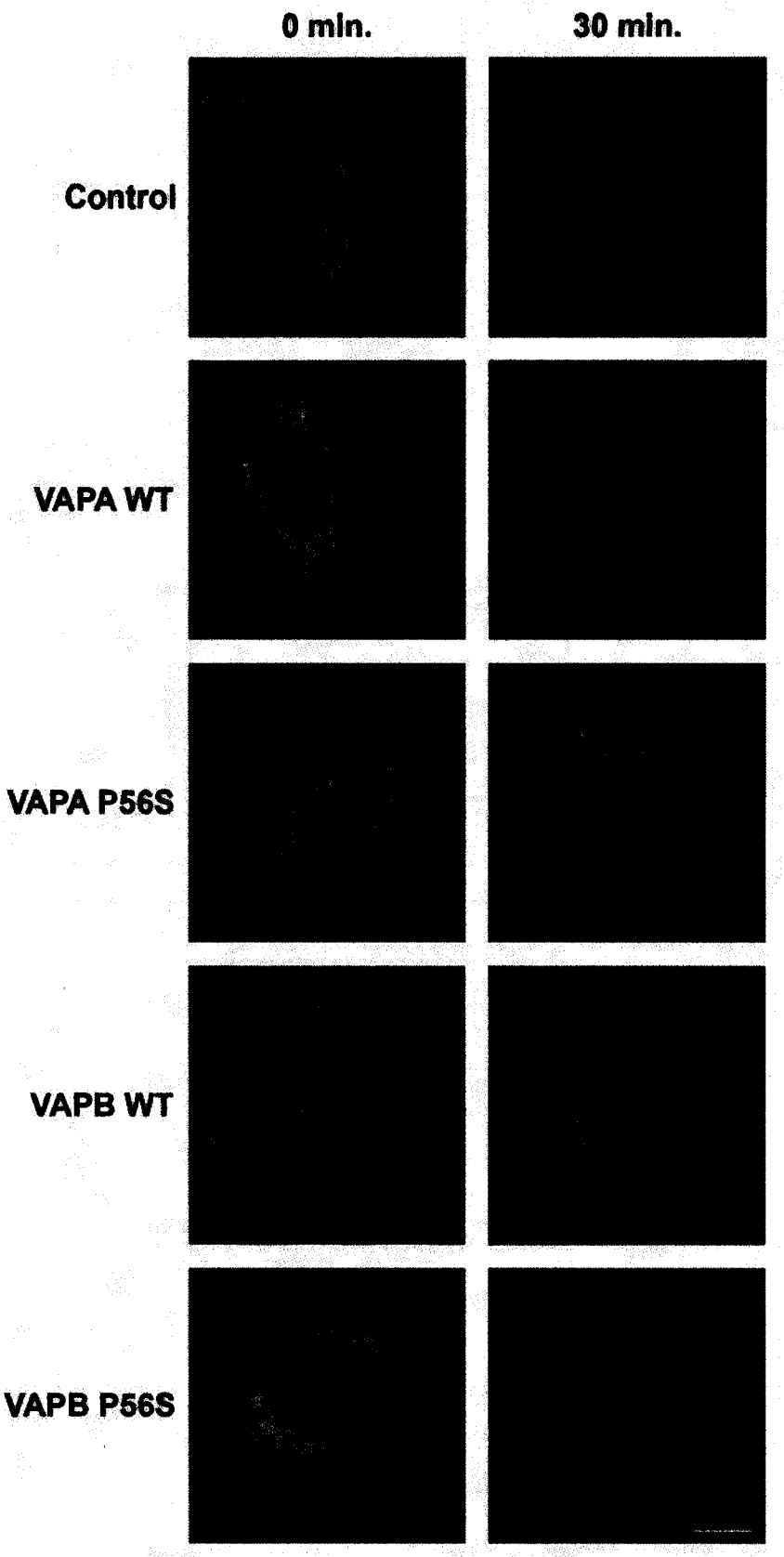
0 min.
30 min.
Control
VAPA WT
VAPA P56S
VAPB WT
VAPB P56S

microtubules and spun through a sucrose cushion, full-length VAPA and VAPB readily co-sedimented with microtubules, although ΔN truncated proteins did not (Figure 36A). Furthermore, Flag-VAP could not sediment through the sucrose cushion in the absence of polymerized microtubules. Thus, these data suggest that the interaction of VAP with microtubules is mediated by the MSP domain. When extracts from cells expressing VAPA P56S were subjected to pulldown with microtubules, the mutant VAPA could still be co-purified with microtubules, suggesting that the P56 residue is not critical for this interaction. However, it was not possible to test VAPB P56S interaction with microtubules under these conditions, since the mutant VAPB formed detergent-insoluble aggregates that were sedimented during the purification of cell extracts (Figure 36B) (Kanekura et al., 2006).

The ability of exogenous FFAT expression to restore defects in lateral diffusion raises the possibility that FFAT interaction with the MSP domain of VAP is able to disrupt interaction with microtubules, thereby relieving the ER of immobile obstacles. Consequently, pulldown experiments were also performed in which increasing concentrations of a synthetic FFAT peptide were applied to cell extracts prior to incubation with microtubules. The same concentrations of a peptide in which the two phenylalanine residues critical for binding to the MSP domain were replaced with alanine residues (AAAT) were used as a control. The relative amount of VAP associated with microtubules under these conditions was normalized to control levels in the absence of peptide, where an equivalent volume of vehicle (DMSO) was added to extracts. When applied to cell extracts, the control AAAT peptide had no effect on microtubule association of P56S mutant VAPA or wild-type VAPB, and only a minor inhibitory effect

Figure 36: Association of VAPs with polymerized microtubules. (A), Detergent-solubilized extracts of transfected cells were pulled down with polymerized microtubules. The lower panel shows 25% of the input signal from cell extracts. (B), Formation of Triton-insoluble aggregates was determined by comparison of the relative amounts of VAPB WT or P56S in crude lysate fraction (INP) and in the high-speed, Triton-insoluble pellet (HSP). Although VAPB P56S expressed at lower levels than WT in the crude lysate, equivalent amounts of each were recovered in the high-speed pellet, indicating that proportionally more VAPB P56S forms insoluble aggregates.

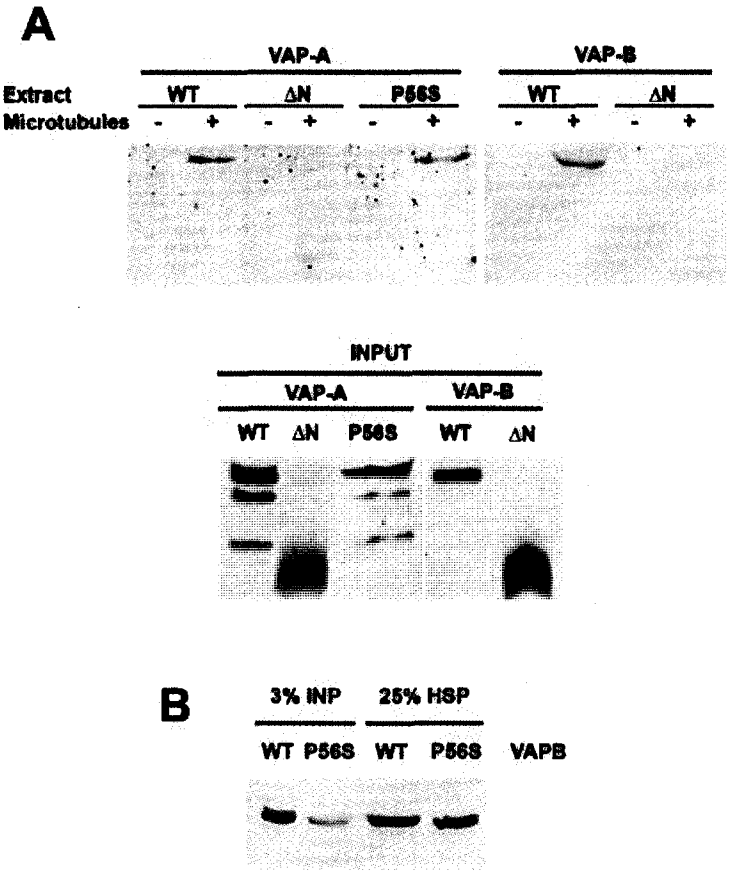
A
VAP-A
VAP-B
Extract
WT
ΔN
P56S
WT
ΔN
Microtubules
- + - + - + - + - +
INPUT
VAP-A
VAP-B
WT ΔN P56S WT ΔN
B
3% INP
25% HSP
WT P56S WT P56S VAPB

on wild-type VAPA association (Figure 37, panels A and B). As shown in Figure 36B, VAPB P56S formed insoluble aggregates, and FFAT or AAAT effects could not be assessed. Consistent with the proposed role of FFAT in disrupting microtubule association, application of this peptide effectively reduced the amount of wild-type VAPA and VAPB or P56S mutant VAPA that co-purified with microtubules at all peptide concentrations tested by 50-75%. Thus, the ability of FFAT to disrupt VAP association with microtubules could provide an explanation for the relief of immobile obstacles and restoration of lateral diffusion defects due to protein overexpression.

Figure 37: Effect of FFAT on association of VAPs with microtubules. Microtubule pulldown was performed as described previously, but in the presence of synthetic AAAT or FFAT peptides. (A), Western immunoblot of VAP recovered with microtubules in the presence of AAAT or FFAT peptide at the indicated concentrations in μM. (B), Quantitative analysis of the effect of AAAT or FFAT on VAP-microtubule association. Values were normalized to the amount of VAP recovered in the absence of either peptide. Solid figures represent microtubule association of VAPA-WT (red ■), VAPA-P56S (blue ●) and VAPB-WT (green ▲) in the presence of AAAT peptide while clear figures represent association of VAPA-WT (red □), VAPA-P56S (blue ○) and VAPB-WT (green Δ) in the presence of FFAT peptide (mean ± SEM; n=3, * $p<0.05$, paired t-test).

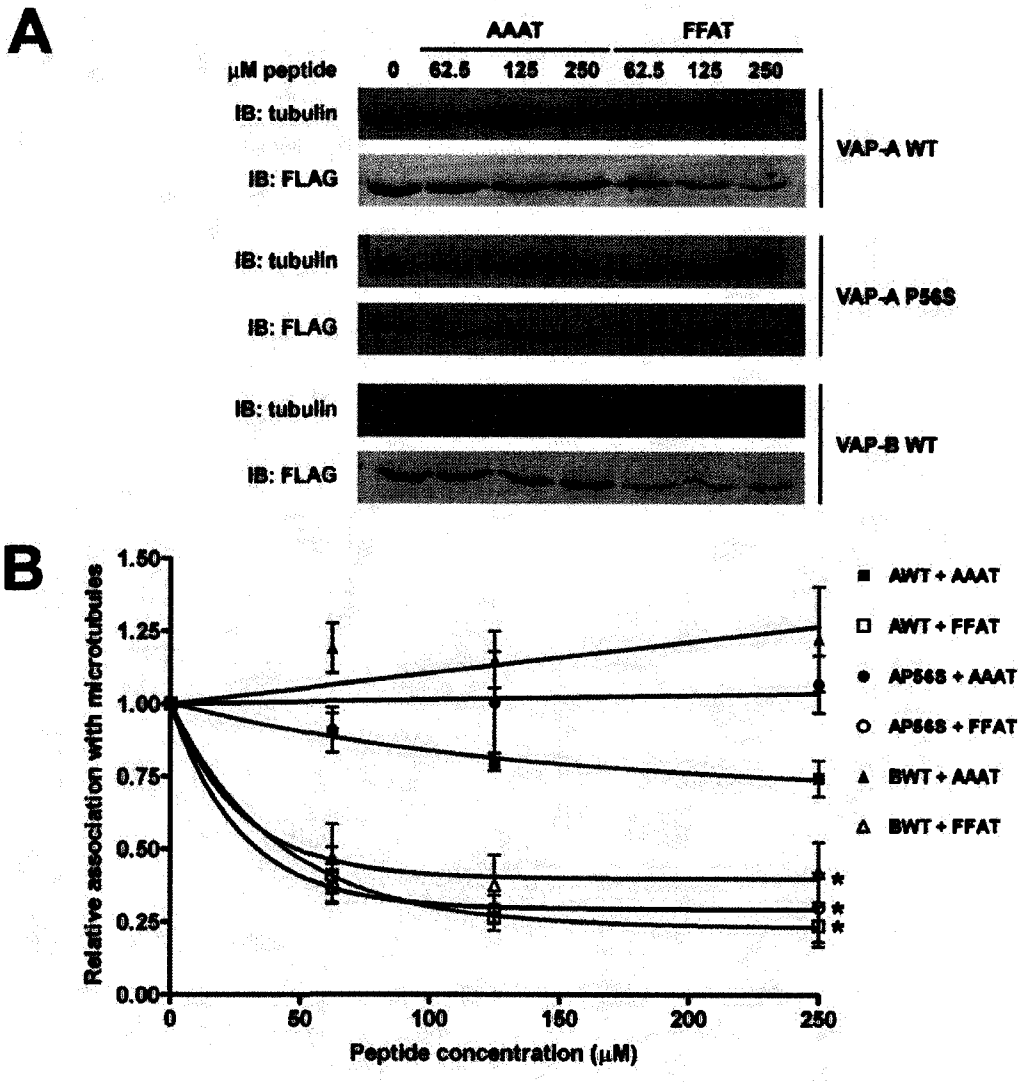
A
AAAT
FFAT
μM peptide
0
62.5
125
250
62.5
125
250
IB: tubulin
IB: FLAG
VAP-A WT
IB: tubulin
IB: FLAG
VAP-A P56S
IB: tubulin
IB: FLAG
VAP-B WT
B
Relative association with microtubules
1.50
1.25
1.00
0.75
0.50
0.25
0.00
0
50
100
150
200
250
Peptide concentration (μM)
AWT + AAAT
AWT + FFAT
AP56S + AAAT
AP56S + FFAT
BWT + AAAT
BWT + FFAT

Chapter III: Novel functions for sorting nexins in modulating actin dynamics

Discussion

SNX1 and SNX2 are novel regulators of RhoG

This study has characterized the interaction of the sorting nexins SNX1 and SNX2 with the actin-modulating Rac1 and RhoG GEF Kalirin-7, and has demonstrated that this interaction can promote membrane remodeling *in vivo*. Although RhoG function is not as well understood as the prototypical GTPases RhoA, Rac1 and Cdc42, emerging evidence supports a role for RhoG in specialized forms of endocytosis. In endothelial cells, activation of RhoG by the SH3-containing guanine nucleotide exchange factor (SGEF) has recently been implicated in macropinocytosis and trans-endothelial migration (Ellerbroek et al., 2004; van Buul et al., 2007). Furthermore, RhoG is known to promote phagocytic uptake of apoptotic cells in mammalian macrophages, as is its orthologue MIG-2 in *C. elegans* (deBakker et al., 2004; Nakaya et al., 2006). Interestingly, MIG-2-dependent clearance of apoptotic cells is mediated by Unc-73, the *C. elegans* orthologue of Kalirin and the closely related GEF Trio (deBakker et al., 2004). Whether SNX1 or SNX2 is involved in this process remains unresolved.

Remarkably, both RhoG and SNX1 have recently been shown to regulate *Salmonella* entry (Bujny et al., 2008; Patel and Galán, 2006), which is a macropinocytosis- or phagocytosis-like process (Alpuche-Aranda et al., 1994). Prior to internalization, the bacterial PI phosphatase SigD is delivered to the host cytosol, and recruits both SGEF and SNX1 to sites of entry. Since SNX1 was shown to interact with inactive RhoG and its GEF Kal7 (this study), it would be interesting to determine whether a similar process might occur whereby SNX1 generates a membrane domain

enriched in RhoG that can subsequently be activated by SGEF. Overall, these endocytic processes require extensive membrane remodeling, and Rho GTPase-dependent actin dynamics must be tightly regulated both spatially and temporally to effectively co-ordinate these activities.

In addition to phagocytosis and macropinocytosis, RhoG is believed to contribute to cell spreading and motility (Katoh et al., 2005; Meller et al., 2008). While the interaction of RhoG with the Dock180/ELMO complex appears to contribute to Rac1-dependent motility, RhoG is also able to stimulate movement in the absence of Rac1. Thus, although some of the effects of RhoG are likely to require Rac1, others appear to be Rac1-independent, as seen by others (Prieto-Sánchez and Bustelo, 2003; Wennerberg et al., 2002). In the present study, Kal7- and SNX-induced lamellipodia were dependent on RhoG, but not RhoA, Rac1 or Cdc42. These data argue against a downstream effect of Rac1 or Cdc42, and instead support parallel signaling of RhoG with these GTPases (Wennerberg et al., 2002).

The observed interaction of SNX1 and SNX2 with inactive, GDP-bound RhoG could provide a potential mechanism for regulation of RhoG. Among the main classes of regulatory proteins binding to inactive GTPases are GDIs, which maintain the pool of inactive GTPases in the cytoplasm. In addition, GEFs rapidly promote GDP release and stabilize the nucleotide-free conformation to allow GTP binding and activation. Since overexpression of SNX1 or SNX2 in singly transfected cells did not promote actin rearrangement, and since neither protein possesses a known GEF motif, these proteins are unlikely to have nucleotide exchange activity. SNX1 and SNX2 are also unlikely to act as classical RhoGDIs, which can inhibit Rho-mediated actin rearrangements when

overexpressed (Dransart et al., 2005), since co-expression with Kal7 promoted RhoG-dependent lamellipodia. Instead, it is possible that SNX1 and SNX2 act as scaffolds that bring inactive RhoG and its GEF Kal7 into close proximity, thereby facilitating nucleotide exchange and activation of RhoG.

BAR domain function is closely linked to actin dynamics

There is a growing body of evidence to suggest that BAR family proteins play a prominent role in multiple endocytic events through their curvature-sensing and membrane tubulating activities, and that actin dynamics are closely coupled to this process (Dawson et al., 2006; Shin et al., 2008; Yarar et al., 2007). For example, actin depolymerizing drugs have been reported to promote membrane tubulation by the BAR proteins amphiphysin 1 and endophilin 1 as well as F-BAR proteins such as syndapin, even though these proteins did not promote tubulation when overexpressed under steady-state conditions (Itoh et al., 2005). The same study reported that actin depolymerization enhanced tubulation induced by the membrane-deforming BAR proteins amphiphysin 2 and endophilin 3, as well as the F-BAR proteins FBP17, CIP4 and Toca-1, suggesting that the requirement of actin dynamics for BAR function is highly conserved. In addition to regulating tubulation of membranes, BAR proteins may be directly involved in other actin-dependent membrane remodeling events. For example, the BAR domain of Arfaptin-2 and the I-BAR domain of IRSp53 can interact with Rac1 to promote membrane ruffling (Miki et al., 2000; Van Aelst et al., 1996). Furthermore, several BAR family proteins, such as Tuba and SNX9, are known to recruit dynamin and actin-nucleating proteins to sites of clathrin-mediated endocytosis (Badour et al., 2007;

Lundmark and Carlsson, 2004; Salazar et al., 2003; Soulet et al., 2005). Thus, the BAR domain of SNX may provide spatial information for localized Rho-dependent actin reorganization.

Implications of co-incidence detection in SNX1 and SNX2 function

Studies of the sorting nexin family have strongly emphasized their established role in sorting of internalized receptors for recycling and degradation; however, cellular mechanisms for this activity remain unclear. The ability of PX domains to recognize specific subsets of PI species is likely to play a key role in SNX function, where the PX domain is critically important for targeting of the protein to the appropriate compartment. In the PX-BAR subfamily of SNXs, these two tandem domains are likely to act as one functional unit. For both SNX1 and SNX9, mutation of either the PX or BAR domain is sufficient to attenuate liposome binding and/or tubulation *in vitro*, suggesting a co-operative effect of the two domains for membrane association (Carlton et al., 2004; Pylypenko et al., 2007; Yarar et al., 2008). Since the PX and BAR domains are both required for interaction of SNX2 with Kal7, and mutation of either domain is sufficient to partially inhibit lamellipodia formation without affecting Kal7 interaction, co-incidence detection might be an important feature in PX-BAR function of SNX1 and SNX2.

Although lamellipodia formation was impaired in cells co-expressing Kal7 with truncated forms of SNX2 that no longer interact (N+PX or BAR) or mutants that show loss of SNX2 function (RRF or KR/AA), the proportion of cells that formed lamellipodia under these conditions was notably greater than that seen for cells expressing Kal7 or SNX2 alone. However, the residual effect seen for truncated or mutant SNX2 was clearly

less effective than that of full-length SNX2. Previous studies have shown that both the N-terminus and BAR domain of SNX1 and SNX2 might be involved in dimerization (Zhong et al., 2002). Consequently, the residual phenotype may result from overexpression of these fragments and clustering with endogenous SNXs. Importantly, endogenous levels of SNX1 or SNX2 are sufficient to promote lamellipodia, since depletion of either SNX was able to inhibit Kal7-dependent lamellipodia. Taken together, these results suggest that SNX1 and SNX2 might act as modulators of Kal7 activity, either through recruitment or activation of Kal7.

A novel role for SNX1 and SNX2 in neurite outgrowth

Analysis of Kal7 tissue distribution has revealed that its expression is largely restricted to the brain, where it plays an important role in formation and maintenance of actin-rich dendritic spines (Alam et al., 1997; Penzes et al., 2001). It has recently become clear that Kalirin is involved in signaling downstream of multiple receptors to regulate numerous morphological responses. At the postsynaptic density, Kal7 acts downstream of the EphB2 receptor, and promotes formation of dendritic spines in response to clustered Ephrin-B1 ligands (Penzes et al., 2003). Co-culture of fibroblasts expressing Ephrin-B ligands or EphB receptors results in trans-endocytosis of the full-length ligand or receptor in contacting cells to promote repulsion (Marston et al., 2003; Zimmer et al., 2003). Uptake of a transmembrane receptor from an apposing cell is likely an engulfment response, since a portion of the membrane itself must also be internalized. Given that both RhoG and SNX1 are implicated in engulfment events, it will be interesting to determine if they are necessary for EphB function downstream of Kal7.

The analysis of Kal7 and SNX2 function was initially performed in epithelial cells that do not normally express Kal7. Although these results may reflect functional similarities between Kal7 and the highly similar, broadly-expressed GEF Trio (Colomer et al., 1997; Debant et al., 1996), interaction of SNXs with Trio was not examined in this study. Thus, these findings were applied to a Kal7- and RhoG-dependent process. Stimulation of the TrkA receptor by NGF is a well-established model for neurite outgrowth in PC12 cells, and has recently been shown to require Kalirin (Chakrabarti et al., 2005). The finding that overexpression of SNX1 or SNX2 could induce formation of short neurites in undifferentiated cells, and that overexpression of Kal7 did not enhance this function, raises several interesting points. First, expression of constitutively active RhoG in PC12 cells is sufficient to promote formation of short neurites in the absence of NGF (Katoh et al., 2000). However, overexpression of wild-type RhoG promotes extension of long neurites, both in the presence and absence of NGF. Given that SNX1 and SNX2 can interact directly with inactive RhoG, it is thus possible that SNX overexpression could promote RhoG activation and neurite initiation by presenting it to an appropriate GEF, although sustained NGF signaling may be necessary for neurite extension. Secondly, the observation that co-expression of wild-type or GEF-inactive Kal7 could not potentiate initiation of short neurites suggests that neurite initiation may not be Kal7-dependent. Alternatively, another RhoG GEF could be involved, or SNX overexpression might saturate the ability of cells to form neurites such that co-expression of Kal7 does not further amplify the effect.

Surprisingly, when this model was used to determine if SNX can enhance NGF-dependent Kalirin function, overexpression of SNX2 potentiated Kal7-dependent neurite

extension, while SNX1 had an inhibitory effect. Considering their high degree of similarity, SNX1 and SNX2 are believed to share largely redundant functions; however, several pieces of information suggest that they have some distinct roles as well. First, although transgenic mice lacking either SNX1 or SNX2 are viable, homozygous deletion of both genes causes embryonic lethality (Schwarz et al., 2002). In these mice, a single copy of the SNX2 gene is sufficient to restore viability, while a single copy of SNX1 cannot fully rescue lethality and developmental defects. Secondly, the subcellular distribution of SNX1 and SNX2 is not identical, suggesting that they may function at different stages of the endocytic pathway (Gullapalli et al., 2004). Finally, while SNX1 is required for lysosomal delivery of PAR1, overexpression of SNX2 blocks receptor degradation, presumably by sequestering endogenous SNX1 (Gullapalli et al., 2006). This last finding could provide a potential explanation for the differential effects of SNX1 and SNX2 on Kal7-dependent neurite outgrowth. Although potential roles for SNX1 or SNX2 in TrkA internalization, sorting and degradation have not yet been established, overexpression of SNX1 could sequester or mistarget endogenous SNX2, thereby preventing appropriate Kal7 signaling downstream of TrkA.

Retromer-independent functions of SNX1 and SNX2

There is currently little evidence for retromer-independent functions of SNX1 or SNX2. The studies of SNX1-dependent sorting and degradation of PAR1 provided the first evidence of retromer-independent activities, since depletion of Vps26 had no effect on delivery of PAR1 to lysosomes for degradation (Gullapalli et al., 2006). In the present study, depletion of Vps35, the cargo-recognition subunit of retromer, was not able to

block lamellipodia formation via Kal7, even though depletion of SNX1 or SNX2 effectively inhibited this phenotype. Although recruitment and function of retromer downstream of lamellipodia induction cannot be ruled out at this time, the membrane remodeling event itself is clearly independent of retromer activity.

In the PC12 model of Kal7-dependent neurite outgrowth, it is not yet known if the actin-dependent processes are independent of retromer, and this issue warrants further study. One pertinent topic is the mode of internalization for TrkA. Although internalized TrkA partially co-localizes with clathrin-positive structures (Grimes et al., 1996), the principal method of TrkA internalization appears to be macropinocytosis mediated by the pinocytic chaperone Pincher (Shao et al., 2002; Valdez et al., 2005). Importantly, inhibition of Pincher function inhibits TrkA internalization and NGF signaling, and macropinosome-localized TrkA is resistant to lysosomal degradation. It is thus possible that SNXs and RhoG might regulate TrkA macropinocytosis, with SNX2 preventing lysosomal delivery. Conversely, SNX1 overexpression could promote TrkA degradation in a manner similar to PAR1 (Gullapalli et al., 2006). TrkA has also been reported to undergo rapid recycling to the plasma membrane following internalization (Chen et al., 2005; Rong et al., 2006). However, the role of SNXs in the above processes is not yet clear. The ability of SNX to promote membrane remodeling in epithelial cells depleted of Vps35 suggests that actin responses in PC12 cells might also be retromer-independent. However, modulation of TrkA internalization or recycling is likely important for prolonged NGF signaling, and it remains possible that retromer contributes to this process.

Interaction with small GTPases may be a general function for BAR domains

Both Arfaptin 2 and Hob3p are BAR-containing proteins that have been shown to interact with Rac1 and Cdc42, respectively (Coll et al., 2007; Shin and Exton, 2001; Tarricone et al., 2001). Unlike the preference of SNX2 for inactive RhoG, Arfaptin 2 and Hob3p may bind promiscuously to active and inactive GTPases. In both cases, GTPase interaction occurs with the BAR domain, suggesting that this might also be the case for SNX and RhoG. Furthermore, the BAR domain of Arfaptin 2 shows structural similarities to the DH domain of the GEF Tiam, which also interacts directly with Rac1 (Cherfils, 2001). DH and BAR domain similarities are thought to have converged during evolution, and interaction with Rho GTPases could be a common function of both domains. It is interesting to note that in the fission yeast *S. pombe*, Hob3p also interacts genetically, and possibly directly, with the Cdc42 exchange factor Gef1p (Coll et al., 2007). This potential interaction is important for recruitment and activation of Cdc42 at the site of cell fission. Another example can be found in interaction of the I-BAR protein IRSp53 with both GTP-bound Rac1 and its GEF Tiam1 to promote lamellipodia formation via WAVE (Connolly et al., 2005; Lee et al., 2007; Miki et al., 2000). Thus, interaction of BAR family proteins with small GTPases and GEFs could be a common theme, and it will be interesting to see if other BAR proteins show similar interactions.

Possible roles for Kal7 and sorting nexins in neurodegenerative diseases

Dysfunction of Kal7, SNX1 or SNX2 has not yet been definitively linked to any known pathological conditions. However, Kal7 was identified as a HAP1-interacting protein (Colomer et al., 1997), suggesting a possible role in Huntington's disease (HD).

HD is an autosomal dominant disorder resulting from an expanded polyglutamine (polyQ) stretch in the Huntingtin (Htt) protein, which causes degeneration of striatal neurons and cortical atrophy (The Huntington's Disease Collaborative Research Group, 1993). Symptoms of HD include uncoordinated movement, personality changes, dementia and cognitive decline, and the disease is typically fatal within 20 years of onset, which generally occurs at 40-50 years of age. Although the precise mechanisms of neurodegeneration in HD are not fully understood, a number of Htt-interacting proteins have been identified, and mutant Htt might alter the function of these proteins. The affinity of HAP1 for Htt appears to be proportional to polyQ length, and it has been suggested that mutant Htt segregates HAP1 into aggregates, leading to impaired endocytic trafficking (Gauthier et al., 2004; Li et al., 1995; Rong et al., 2006). The regions of HAP1 that interact with Kal7 and Htt do not overlap, suggesting that these proteins might form sequential or ternary complexes (Colomer et al., 1997). Although the physiological significance of Kal7-HAP1 interaction is unclear, it is possible that mutant Htt might also sequester Kal7, or that it could disrupt Kal7-HAP1 complexes. Either case could result in loss of Kal7 localization or function at dendritic spines. Studies have shown that Kal7 is important in dendritic spine maintenance (Ma et al., 2003; Penzes et al., 2003; Penzes et al., 2001), thus a reduction in Kal7 activity could promote spine loss, which is a pathological feature of HD (Ferrante et al., 1991; Klapstein et al., 2001; Spires et al., 2004). It is also possible that Kal7 is not involved in HD; however, this topic clearly warrants further study.

In addition to a possible role in HD, Kal7 downregulation has recently been reported in postmortem hippocampal tissue from patients with Alzheimer's disease

(Youn et al., 2007a; Youn et al., 2007b). Kalirin isoforms interact with and inhibit the inducible nitric-oxide synthase (iNOS), thereby preventing NO production (Ratovitski et al., 1999). While NO can act as a neurotransmitter, elevated levels are neurotoxic and promote inflammatory responses. Reduced levels of Kalirin appear to coincide with increased iNOS activity in the brain, suggesting that Kal-mediated dysregulation of iNOS could contribute to cell inflammatory responses to β-amyloid plaque deposition (Youn et al., 2007b). Notably, Kal7 is the main isoform expressed in adult brain, while other isoforms appear to be expressed at higher levels during development, and decreased Kalirin activity may specifically reflect loss of Kal7 (McPherson et al., 2002). However, it is not clear whether this process is a causative factor for neurodegeneration, or if reduced Kalirin levels are merely indicative of cell death in affected regions of the brain.

Interestingly, HAP1 localizes to an electron-dense cytoplasmic structure known as the stigmoid body, which also contains the sorting receptors sortilin and SorLA (Gutekunst et al., 2003). SorLA is involved in endosome-to-TGN recycling of amyloid precursor protein, and prevents its processing into pathogenic β-amyloid (Nielsen et al., 2007; Rogaeva et al., 2007). Notably, sortilin and SorLA are recycled in a retromer- and SNX1-dependent fashion (Nielsen et al., 2007; Rogaeva et al., 2007; Seaman, 2004). This interaction is mediated by a Vps10p-like domain in sortilin and SorLA, which bears similarity to the yeast Vps10p receptor that is sorted by retromer. Thus, retromer or SNX deficiency could contribute to pathogenesis in multiple neurological disorders, and it is possible that Kalirin dysfunction might also directly or indirectly affect sortilin or SorLA function.

A model for SNX-mediated recruitment of RhoG to its GEF Kal7

Overall, the results of this study support a model where SNXs 1 and 2 interact directly with inactive RhoG to present it to its GEF Kal7 for activation (Figure 38). Through co-incidence detection of membrane composition and curvature, SNX might be able to recruit Kal7 and RhoG to an appropriate compartment for activation. Alternatively, both Kalirin and SNXs have been shown to interact with cell surface receptors such as TrkA and EGFR (Chakrabarti et al., 2005; Kurten et al., 1996), which could mediate recruitment to sites of receptor activation. Although the order of SNX and Kal7 recruitment is not yet known, either scenario would result in the formation of a membrane domain that is enriched in both an inactive Rho GTPase and its activating GEF. Subsequent activation of RhoG promotes formation of lamellipodia or membraneruffles through a pathway that does not appear to require subsequent activation of Rac1 or other Rho GTPases, and could facilitate specialized forms of endocytosis. While retromer does not appear to play a role in SNX enhancement of Kal7-dependent actin remodeling, these findings do not preclude a downstream function of retromer in this model.

A similar phenomenon has already been described for the early endosomal GTPase Rab5, where the effector Rabaptin-5 interacts with and is required for recruitment of its exchange factor Rabex-5 (Horiuchi et al., 1997; Lippé et al., 2001). The complex formed between a Rab, its effector and its exchange factor is thus essential for signal amplification by generating domains that contain both Rab5 and its GEF Rabex-5. In this model, SNX1 or SNX2 could serve as a direct link between RhoG and Kal7 to create a localized enrichment and functional amplification of the Rho GTPase.

Figure 38: Model of Kalirin- and SNX-dependent membrane remodeling. SNX proteins are known to interact with a variety of activated receptors, and may also be recruited to specific compartments within the endocytic pathway via the PI-sensing PX domain or to regions of membrane curvature through the BAR domain. This may in turn serve to recruit Kal7 to an appropriate signaling complex or compartment. Alternatively, Kal7 may be recruited to an activated receptor, and subsequent interaction with SNX1 or SNX2 would bring these two proteins to the same region. SNX1 and SNX2 interact directly with inactive, GDP-bound RhoG, and could thereby present GDP-RhoG to Kal7 for subsequent activation. In this system, activated RhoG stimulates formation of lamellipodia independently of Rac1. However, it remains possible that RhoG could still activate Rac1 via interaction with the ELMO-Dock180 complex, which could contribute to other actin-dependent processes such as macropinocytosis or phagocytosis. Finally, although retromer is not required for lamellipodia formation, this model does not preclude retromer-dependent functions downstream of Kal7 and SNX. Note that broken arrows correspond to interactions that are not required for actin remodeling as observed in this study, but may contribute to downstream signals or alternative interactions.

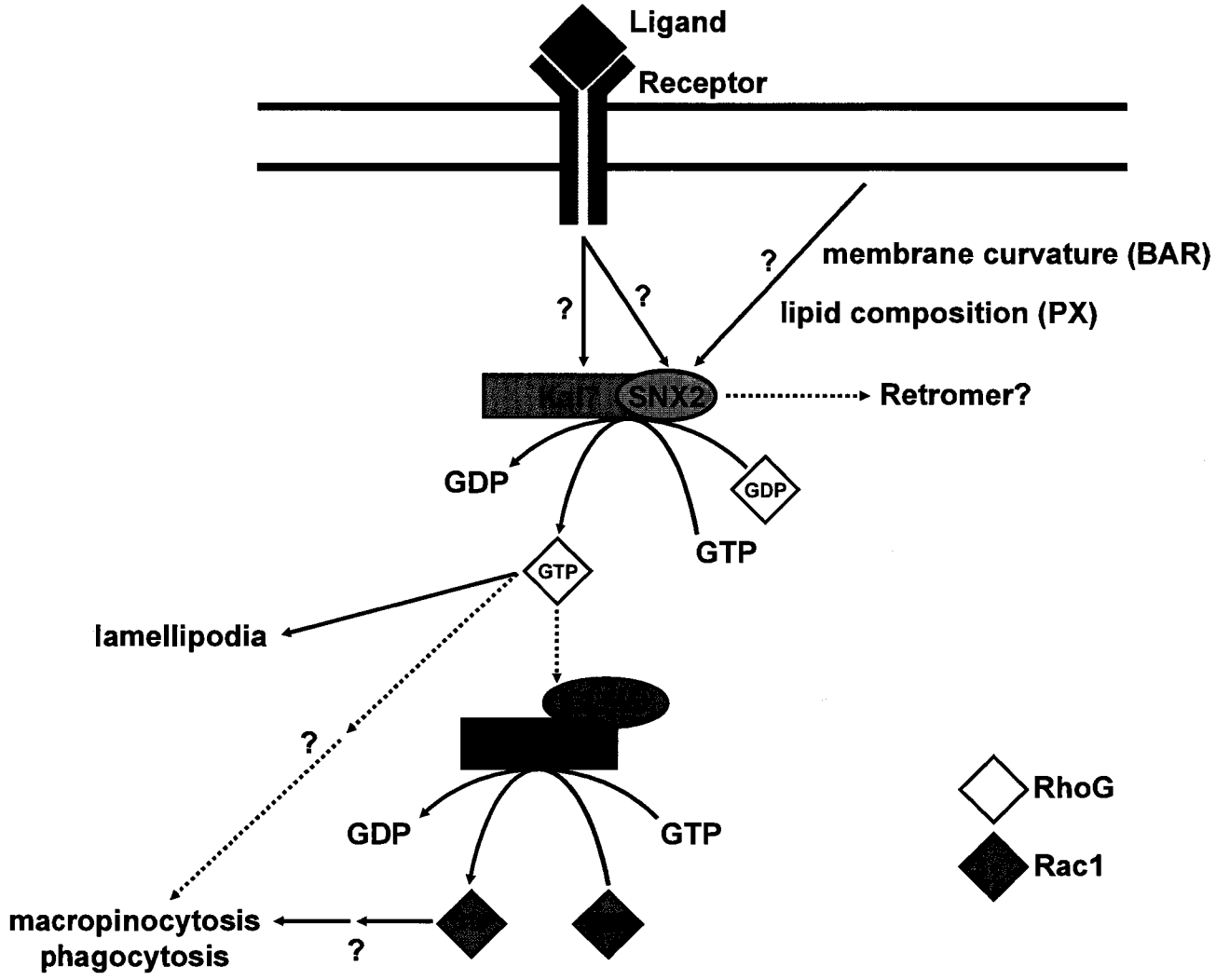
Ligand
Receptor
?
membrane curvature (BAR)
?
?
lipid composition (PX)
SNX2
Retromer?
GDP
GDP
GTP
GTP
lamellipodia
?
GDP
GTP
macropinocytosis
phagocytosis
?
RhoG
Rac1

Chapter IV: VAPs and FFAT regulate lateral diffusion and anterograde transport of ER cargo

Discussion

Differential regulation of anterograde transport by VAPA and VAPB

In the present study, overexpression of VAPA severely impeded anterograde transport of the transmembrane cargo protein VSVG. In contrast, VAPB overexpression had no effect on VSVG trafficking. Although VAPA and VAPB have a high degree of sequence similarity and are both ER-localized proteins, these data suggest that the two VAP isoforms have distinct functions. It is possible that VAPA and VAPB regulate transport of different sets of cargo proteins, or alternatively that they exert their effects on different ER subcompartments or transport pathways. Although selectivity for different cargo proteins has not been established for VAPA and VAPB, there is evidence to support regulation of different transport steps. For example, while overexpression of VAPA appears to block incorporation of VSVG into ER-derived COPII vesicles *in vitro* (Prosser et al., 2008), antibody-mediated inhibition of VAPB function appears to affect COPI-mediated transport, either from the ERGIC or within the Golgi complex (Soussan et al., 1999). The ability of VSVG to efficiently transit from ER to plasma membrane in VAPB-overexpressing cells indicates that VAPB is unlikely to affect anterograde transport through the secretory pathway (Amarilio et al., 2005; Prosser et al., 2008), and these data are consistent with a potential role for VAPB in regulating retrograde Golgi-to-ER retrieval (Soussan et al., 1999). Additionally, VAPA and VAPB distributions within the ER do not overlap completely, suggesting that they regulate processes in discrete ER subdomains (Gkogkas et al., 2008). Importantly, the observed differences in anterograde

transport are not likely due to differences in expression levels of Flag-VAPA and VAPB, since both proteins appeared to express at similar levels (for example, compare wild-type input immunoblots from Figure 36A). While it is not yet clear whether similar effects will be seen for other membrane-associated cargo proteins, these data support differential regulation of protein sorting and/or transport by VAPA and VAPB.

VAPA immobile obstacles as regulators of lateral diffusion

When expressed at endogenous levels, VAPA and VAPB do not appear to impede lateral diffusion or anterograde trafficking of membrane cargo. However, elevated levels of VAPA inhibited lateral diffusion of VSVG within the ER membrane, leading to a consequent reduction in transport to the Golgi complex. Although a number of factors are likely to contribute to the regulation of lateral diffusion, membrane viscosity and the presence of immobile obstacles have been proposed as key regulators of this process (Saxton, 1987). Since VAPs have a microtubule-associated MSP domain as well as a transmembrane domain, they could serve as immobile obstacles in the ER membrane. If overexpression of VAPA forms immobile obstacles by linking the ER to the microtubule network, expression of a truncated VAP lacking either the MSP or the transmembrane domain would be predicted to have no effect on lateral diffusion. Consistent with this idea, deletion of the transmembrane of VAPA resulted in a protein that was unable to block ER-to-Golgi transport of VSVG, while deletion of the central coiled-coil region could still effectively block trafficking (P. Gougeon, unpublished results). When the VAPA ΔN mutant lacking the MSP domain was tested for its ability to block transport, cells showed only a partial rescue in ER-to-Golgi transport as assessed by Endo H

resistance of VSVG. VAPA ΔN-expressing cells also showed a slight increase in the initial recovery rate of VSVG-GFP lateral diffusion in FRAP experiments; however, the overall recovery was similar to wild-type VAPA. Overall, the results obtained for VAPA ΔN are difficult to interpret, since dimerization occurs at least in part through the transmembrane domain, and VAPA ΔN could still create immobile obstacles by clustering endogenous VAPs.

Whether endogenous VAPs can form immobile obstacles is currently unclear. The ability of VSVG to diffuse freely in empty vector-transfected cells suggests that immobile obstacles are not present at sufficient concentrations to prevent incorporation of cargo into ER exit sites. However, it is possible that endogenous VAP might be able to form clusters or islands of immobile obstacles. Such structures could in theory play a role in regulating diffusion during protein folding or complex assembly, either under normal conditions or during periods of ER stress. In the case of VAPB, it appears unlikely that immobile obstacles regulate anterograde trafficking, but may instead play a role in incorporation of cargo into retrograde transport vesicles (Soussan et al., 1999). However, P56S mutant VAPB forms insoluble aggregates that might block anterograde transport at endogenous levels, and this is likely to contribute to pathogenesis in ALS8 patients (Nishimura et al., 2004; Teuling et al., 2007).

Other ER-localized transmembrane proteins such as CLIMP-63 and p180 can also interact with microtubules (Klopfenstein et al., 1998; Ogawa-Goto et al., 2007), and may regulate protein diffusion. For example, depletion of endogenous CLIMP-63 increases mobility of the translocon complex involved in membrane insertion or translocation of proteins into the ER lumen (Nikonov et al., 2007). Since the translocon is a very large

complex (~950 kDa), it diffuses much more slowly than smaller proteins, thus its mobility is likely restricted at endogenous protein levels (Nikonov et al., 2002). Although CLIMP-63 and VAPA are likely to create immobile obstacles in the ER, they might do so through different mechanisms. While CLIMP-63 interacts directly with microtubules (Klopfenstein et al., 1998), recombinant VAPA does not co-purify with microtubules, suggesting that their interaction is indirect (Kaiser et al., 2005) (P. Gougeon, unpublished results). Furthermore, overexpression of CLIMP-63 promotes bundling and rearrangement of the microtubule network, and appears to play a critical role in maintaining ER structure (Vedrenne et al., 2005). In contrast, VAP overexpression does not alter microtubule organization *in vivo*. Thus, VAPs might be able to reversibly associate with or dissociate from microtubules without affecting their morphology, and could thus form temporary immobile obstacles.

VAP-mediated transport defects are restricted to membrane-associated cargo

Based on their predicted topology, very little of the VAPA or VAPB protein is expected to span into the ER lumen (Figure 9). Consequently, overexpression of VAP isoforms is unlikely to alter the viscosity of the ER lumen, and luminal proteins are expected to diffuse freely. Consistent with this prediction, the secreted protein CgB was rapidly transported from the ER to the Golgi complex in cells overexpressing VAPA or VAPB, even though transport of transmembrane cargo was severely inhibited. Surprisingly, the ability of CgB to transport out of VAPB P56S-containing ER aggregates within the same time frame as control cells indicates that the collapsed ER observed in these cells retains at least some residual function. Importantly, the ability of CgB to exit

from the ER suggests that VAPA overexpression results in a protein sorting defect rather than an inability to form ER-derived transport vesicles. This idea is supported by the observation that overexpression of wild-type or mutant VAPA inhibits incorporation of membrane-associated VSVG into ER-derived COPII vesicles *in vitro*, indicating impaired sorting of VSVG into ER exit sites (Prosser et al., 2008).

FFAT motif-containing proteins modulate VAP function

Since FFAT motif-containing proteins are known to interact with the MSP domain of VAPs, it is likely that there is a functional interrelation between these two families of proteins. For example, the FFAT motif is necessary and sufficient for ER recruitment of Nir/RdgB proteins, ORP3, ORP9 and CERT (Amarilio et al., 2005; Kawano et al., 2006; Teuling et al., 2007; Wyles and Ridgway, 2004), and mutation of the two phenylalanines abolishes interaction with VAP and results in protein mistargeting. Similarly, overexpression of FFAT motif-containing proteins causes variable alterations in ER morphology, including formation of ER membrane stacks, vacuoles or varicosities, and can also induce microtubule bundling (Amarilio et al., 2005; Wyles and Ridgway, 2004). The present study establishes for the first time that a FFAT motif can interfere with the ability of VAP MSP domains to interact with microtubules *in vitro*. This finding further supports the ability of VAPA to form immobile obstacles in the ER membrane, since co-expression of FFAT and VAPA relieved defects in lateral diffusion compared to overexpression of VAPA alone. By interfering with VAPA-microtubule associations *in vivo*, FFAT could reduce the proportion of immobile obstacles in the ER membrane, allowing increased mobility of cargo proteins. It is

important to note that the effects observed in this study are likely exerted by the FFAT motif itself, since the synthetic peptides and mammalian expression constructs used did not contain any other functional domains. However, in the context of a full-length protein, other effects might be observed such as interaction with or synthesis of lipids. In addition, it is possible that exogenous expression of the FFAT motif could interfere with the association of endogenous FFAT-containing proteins with VAPs. Mislocalization of FFAT-containing proteins could affect ER membrane viscosity by altering normal lipid synthesis or shuttling; however, this possibility remains to be addressed in future studies.

In addition to restoring lateral diffusion in VAPA-overexpressing cells, co-expression of FFAT corrected VAPB P56S mutant ER aggregates. Although the mechanism for this phenomenon is not yet clear, it is possible that FFAT could disrupt aggregates or, alternatively, that it interacts with free VAP to prevent aggregation. In contrast to the present study, Teuling *et al.* reported that co-expression of GFP-tagged FFAT could not rescue VAPB P56S aggregates, and that GFP-FFAT did not interact with VAPB P56S (Teuling et al., 2007). While these findings are apparently contradictory, it is possible that differences in FFAT constructs could account for the observed discrepancies. The present study made use of a myc-tagged FFAT motif from OSBP, while Teuling *et al.* generated a GFP-tagged FFAT motif from Nir2. Although both FFAT motifs can interact directly with VAPs (Amarilio et al., 2005; Loewen et al., 2003), it is possible that they do so with different affinities. It is also possible that the large, N-terminal GFP tag reduces the ability of FFAT to associate with the MSP domain by steric hindrance. While GFP-FFAT could interact efficiently with wild-type VAPB, the P56S mutation could alter the conformation of the MSP domain. The Pro56 residue is

not located directly within the FFAT-binding pocket, but it could indirectly alter the accessibility of this region to FFAT containing a large GFP tag (Teuling et al., 2007).

Overall, the ability of myc-FFAT to resolve VAPB-P56S aggregates in the present study indicates that FFAT might still interact with mutant VAPB. Attempts to co-immunoprecipitate VAPs with the myc-FFAT motif were unsuccessful, since co-expression of myc-FFAT resulted in downregulation of VAPA and VAPB, and this effect might also contribute to the ability of FFAT to restore anterograde cargo transport (data not shown). Notably, a K87D/M87D double mutant in the FFAT-binding pocket within the MSP domain of VAPA fails to interact with FFAT, but does not form aggregates (Kaiser et al., 2005). Although this mutant formed abnormal ER structures, they do not reflect the morphology of VAPB P56S aggregates, and could arise from deficient interaction with FFAT-containing proteins. Thus, the K87D/M89D mutant is likely to reflect a loss of function, while P56S promotes aggregation and ER collapse, which could constitute a toxic gain of function.

Implications of VAPB dysfunction in ALS8

Since P56S mutant VAPB has been linked to motor neuron degeneration in ALS8, it is likely that the observed ER aggregates contribute to pathogenesis and cell death. Given that ER aggregates showed a delay in lateral diffusion and exit of membrane cargo proteins (Prosser et al., 2008; Teuling et al., 2007), a reduction in transport through the secretory pathway might have adverse effects on cell function. In addition, while overexpression of wild-type VAPB elevated the steady-state expression levels of the UPR marker XBP1, depletion of VAPB by siRNA attenuated expression of mature XBP1

(Kanekura et al., 2006). In contrast, overxpression of VAPB P56S failed to induce UPR at steady-state levels, and also inhibited UPR activation in response to ER stress, possibly by sequestering endogenous VAPB into ER aggregates. Similarly, both VAPA and VAPB have been found to interact with the UPR-activated transcription factor ATF6 (Gkogkas et al., 2008). While overexpression of wild-type VAPB inhibited ATF6 activity during ER stress, VAPB P56S had a more potent inhibitory effect, and ATF6 inhibition might be attributed to its retention in the ER by VAPB. These findings suggest that VAP P56S could inhibit UPR-mediated responses to ER stress, which might render motor neurons susceptible to degeneration over extended periods of time.

A recent study has demonstrated that the MSP domain of *Drosophila* VAPB can be cleaved and secreted into the extracellular space, where it acts as a ligand for the A class of Eph receptors (Tsuda et al., 2008). This finding is consistent with the established role of *C. elegans* MSP as a secreted ligand for variable-abnormal (VAB)/Eph receptors (Govindan et al., 2006; Miller et al., 2003b). Since worm MSP and the MSP domain of VAPs are localized to the cytoplasm, they cannot enter the classical secretory pathway, and must instead be secreted through unconventional mechanisms (Kosinski et al., 2005). Interestingly, while wild-type VAPB can be readily detected in the extracellular space, the *Drosophila* P58S mutant VAPB, which is equivalent to mammalian P56S, fails to be cleaved and secreted and may also prevent processing of wild-type VAPB (Tsuda et al., 2008). Since Eph receptors play a key role in neuronal morphology, axon guidance and dendritic spine regulation, a loss of secreted VAPB MSP domains in ALS8 patients might also contribute to dysfunction and neurodegeneration (Klein, 2004).

A third possible mechanism for VAPB P56S-mediated neurodegeneration was recently reported, where mutant VAPB sequestered wild-type VAPA and VAPB into aggregates (Teuling et al., 2007). In this study, the authors found that depletion of VAPA, but not VAPB, in motor neurons reduced cell viability, suggesting that VAPA function plays a role in cell survival. Furthermore, overexpression of VAPB P56S reduced motor neuron viability, which could be explained by sequestration of VAPA in mutant VAPB-containing aggregates. Interestingly, mutant SOD1 G93A transgenic mice, which are an established model for SOD1-dependent ALS, also showed reduced levels of VAPA and VAPB in spinal cord lysates (Teuling et al., 2007). Although this finding might reflect motor neuron loss rather than VAP downregulation, it is possible that loss of VAPA could contribute to cell death resulting from mutant SOD1. The inability of VAPA P56S to form large ER aggregates (Figure 26) suggests that the equivalent mutation in VAPA might not sequester wild-type VAPs into insoluble aggregates. Additionally, although mutant VAPB has been reported to associate with microtubules less efficiently than wild-type VAPB (Mitne-Neto et al., 2007), the present study demonstrates that wild-type and mutant VAPA associate with microtubules at similar efficiencies. Although trafficking defects in VAPA P56S-expressing cells were more severe than those of wild-type VAPA (Prosser et al., 2008), mutant VAPA and VAPB clearly have different cellular effects.

FFAT peptides could have therapeutic applications for ALS

The present study demonstrates that exogenous expression of FFAT-containing peptides resolves ER aggregates in VAPB P56S-expressing epithelial cells, and restores the transport defects associated with mutant VAPB. As such, it is interesting to speculate

that application of FFAT might exert similar effects in motor neurons to protect against neurodegeneration in ALS8. While FFAT may exert its effects by preventing aggregation of newly synthesized VAPB P56S, dissociating pre-existing aggregates or enhancing downregulation of mutant VAPB, any of these mechanisms could restore function of wild-type VAPA. In an animal model, delivery of the peptide across the blood-brain barrier could prove difficult; however, this might be resolved by viral transduction of the FFAT peptide in affected areas. Regulation of FFAT expression levels will also be critical, since overexpression could affect wild-type proteins to promote their dissociation from microtubules, or could compete with endogenous FFAT-containing proteins for interaction with VAPs. Whether FFAT could be used in a therapeutic program for treatment of ALS8, or other forms of ALS in which VAP function might be reduced, merits further study.

A model for VAP function in regulation of diffusion through the ER membrane

Overall, the above results are in agreement with a model where VAPA overexpression forms immobile obstacles by anchoring the ER membrane to the microtubule network (Figure 39). At endogenous levels, VAP does not impede lateral diffusion of cargo through the ER, but may instead play a role in maintenance of ER structure through its interaction with microtubules. Recruitment of FFAT-containing proteins could also regulate ER structure or function through synthesis, metabolism or shuttling of lipids. Clustering of VAP immobile obstacles could inhibit diffusion within the ER membrane, thereby preventing incorporation of membrane-associated cargo into ER exit sites for subsequent transport. Whether this is a normal function for VAPs is not

Figure 39: Model of VAP function. (A), VAPs are dimeric proteins that embed into the ER via a transmembrane domain and interact with the microtubule network through the N-terminal MSP domain to form immobile obstacles. At endogenous VAP concentrations, membrane and luminal cargo proteins diffuse freely through the ER membrane and are efficiently incorporated into ER exit sites for transport to the ERGIC and Golgi complex. (B), Under conditions of VAPA overexpression or VAPB P56S aggregation, the increased concentration of immobile obstacles in the ER impedes lateral diffusion of membrane-associated cargoes, preventing their incorporation into ER exit sites. However, soluble proteins can still diffuse freely and are rapidly transported to post-ER structures. (C), Co-expression of FFAT peptides or FFAT-containing proteins interferes with VAP-microtubule interactions, or prevents aggregation of mutant VAPB. Release of VAPs from microtubules and/or resolution of aggregates relieves one anchor point from the immobile obstacles, and loss of immobile obstacles restores lateral mobility of membrane-associated cargo.

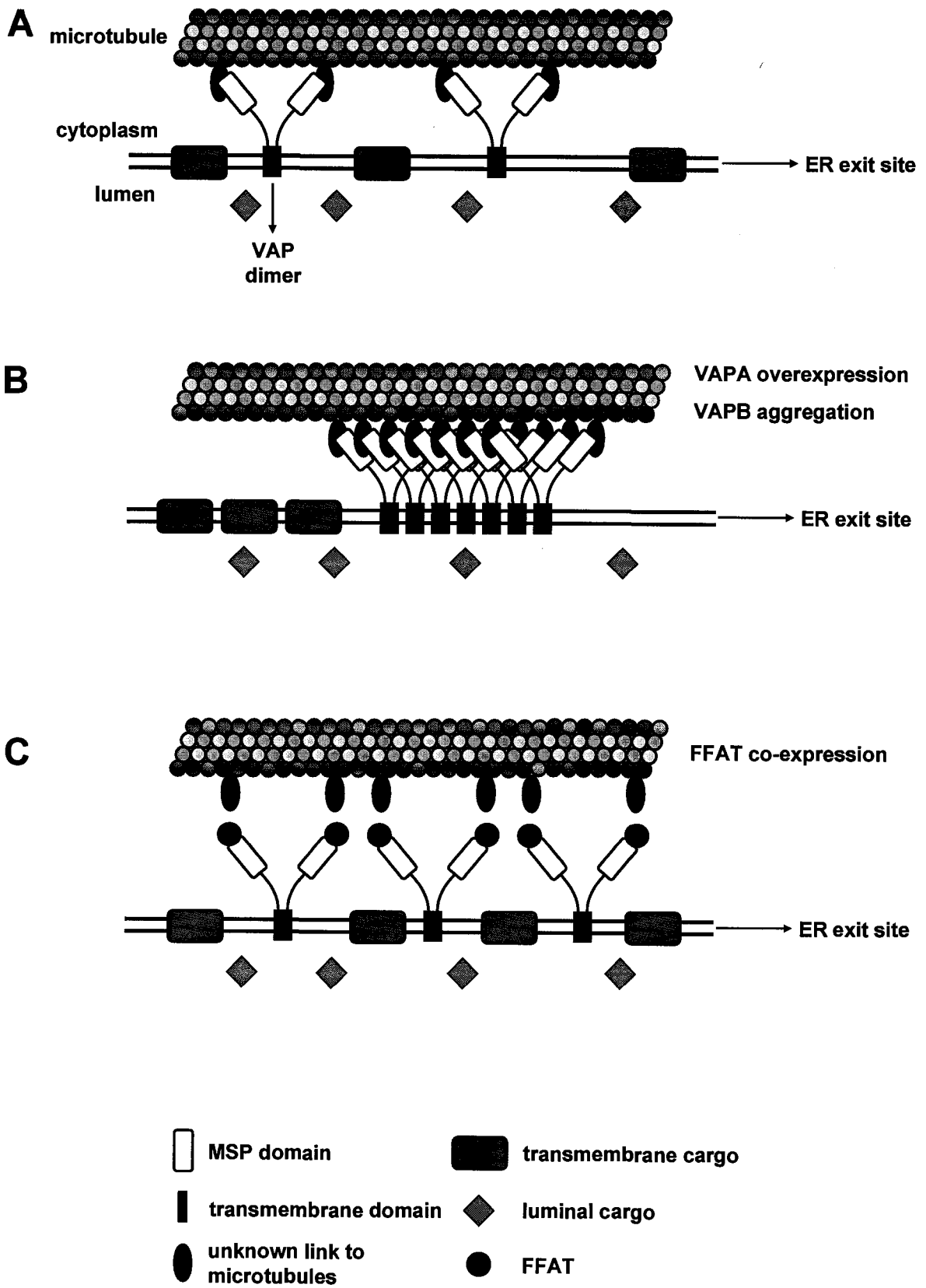
A
microtubule
cytoplasm
lumen
VAP
dimer
ER exit site
B
VAPA overexpression
VAPB aggregation
ER exit site
C
FFAT co-expression
ER exit site
MSP domain
transmembrane domain
unknown link to
microtubules
transmembrane cargo
luminal cargo
FFAT

yet clear, but immobile obstacles might be enhanced during ER stress or by VAPB P56S aggregation or VAPA overexpression. Under conditions of increased VAP immobile obstacles (either through overexpression or aggregation), exogenous expression of FFAT restores lateral diffusion of membrane-associated proteins, which could indicate a reduction in the level of immobile obstacles. Consistent with this possibility, application of FFAT prevents association of VAP with microtubules and reduces the incidence of mutant VAPB aggregates. Thus, VAPs are likely to interact reversibly with microtubules *in vivo*, and FFAT-containing proteins could provide a means to modulate VAP-microtubule interactions.

References

Abdul-Ghani, M., K.L. Hartman, and J.K. Ngsee. 2005. Abstrakt interacts with and regulates the expression of sorting nexin-2. *J. Cell. Physiol.* 204:210-218.

Alam, M.R., R.C. Johnson, D.N. Darlington, T.A. Hand, R.E. Mains, and B.A. Eipper. 1997. Kalirin, a cytosolic protein with spectrin-like and GDP/GTP exchange factor-like domains that interacts with peptidylglycine α-amidating monooxygenase, an integral membrane peptide-processing enzyme. *J. Biol. Chem.* 292:12667-12675.

Alberts, A.S., N. Bouquin, L.H. Johnston, and R. Treisman. 1998. Analysis of RhoA-binding proteins reveals an interaction domain conserved in heterotrimeric G protein β subunits and the yeast response regulator protein Skn7. *J. Biol. Chem.* 273:8616-8622.

Alpuche-Aranda, C.M., E.L. Racoosin, J.A. Swanson, and S.I. Miller. 1994. *Salmonella* stimulate macrophage macropinocytosis and persist within spacious phagosomes. *J. Exp. Med.* 179:601-608.

Amarilio, R., S. Ramachandran, H. Sabanay, and S. Lev. 2005. Differential regulation of endoplasmic reticulum structure through VAP-Nir protein interaction. *J. Biol. Chem.* 280:5934-5944.

Arighi, C.N., L.M. Hartnell, R.C. Aguilar, C.R. Haft, and J.S. Bonifacino. 2004. Role of the mammalian retromer in sorting of the cation-independent mannose 6-phosphate receptor. *J. Cell Biol.* 165:123-133.

Bache, K.G., A. Brech, A. Mehlum, and H. Stenmark. 2003. Hrs regulates multivesicular body formation via ESCRT recruitment to endosomes. *J. Cell Biol.* 162:435-442.

Badour, K., M.K.H. McGavin, J. Zhang, S. Freeman, C. Vieira, D. Filipp, M. Julius, G.B. Mills, and K.A. Siminovitch. 2007. Interaction of the Wiskott-Aldrich syndrome protein with sorting nexin 9 is required for CD28 endocytosis and cosignaling in T cells. *Proc. Natl. Acad. Sci. USA*. 104:1593-1598.

Baker, A.M.E., T.M. Roberts, and M. Stewart. 2002. 2.6 Å resolution crystal structure of helices of the motile major sperm protein (MSP) of *Caenorhabditis elegans*. *J. Mol. Biol.* 319:491-499.

Bankaitis, V.A., L.M. Johnson, and S.D. Emr. 1986. Isolation of yeast mutants defective in protein targeting to the vacuole. *Proc. Natl. Acad. Sci. USA*. 83:9075-9079.

Banta, L.M., J.S. Robinson, D.J. Klionsky, and S.D. Emr. 1988. Organelle assembly in yeast: characterization of yeast mutants defective in vacuolar biogenesis and protein sorting. *J. Cell Biol.* 107:1369-1383.

Barlowe, C., L. Orci, T. Yeung, M. Hosobuchi, S. Hamamoto, N. Salama, M.F. Rexach, M. Ravazzola, M. Amherdt, and R. Schekman. 1994. COPII: a membrane coat formed by Sec proteins that drive vesicle budding from the endoplasmic reticulum. *Cell.* 77:895-907.

Benesch, S., S. Lommel, A. Steffen, T.E.B. Stradal, N. Scaplehorn, M. Way, J. Wehland, and K. Rottner. 2002. Phosphatidylinositol 4,5-biphosphate (PIP2)-induced vesicle movement depends on N-WASP and involves Nck, WIP, and Grb2. *J. Biol. Chem.* 277:37771-37776.

Bergmann, J.E., K.T. Tokuyasu, and S.J. Singer. 1981. Passage of an integral membrane protein, the vesicular stomatitis virus glycoprotein, through the Golgi apparatus en route to the plasma membrane. *Proc. Natl. Acad. Sci. USA.* 78:1746-1750.

Boillée, S., C.V. Velde, and D.W. Cleveland. 2006. ALS: a disease of motor neurons and their nonneuronal neighbors. *Neuron.* 52:39-59.

Bompard, G., S.J. Sharp, G. Freiss, and L.M. Machesky. 2005. Involvement of Rac in actin cytoskeleton rearrangements induced by MIM-B. *J. Cell Sci.* 118:5393-5403.

Bonifacino, J.S., and B.S. Glick. 2004. The mechanisms of vesicle budding and fusion. *Cell.* 116:153-166.

Bonifacino, J.S., and L.M. Traub. 2003. Signals for sorting of transmembrane proteins to endosomes and lysosomes. *Annu. Rev. Biochem.* 72:395-447.

Bravo, J., D. Karathanassis, C.M. Pacold, M.E. Pacold, C.D. Ellson, K.E. Anderson, P.J.G. Butler, I. Lavenir, O. Perisic, P.T. Hawkins, L. Stephens, and R.L. Williams. 2001. The crystal structure of the PX domain from p40phox bound to phosphatidylinositol 3-phosphate. *Mol. Cell.* 8:829-839.

Brickner, J.H., and P. Walter. 2004. Gene recruitment of the activated INO1 locus to the nuclear membrane. *PLoS Biol.* 2:e342.

Bujny, M.V., P.A. Ewels, S. Humphrey, N. Attar, M.A. Jepson, and P.J. Cullen. 2008. Sorting nexin-1 defines an early phase of *Salmonella*-containing vacuole-remodeling during *Salmonella* infection. *J. Cell Sci.* 121:2027-2036.

Bullock, T.L., T.M. Roberts, and M. Stewart. 1996. 2.5 Å resolution crystal structure of the motile major sperm protein (MSP) of *Ascaris suum*. *J. Mol. Biol.* 263:284-296.

Burridge, K., and K. Wennerberg. 2004. Rho and Rac take center stage. *Cell.* 116:167-179.

Buss, F., S.D. Arden, M. Lindsay, J.P. Luzio, and J. Kendrick-Jones. 2001. Myosin VI isoform localized to clathrin-coated vesicles with a role in clathrin-mediated endocytosis. *EMBO J.* 20:3676-3684.

Cai, H., K. Reinisch, and S. Ferro-Novick. 2007. Coats, tethers, Rabs, and SNAREs work together to mediate the intracellular destination of a transport vesicle. *Dev. Cell.* 12:671-682.

Carlton, J., M. Bujny, B.J. Peter, V.M.J. Oorschot, A. Rutherford, H. Mellor, J. Klumperman, H.T. McMahon, and P.J. Cullen. 2004. Sorting nexin-1 mediates tubular endosome-to-TGN transport through coincidence sensing of high-curvature membranes and 3-phosphoinositides. *Curr. Biol.* 14:1791-1800.

Carlton, J.G., M.V. Bujny, B.J. Peter, V.M.J. Oorschot, A. Rutherford, R.S. Arkell, J. Klumperman, H.T. McMahon, and P.J. Cullen. 2005. Sorting nexin-2 is associated with tubular elements of the early endosome, but is not essential for retromer-mediated endosome-to-TGN transport. *J. Cell Sci.* 118:4527-4539.

Chakrabarti, K., R. Lin, N.I. Schiller, Y. Wang, D. Koubi, Y.-X. Fan, B.B. Rudkin, G.R. Johnson, and M.R. Schiller. 2005. Critical role for Kalirin in nerve growth factor signaling through TrkA. *Mol. Cell. Biol.* 25:5106-5118.

Chen, Z.-Y., A. Ieraci, M. Tanowitz, and F.S. Lee. 2005. A novel endocytic recycling signal distinguishes biological responses of Trk neurotrophin receptors. *Mol. Biol. Cell.* 16:5761-5772.

Cherfils, J. 2001. Structural mimicry of DH domains by Arfaptin suggests a model for the recognition of Rac-GDP by its guanine nucleotide exchange factors. *FEBS Lett.* 507:280-284.

Coll, P.M., S.A. Rincon, R.A. Izquierdo, and P. Perez. 2007. Hob3p, the fission yeast ortholog of human BIN3, localizes Cdc42p to the division site and regulates cytokinesis. *EMBO J.* 26:1865-1877.

Collins, B.M., S.J. Norwood, M.C. Kerr, D. Mahony, M.N.J. Seaman, R.D. Teasdale, and D.J. Owen. 2008. Structure of Vps26B and mapping of its interaction with the retromer protein complex. *Traffic.* 9:366-379.

Colomer, V., S. Engelender, A.H. Sharp, K. Duan, J.K. Cooper, A. Lanahan, G. Lyford, P. Worley, and C.A. Ross. 1997. Huntingtin-associated protein 1 (HAP1) binds to a Trio-like polypeptide, with a rac1 guanine nucleotide exchange factor domain. *Hum. Mol. Genet.* 6:1519-1525.

Connolly, B.A., J. Rice, L.A. Feig, and R.J. Buchsbaum. 2005. Tiam1-IRSp53 complex formation directs specificity of Rac-mediated actin cytoskeleton regulation. *Mol. Cell. Biol.* 25:4602-4614.

Cox, D., P. Chang, Q. Zhang, P.G. Reddy, G.M. Bokoch, and S. Greenberg. 1997. Requirements for both Rac1 and Cdc42 in membrane ruffling and phagocytosis in leukocytes. *J. Exp. Med.* 186:1487-1494.

Cozier, G.E., J. Carlton, A.H. McGregor, P.A. Gleeson, R.D. Teasdale, H. Mellor, and P.J. Cullen. 2002. The Phox homology (PX) domain-dependent, 3-phosphoinositide-mediated association of sorting nexin-1 with an early sorting endosomal compartment is required for its ability to regulate epidermal growth factor receptor degradation. *J. Biol. Chem.* 277:48730-48736.

Cullen, P.J. 2008. Endosomal sorting and signalling: an emerging role for sorting nexins. *Nat. Rev. Mol. Cell Biol.* 9:574-582.

d'Enfert, C., L.J. Wuestehube, T. Lila, and R. Schekman. 1991. Sec12p-dependent membrane binding of the small GTP-binding protein Sar1p promotes formation of transport vesicles from the ER. *J. Cell Biol.* 114:663-670.

D'Souza-Schorey, C., R.L. Boshans, M. McDonough, P.D. Stahl, and L. Van Aelst. 1997. A role for POR1, a Rac1-interacting protein, in ARF6-mediated cytoskeletal rearrangements. *EMBO J.* 16:5445-5454.

Dawson, J.C., J.A. Legg, and L.M. Machesky. 2006. Bar domain proteins: a role in tubulation, scission and actin assembly in clathrin-mediated endocytosis. *Trends Cell Biol.* 16:493-498.

deBakker, C.D., L.B. Haney, J.M. Kinchen, C. Grimsley, M. Lu, D. Klingele, P.-K. Hsu, B.-K. Chou, L.-C. Cheng, A. Blangy, J. Sondek, M.O. Hengartner, Y.-C. Wu, and K.S. Ravichandran. 2004. Phagocytosis of apoptotic cells is regulated by a UNC-73/TRIO-MIG-2/RhoG signaling module and armadillo repeats of CED-12/ELMO. *Curr. Biol.* 14:2208-2216.

Debant, A., C. Serra-Pagès, K. Seipel, S. O'Brien, M. Tang, S.-H. Park, and M. Streuli. 1996. The multidomain protein Trio binds the LAR transmembrane tyrosine phosphatase, contains a protein kinase domain, and has separate rac-specific and rho-specific guanine nucleotide exchange factor domains. *Proc. Natl. Acad. Sci. USA.* 93:5466-5471.

DerMardirossian, C., and G.M. Bokoch. 2005. GDIs: central regulatory molecules in Rho GTPase activation. *Trends Cell Biol.* 15:356-363.

Dransart, E., A. Morin, J. Cherfils, and B. Olofsson. 2005. Uncoupling of inhibitory and shuttling functions of Rho GDP dissociation inhibitors. *J. Biol. Chem.* 280:4674-4683.

Dukhovny, A., A. Papadopulos, and K. Hirschberg. 2008. Quantitative live-cell analysis of microtubule-uncoupled cargo-protein sorting in the ER. *J. Cell Sci.* 121:865-876.

Eby, J.J., S.P. Holly, F. van Drogen, A.V. Grishin, M. Peter, D.G. Drubin, and K.J. Blumer. 1998. Actin cytoskeleton organization regulated by the PAK family of protein kinases. *Curr. Biol.* 8:967-970.

Eden, S., R. Rohatgi, A.V. Podtelejnikov, M. Mann, and M.W. Kirschner. 2002. Mechanism of regulation of WAVE1-induced actin nucleation by Rac1 and Nck. *Nature*. 418:790-793.

Edgar, A.J., and J.M. Polak. 2000. Human homologues of yeast vacuolar protein sorting 29 and 35. *Biochem. Biophys. Res. Commun.* 277:622-630.

Ellerbroek, S.M., K. Wennerberg, W.T. Arthur, J.M. Dunty, D.R. Bowman, K.A. DeMali, C. Der, and K. Burridge. 2004. SGEF, a RhoG guanine nucleotide exchange factor that stimulates macropinocytosis. *Mol. Biol. Cell*. 15:3309-3319.

Estrach, S., S. Schmidt, S. Diriong, A. Penna, A. Blangy, P. Fort, and A. Debant. 2002. The human Rho-GEF trio and its target GTPase RhoG are involved in the NGF pathway, leading to neurite outgrowth. *Curr. Biol.* 12:307-312.

Farsad, K., N. Ringstad, K. Takei, S.R. Floyd, K. Rose, and P. De Camilli. 2001. Generation of high curvature membranes mediated by direct endophilin bilayer interactions. *J. Cell Biol.* 155:193-200.

Feiguin, F., A. Ferreira, K.S. Kosik, and A. Caceres. 1994. Kinesin-mediated organelle translocation revealed by specific cellular manipulations. *J. Cell Biol.* 127:1021-1039.

Ferrante, R.J., N.W. Kowall, and E.P. Richardson. 1991. Proliferative and degenerative changes in striatal spiny neurons in Huntington's disease: a combined study using the section-Golgi method and calbindin D28k immunocytochemistry. *J. Neurosci.* 11:3877-3887.

Foster, L.J., M.L. Weir, D.Y. Lim, Z. Liu, W.S. Trimble, and A. Klip. 2000. A functional role for VAP-33 in insulin-stimulated GLUT4 traffic. *Traffic*. 1:512-521.

Frost, A., R. Perera, A. Roux, K. Spasov, O. Destaing, E.H. Egelman, P. De Camilli, and V.M. Unger. 2008. Structural basis of membrane invagination by F-BAR domains. *Cell*. 132:807-817.

Futter, C.E., A. Pearse, L.J. Hewlett, and C.R. Hopkins. 1996. Multivesicular endosomes containing internalized EGF-EGF receptor complexes mature and then fuse directly with lysosomes. *J. Cell Biol.* 132:1011-1023.

Gabel, C.A., and J.E. Bergmann. 1985. Processing of the asparagine-linked oligosaccharides of secreted and intracellular forms of the vesicular stomatitis virus G protein: in vivo evidence of Golgi apparatus compartmentalization. *J. Cell Biol.* 101:460-469.

Gallione, C.J., and J.K. Rose. 1985. A single amino acid substitution in a hydrophobic domain causes temperature-sensitive cell-surface transport of a mutant viral glycoprotein. *J. Virol.* 54:374-382.

Gallop, J.L., C.C. Jao, H.M. Kent, P.J.G. Butler, P.R. Evans, R. Langen, and H.T. McMahon. 2006. Mechanism of endophilin N-BAR domain-mediated membrane curvature. *EMBO J.* 25:2898-2910.

Gauthier-Rouvière, C., E. Vignal, M. Mériane, P. Roux, P. Montcourier, and P. Fort. 1998. RhoG GTPase controls a pathway that independently activates Rac1 and Cdc42Hs. *Mol. Biol. Cell.* 9:1379-1394.

Gauthier, L.R., B.C. Charrin, M. Borrell-Pagès, J.P. Dompierre, H. Rangone, F.P. Cordelières, J.D. Mey, M.E. MacDonald, V. Leßmann, S. Humbert, and F. Saudou. 2004. Huntingtin controls neurotrophic support and survival of neurons by enhancing BDNF vesicular transport along microtubules. *Cell.* 118:127-138.

Gkogkas, C., S. Middleton, A.M. Kremer, C. Wardrope, M. Hannah, T.H. Gillingwater, and P. Skehel. 2008. VAPB interacts with and modulates the activity of ATF6. *Hum. Mol. Genet.* 17:1517-1526.

Gokool, S., D. Tattersall, J.V. Reddy, and M.N.J. Seaman. 2007. Identification of a conserved motif required for Vps35p/Vps26p interaction and assembly of the retromer complex. *Biochem J.* 408:287-295.

Gougeon, P.-Y., D.C. Prosser, L.F. Da-Silva, and J.K. Ngsee. 2002. Disruption of Golgi morphology and trafficking in cells expressing mutant prenylated Rab acceptor-1. *J. Biol. Chem.* 277:36408-36414.

Govindan, J.A., H. Cheng, J.E. Harris, and D. Greenstein. 2006. $G\alpha_{o/i}$ and $G\alpha_s$ signaling function in parallel with the MSP/Eph receptor to control meiotic diapause in *C. elegans*. *Curr. Biol.* 16:1257-1268.

Grimes, M.L., J. Zhou, E.C. Beattie, E.C. Yuen, D.E. Hall, J.S. Valletta, K.S. Topp, J.H. LaVail, N.W. Bunnett, and W.C. Mobley. 1996. Endocytosis of activated TrkA:

evidence that nerve growth factor induces formation of signaling endosomes. *J. Neurosci.* 16:7950-7964.

Gullapalli, A., T.A. Garrett, M.M. Paing, C.T. Griffin, Y. Yang, and J. Trejo. 2004. A role for sorting nexin 2 in epidermal growth factor receptor down-regulation: evidence for distinct functions of sorting nexin 1 and 2 in protein trafficking. *Mol. Biol. Cell.* 15:2143-2155.

Gullapalli, A., B.L. Wolfe, C.T. Griffin, T. Magnuson, and J. Trejo. 2006. An essential role for SNX1 in lysosomal sorting of protease-activated receptor-1: evidence for retromer-, Hrs-, and Tsg101-independent functions of sorting nexins. *Mol. Biol. Cell.* 17:1228-1238.

Gutekunst, C.-A., E.R. Torre, Z. Sheng, H. Yi, S.H. Coleman, I.B. Riedel, and H. Bujo. 2003. Stigmoid bodies contain type I receptor proteins SorLA/LR11 and sortilin: new perspectives on their function. *J. Histochem. Cytochem.* 51:841-852.

Haaf, A., L. LeClaire, G. Roberts, H.M. Kent, T.M. Roberts, M. Stewart, and D. Neuhaus. 1998. Solution structure of the motile major sperm protein (MSP) of *Ascaris suum* - evidence for two manganese binding sites and the possible role of divalent cations in filament formation. *J. Mol. Biol.* 284:1611-1624.

Habermann, B. 2004. The BAR-domain family of proteins: a case of bending and binding? *EMBO Rep.* 5:250-255.

Haft, C.R., M. de la Luz Sierra, R. Bafford, M.A. Lesniak, V.A. Barr, and S.I. Taylor. 2000. Human orthologs of yeast vacuolar protein sorting proteins Vps26, 29, and 35: assembly into multimeric complexes. *Mol. Biol. Cell.* 11:4105-4116.

Haft, C.R., M. de la Luz Sierra, V.A. Barr, D.H. Haft, and S.I. Taylor. 1998. Identification of a family of sorting nexin molecules and characterization of their association with receptors. *Mol. Cell. Biol.* 18:7278-7287.

Harding, H.P., Y. Zhang, and D. Ron. 1999. Protein translation and folding are coupled by an endoplasmic-reticulum-resident kinase. *Nature*. 397:271-274.

Harmer, A.R., D.V. Gallacher, and P.M. Smith. 2002. Correlations between the functional integrity of the endoplasmic reticulum and polarized Ca^{2+} signalling in mouse lacrimal acinar cells : a role for inositol 1,3,4,5-tetrakisphosphate. *Biochem J.* 367:137-143.

Henne, W.M., H.M. Kent, M.G.J. Ford, B.G. Hegde, O. Daumke, P.J.G. Butler, R. Mittal, R. Langen, P.R. Evans, and H.T. McMahon. 2007. Structure and analysis of FCHo2 F-BAR domain: a dimerizing and membrane recruitment module that effects membrane curvature. *Structure*. 15:839-852.

Hierro, A., A.L. Rojas, R. Rojas, N. Murthy, G. Effantin, A.V. Kajava, A.C. Steven, J.S. Bonifacino, and J.H. Hurley. 2007. Functional architecture of the retromer cargo-recognition complex. *Nature*. 449:1063-1067.

Hiroaki, H., T. Ago, T. Ito, H. Sumimoto, and D. Kohda. 2001. Solution structure of the PX domain, a target of the SH3 domain. *Nat. Struct. Biol.* 8:526-530.

Horazdovsky, B.F., B.A. Davies, M.N.J. Seaman, S.A. McLaughlin, S.-h. Yoon, and S.D. Emr. 1997. A sorting nexin-1 homologue, Vps5p, forms a complex with Vpsl7p and is required for recycling the vacuolar protein-sorting receptor. *Mol. Biol. Cell.* 8:1529-1541.

Horiuchi, H., R. Lippé, H.M. McBride, M. Rubino, P. Woodman, H. Stenmark, V. Rybin, M. Wilm, K. Ashman, M. Mann, and M. Zerial. 1997. A novel Rab5 GDP/GTP exchange factor complexed to Rabaptin-5 links nucleotide exchange to effector recruitment and function. *Cell.* 90:1149-1159.

Itoh, T., K.S. Erdmann, A. Roux, B. Habermann, H. Werner, and P. De Camilli. 2005. Dynamin and the actin cytoskeleton cooperatively regulate plasma membrane invagination by BAR and F-BAR proteins. *Dev. Cell.* 9:791-804.

Jackson, M.R., T. Nilsson, and P.A. Peterson. 1993. Retrieval of transmembrane proteins to the endoplasmic reticulum. *J. Cell Biol.* 121:317-333.

Jacobson, K., A. Ishihara, and R. Inman. 1987. Lateral diffusion of proteins in membranes. *Annu. Rev. Physiol.* 49:163-175.

Jaffe, A.B., and A. Hall. 2005. Rho GTPases: biochemistry and biology. *Annu. Rev. Cell Dev. Biol.* 21:247-269.

Johnson, R.C., P. Penzes, B.A. Eipper, and R.E. Mains. 2000. Isoforms of Kalirin, a neuronal Dbl family member, generated through use of different 5'- and 3'-ends along with an internal translational initiation site. *J. Biol. Chem.* 275:19324-19333.

Kagiwada, S., K. Hosaka, M. Murata, J.-I. Nikawa, and A. Takatsuki. 1998. The *Saccharomyces cerevisiae* SCS2 gene product, a homolog of a synaptobrevin-associated protein, is an integral membrane protein of the endoplasmic reticulum and is required for inositol metabolism. *J. Bacteriol.* 1998.

Kaiser, S.E., J.H. Brickner, A.R. Reilein, T.D. Fenn, P. Walter, and A.T. Brunger. 2005. Structural basis of FFAT motif-mediated ER targeting. *Structure*. 13:1035-1045.

Kanekura, K., I. Nishimoto, S. Aiso, and M. Matsuoka. 2006. Characterization of amyotrophic lateral sclerosis-linked P56S mutation of vesicle-associated

membrane protein-associated protein B (VAPB/ALS8). *J. Biol. Chem.* 40:30223-30233.

Katoh, H., K. Hiramoto, and M. Negishi. 2005. Activation of Rac1 by RhoG regulates cell migration. *J. Cell Sci.* 119:56-65.

Katoh, H., and M. Negishi. 2003. RhoG activates Rac1 by direct interaction with the Dock180-binding protein Elmo. *Nature*. 424:461-464.

Katoh, H., H. Yasui, Y. Yamaguchi, J. Aoki, H. Fujita, K. Mori, and M. Negishi. 2000. Small GTPase RhoG is a key regulator for neurite outgrowth in PC12 cells. *Mol. Cell. Biol.* 20:7378-7387.

Katzmann, D.J., M. Babst, and S.D. Emr. 2001. Ubiquitin-dependent sorting into the multivesicular body pathway requires the function of a conserved endosomal protein sorting complex, ESCRT-I. *Cell*. 106:145-155.

Kawano, M., K. Kumagai, M. Nishijima, and K. Hanada. 2006. Efficient trafficking of ceramide from the endoplasmic reticulum to the Golgi apparatus requires a VAMP-associated protein-interacting FFAT motif of CERT. *J. Biol. Chem.* 281:30279-30288.

Kittler, J.T., P. Thomas, V. Tretter, Y.D. Bogdanov, V. Haucke, T.G. Smart, and S.J. Moss. 2004. Huntingtin-associated protein 1 regulates inhibitory synaptic transmission by modulating γ-aminobutyric acid type A receptor membrane trafficking. *Proc. Natl. Acad. Sci. USA*. 101:12736-12741.

Klapstein, G.J., R.S. Fisher, H. Zanjani, C. Cepeda, E.S. Jokel, M.-F. Chesselet, and M.S. Levine. 2001. Electrophysiological and morphological changes in striatal spiny neurons in R6/2 Huntington's disease transgenic mice. *J. Neurophysiol.* 86:2667-2677.

Klein, R. 2004. Eph/ephrin signaling in morphogenesis, neural development and plasticity. *Curr. Opin. Cell Biol.* 16:580-589.

Klopfenstein, D.R.C., F. Kappeler, and H.-P. Hauri. 1998. A novel direct interaction of endoplasmic reticulum with microtubules. *EMBO J.* 17:6168-6177.

Koo, T.H., B.A. Eipper, and J.G. Donaldson. 2007. Arf6 recruits the Rac GEF Kalirin to the plasma membrane facilitating Rac activation. *BMC Cell Biol.* 8:29.

Korolchuk, V.I., M.M. Schütz, C. Gómez-Llorente, J. Rocha, N.R. Lansu, S.M. Collins, Y.P. Wairkar, I.M. Robinson, and C.J. O'Kane. 2007. *Drosophila* Vps35 function is necessary for normal endocytic trafficking and actin cytoskeleton organisation. *J. Cell Sci.* 120:4367-4376.

Kosinski, M., K. McDonald, J. Schwartz, I. Yamamoto, and D. Greenstein. 2005. *C. elegans* sperm bud vesicles to deliver a meiotic maturation signal to distant oocytes. *Development.* 132:3357-3369.

Kovacs, E.M., R.S. Makar, and F.B. Gertler. 2006. Tuba stimulates intracellular N-WASP-dependent actin assembly. *J. Cell Sci.* 119:2715-2726.

Kozma, R., S. Sarner, S. Ahmed, and L. Lim. 1997. Rho family GTPases and neuronal growth cone remodelling: relationship between increased complexity induced by Cdc42Hs, Rac1, and acetylcholine and collapse induced by RhoA and lysophosphatidic acid. *Mol. Cell. Biol.* 17:1201-1211.

Kurten, R.C., D.L. Cadena, and G.N. Gill. 1996. Enhanced degradation of EGF receptors by a sorting nexin, SNX1. *Science.* 272:1008-1010.

Kusumi, A., C. Nakada, K. Ritchie, K. Murase, K. Suzuki, H. Murakoshi, R.S. Kasai, J. Kondo, and T. Fujiwara. 2005. Paradigm shift of the plasma membrane concept from the two-dimensional continuum fluid to the partitioned fluid: high-speed single-molecule tracking of membrane molecules. *Annu. Rev. Biophys. Biomol. Struct.* 34:351-378.

Lane, J.D., and V.J. Allan. 1999. Microtubule-based endoplasmic reticulum motility in *Xenopus laevis*: activation of membrane-associated kinesin during development. *Mol. Biol. Cell.* 10:1909-1922.

Lee, M.C.S., E.A. Miller, J. Goldberg, L. Orci, and R. Schekman. 2004. Bi-directional protein transport between the ER and Golgi. *Annu. Rev. Cell Dev. Biol.* 20:87-123.

Lee, S.H., F. Kerff, D. Chereau, F. Ferron, A. Klug, and R. Dominguez. 2007. Structural basis for the actin-binding function of missing-in-metastasis. *Structure.* 15:145-155.

Lemmon, M.A. 2008. Membrane recognition by phospholipid-binding domains. *Nat. Rev. Mol. Cell Biol.* 9:99-111.

Li, J., X. Mao, L.Q. Dong, F. Liu, and L. Tong. 2007. Crystal structures of the BAR-PH and PTB domains of human APPL1. *Structure.* 15:525-533.

Li, X.J., S.H. Li, A.H. Sharp, F.C. Nucifora, G. Schilling, A. Lanahan, P. Worley, S.H. Snyder, and C.A. Ross. 1995. A huntingtin-associated protein enriched in brain with implications for pathology. *Nature.* 378:398-402.

Li, Y., L.-S. Chin, A.I. Levey, and L. Li. 2002. Huntingtin-associated protein 1 interacts with hepatocyte growth factor-regulated tyrosine kinase substrate and functions in endosomal trafficking. *J. Biol. Chem.* 277:28212-28221.

Lippé, R., M. Miaczynska, V. Rybin, A. Runge, and M. Zerial. 2001. Functional synergy between Rab5 effector Rabaptin-5 and exchange factor Rabex-5 when physically associated in a complex. *Mol. Biol. Cell.* 12:2219-2228.

Loewen, C.J.R., M.L. Gaspar, S.A. Jesch, C. Delon, N.T. Ktistakis, S.A. Henry, and T.P. Levine. 2004. Phospholipid metabolism regulated by a transcription factor sensing phosphatidic acid. *Science.* 304:1644-1647.

Loewen, C.J.R., and T.P. Levine. 2006. A highly conserved binding site in vesicle-associated membrane protein-associated protein (VAP) for the FFAT motif of lipid-binding proteins. *J. Biol. Chem.* 280:14097-14104.

Loewen, C.J.R., A. Roy, and T.P. Levine. 2003. A conserved ER targeting motif in three families of lipid binding proteins and in Opi1p binds VAP. *EMBO J.* 22:2025-2035.

Lundmark, R., and S.R. Carlsson. 2003. Sorting nexin 9 participates in clathrin-mediated endocytosis through interactions with the core components. *J. Biol. Chem.* 278:46772-46781.

Lundmark, R., and S.R. Carlsson. 2004. Regulated membrane recruitment of dynamin-2 mediated by sorting nexin 9. *J. Biol. Chem.* 279:42694-42702.

Ma, X.-M., J. Huang, Y. Wang, B.A. Eipper, and R.E. Mains. 2003. Kalirin, a multifunctional Rho guanine nucleotide exchange factor, is necessary for maintenance of hippocampal pyramidal neuron dendrites and dendritic spines. *J. Neurosci.* 23:10593-10603.

Marston, D.J., S. Dickinson, and C.D. Nobes. 2003. Rac-dependent trans-endocytosis of ephrinBs regulates Eph–ephrin contact repulsion. *Nat. Cell Biol.* 5:879-888.

Mattila, P.K., A. Pykäläinen, J. Saarikangas, V.O. Paavilainen, H. Vihinen, E. Jokitalo, and P. Lappalainen. 2007. Missing-in-metastasis and IRSp53 deform PI(4,5)P2-rich membranes by an inverse BAR domain–like mechanism. *J. Cell Biol.* 7:953-964.

May, V., M.R. Schiller, B.A. Eipper, and R.E. Mains. 2002. Kalirin Dbl-homology guanine nucleotide exchange factor 1 domain initiates new axon outgrowths via RhoG-mediated mechanisms. *J. Neurosci.* 22:6980-6990.

McAuliffe, M.J., F.M. Lalonde, D. McGarry, W. Gandler, K. Csaky, and B.L. Trus. 2001. Medical image processing, analysis & visualization in clinical research. *IEEE Computer-based Medical Systems (CBMS)*:381-386.

McPherson, C.E., B.A. Eipper, and R.E. Mains. 2002. Genomic organization and differential expression of Kalirin isoforms. *Gene*. 284:41-51.

Meller, J., L. Vidali, and M.A. Schwartz. 2008. Endogenous RhoG is dispensable for integrin-mediated cell spreading but contributes to Rac-independent migration. *J. Cell Sci.* 121:1981-1989.

Merrifield, C.J., M.E. Feldman, L. Wan, and W. Almers. 2002. Imaging actin and dynamin recruitment during invagination of single clathrin-coated pits. *Nat. Cell Biol.* 4:691-698.

Meusser, B., C. Hirsch, E. Jarosch, and T. Sommer. 2005. ERAD: the long road to destruction. *Nat. Cell Biol.* 7:766-772.

Miki, H., T. Sasaki, Y. Takai, and T. Takenawa. 1998a. Induction of filopodium formation by a WASP-related actin-depolymerizing protein N-WASP. *Nature*. 391:93-96.

Miki, H., S. Suetsugu, and T. Takenawa. 1998b. WAVE, a novel WASP-family protein involved in actin reorganization induced by Rac. *EMBO J.* 17:6932-6941.

Miki, H., H. Yamaguchi, S. Suetsugu, and T. Takenawa. 2000. IRSp53 is an essential intermediate between Rac and WAVE in the regulation of membrane ruffling. *Nature*. 408:732-735.

Millard, T.H., G. Bompard, M.Y. Heung, T.R. Dafforn, D.J. Scott, L.M. Machesky, and K. Fütterer. 2005. Structural basis of filopodia formation induced by the IRSp53/MIM homology domain of human IRSp53. *EMBO J.* 24:240-250.

Miller, E.A., T.H. Beilharz, P.N. Malkus, M.C.S. Lee, S. Hamamoto, L. Orci, and R. Schekman. 2003a. Multiple cargo binding sites on the COPII subunit Sec24p ensure capture of diverse membrane proteins into transport vesicles. *Cell*. 114:497-509.

Miller, M.A., P.J. Ruest, M. Kosinski, S.K. Hanks, and D. Greenstein. 2003b. An Eph receptor sperm-sensing control mechanism for oocyte meiotic maturation in *Caenorhabditis elegans*. *Genes Dev.* 17:187-200.

Mitne-Neto, M., C.R.R. Ramos, D.C. Pimenta, J.S. Luz, A.L. Nishimura, F.A. Gonzales, C.C. Oliveira, and M. Zatz. 2007. A mutation in human VAP-B-MSP domain, present in ALS patients, affects the interaction with other cellular proteins. *Prot. Exp. Purif.* 55:139-146.

Mizuno, M., and S.J. Singer. 1994. A possible role for stable microtubules in intracellular transport from the endoplasmic reticulum to the Golgi apparatus. *J. Cell Sci.* 107:1321-1331.

Nakaya, M., M. Tanaka, Y. Okabe, R. Hanayama, and S. Nagata. 2006. Opposite effects of Rho family GTPases on engulfment of apoptotic cells by macrophages. *J. Biol. Chem.* 281:8836-8842.

Nicolau, D.V., J.F. Hancock, and K. Burrage. 2007. Sources of anomalous diffusion on cell membranes: a Monte Carlo study. *Biophys. J.* 92:1975-1987.

Nielsen, M.S., C. Gustafsen, P. Madsen, J.R. Nyengaard, G. Hermey, O. Bakke, M. Mari, P. Schu, R. Pohlmann, A. Dennes, and C.M. Petersen. 2007. Sorting by the cytoplasmic domain of the amyloid precursor protein binding receptor SorLA. *Mol. Cell. Biol.* 27:6842-6851.

Nikonov, A.V., H.-P. Hauri, B. Lauring, and G. Kreibich. 2007. Climp-63-mediated binding of microtubules to the ER affects the lateral mobility of translocon complexes. *J. Cell Sci.* 120:2248-2258.

Nikonov, A.V., E. Snapp, J. Lippincott-Schwartz, and G. Kreibich. 2002. Active translocon complexes labeled with GFP–Dad1 diffuse slowly as large polysome arrays in the endoplasmic reticulum. *J. Cell Biol.* 158:497-506.

Nishimura, A.L., A. Al-Chalabi, and M. Zatz. 2005. A common founder for amyotrophic lateral sclerosis type 8 (ALS8) in the Brazilian population. *Hum. Genet.* 118:499-500.

Nishimura, A.L., M. Mitne-Neto, H.C.A. Silva, A. Richieri-Costa, S. Middleton, D. Cascio, F. Kok, J.R.M. Oliveira, T. Gillingwater, J. Webb, P. Skehel, and M. Zatz. 2004. A mutation in the vesicle-trafficking protein VAPB causes late-onset spinal muscular atrophy and amyotrophic lateral sclerosis. *Am. J. Hum. Genet.* 75:822-831.

Nishimura, N., and W.E. Balch. 1997. A di-acidic signal required for selective export from the endoplasmic reticulum. *Science*. 277:556-558.

Nishimura, Y., M. Hayashi, H. Inada, and T. Tanaka. 1999. Molecular cloning and characterization of mammalian homologues of vesicle-associated membrane protein-associated (VAMP-associated) proteins. *Biochem. Biophys. Res. Commun.* 254:21-26.

Nobes, C.D., and A. Hall. 1995. Rho, Rac, and Cdc42 GTPases regulate the assembly of multimolecular focal complexes associated with actin stress fibers, lamellipodia, and filopodia. *Cell*. 81:53-62.

Nothwehr, S.F., P. Bruinsma, and L.A. Strawn. 1999. Distinct domains within Vps35p mediate the retrieval of two different cargo proteins from the yeast prevacuolar/endosomal compartment. *Mol. Biol. Cell*. 10:875-890.

Nothwehr, S.F., S.-A. Ha, and P. Bruinsma. 2000. Sorting of yeast membrane proteins into an endosome-to-Golgi pathway involves direct interaction of their cytosolic domains with Vps35p. *J. Cell Biol.* 151:297-309.

Nothwehr, S.F., and A.E. Hindes. 1997. The yeast VPS5/GRD2 gene encodes a sorting nexin-1-like protein required for localizing membrane proteins to the late Golgi. *J. Cell Sci.* 110:1063-1072.

Ogawa-Goto, K., K. Tanaka, T. Ueno, K. Tanaka, T. Kurata, T. Sata, and S. Irie. 2007. p180 is involved in the interaction between the endoplasmic reticulum and microtubules through a novel microtubule-binding and bundling domain. *Mol. Biol. Cell.* 18:3741-3751.

Patel, J.C., and J.E. Galán. 2006. Differential activation and function of Rho GTPases during *Salmonella*-host cell interactions. *J. Cell Biol.* 175:453-463.

Pechlivanis, M., and J. Kuhlmann. 2006. Hydrophobic modifications of Ras proteins by isoprenoid groups and fatty acids—more than just membrane anchoring. *Biochim. Biophys. Acta.* 1764:1914-1931.

Pelham, H.R.B. 1988. Evidence that luminal ER proteins are sorted from secreted proteins in a post-ER compartment. *EMBO J.* 7:913-918.

Peng, J., B.J. Wallar, A. Flanders, P.J. Swiatek, and A.S. Alberts. 2003. Disruption of the diaphanous-related formin Drf1 gene encoding mDia1 reveals a role for Drf3 as an effector for Cdc42. *Curr. Biol.* 13:534-545.

Pennetta, G., P.R. Hiesinger, R. Fabian-Fine, I.A. Meinertzhagen, and H.J. Bellen. 2002. Drosophila VAP-33A directs bouton formation at neuromuscular junctions in a dosage-dependent manner. *Neuron.* 35:291-306.

Penzes, P., A. Beeser, J. Chernoff, M.R. Schiller, B.A. Eipper, R.E. Mains, and R.L. Huganir. 2003. Rapid induction of dendritic spine morphogenesis by trans-synaptic EphrinB-EphB receptor activation of the Rho-GEF Kalirin. *Neuron.* 37:263-274.

Penzes, P., R.C. Johnson, M.R. Alam, V. Kambampati, R.E. Mains, and B.A. Eipper. 2000. An isoform of Kalirin, a brain-specific GDP/GTP exchange factor, is enriched in the postsynaptic density fraction. *J. Biol. Chem.* 275:6395-6403.

Penzes, P., R.C. Johnson, R. Sattler, X. Zhang, R.L. Huganir, V. Kambampati, R.E. Mains, and B.A. Eipper. 2001. The neuronal Rho-GEF Kalirin-7 interacts with PDZ domain-containing proteins and regulates dendritic morphogenesis. *Neuron.* 29:229-242.

Perry, R.J., and N.D. Ridgway. 2006. Oxysterol-binding protein and vesicle-associated membrane protein-associated protein are required for sterol-dependent activation of the ceramide transport protein. *Mol. Biol. Cell.* 17:2604-2616.

Peter, B.J., H.M. Kent, I.G. Mills, Y. Vallis, P.J.G. Butler, P.R. Evans, and H.T. McMahon. 2004. BAR domains as sensors of membrane curvature: the amphiphysin BAR structure. *Science*. 303:495-499.

Pevsner, J., S.-C. Hsu, J.E.A. Braun, N. Calakos, A.E. Ting, M.K. Bennett, and R.H. Scheller. 1994. Specificity and regulation of a synaptic vesicle docking complex. *Neuron*. 13:353-361.

Prieto-Sánchez, R.M., and X.R. Bustelo. 2003. Structural basis for the signaling specificity of RhoG and Rac1 GTPases. *J. Biol. Chem.* 278:37916-37925.

Prosser, D.C., D. Tran, P.-Y. Gougeon, C. Verly, and J.K. Ngsee. 2008. FFAT rescues VAPA-mediated inhibition of ER-to-Golgi transport and VAPB-mediated ER aggregation. *J. Cell Sci.* 121:3052-3061.

Pylypenko, O., R. Lundmark, E. Rasmuson, S.R. Carlsson, and A. Rak. 2007. The PX-BAR membrane-remodeling unit of sorting nexin 9. *EMBO J.* 26:4788-4800.

Radice, G., J.J. Lee, and F. Costantini. 1991. Hβ58, an insertional mutation affecting early postimplantation development of the mouse embryo. *Development*. 111:801-811.

Raiborg, C., K.G. Bache, D.J. Gillooly, I.H. Madshus, E. Stang, and H. Stenmark. 2002. Hrs sorts ubiquitinated proteins into clathrin-coated microdomains of early endosomes. *Nat. Cell Biol.* 4:394-398.

Ratovitski, E.A., M.R. Alam, R.A. Quick, A. McMillan, C. Bao, C. Kozlovsky, T.A. Hand, R.C. Johnson, R.E. Mains, B.A. Eipper, and C.J. Lowenstein. 1999. Kalirin inhibition of inducible nitric-oxide synthase. *J. Biol. Chem.* 274:993-999.

Razzaq, A., I.M. Robinson, H.T. McMahon, J.N. Skepper, Y. Su, A.C. Zelhof, A.P. Jackson, N.J. Gay, and C.J. O'Kane. 2001. Amphiphysin is necessary for organization of the excitation-contraction coupling machinery of muscles, but not for synaptic vesicle endocytosis in *Drosophila*. *Genes Dev.* 15:2967-2979.

Reddy, J.V., and M.N.J. Seaman. 2001. Vps26p, a component of retromer, directs the interactions of Vps35p in endosome-to-Golgi retrieval. *Mol. Biol. Cell.* 12:3242-3256.

Reits, E.A.J., and J.J. Neefjes. 2001. From fixed to FRAP: measuring protein mobility and activity in living cells. *Nat. Cell Biol.* 3:E145-E147.

Ridley, A.J. 2006. Rho GTPases and actin dynamics in membrane protrusions and vesicle trafficking. *Trends Cell Biol.* 16:522-529.

Ridley, A.J., and A. Hall. 1992. The small GTP-binding protein rho regulates the assembly of focal adhesions and actin stress fibers in response to growth factors. *Cell.* 70:389-399.

Ridley, A.J., H.F. Paterson, C.L. Johnston, D. Diekmann, and A. Hall. 1992. The small GTP-binding protein rac regulates growth factor-induced membrane ruffling. *Cell.* 70:401-410.

Riento, K., and A.J. Ridley. 2003. ROCKs: multifunctional kinases in cell behaviour. *Nat. Rev. Mol. Cell Biol.* 4:446-456.

Roberts, T.M., and M. Stewart. 2000. Acting like actin: the dynamics of the nematode major sperm protein (MSP) cytoskeleton indicate a push-pull mechanism for amoeboid cell motility. *J. Cell Biol.* 149:7-12.

Robinson, J.S., D.J. Klionsky, L.M. Banta, and S.D. Emr. 1988. Protein sorting in *Saccharomyces cerevisiae*: isolation of mutants defective in the delivery and processing of multiple vacuolar hydrolases. *Mol. Cell. Biol.* 8:4936-4948.

Rogaeva, E., Y. Meng, J.H. Lee, Y. Gu, T. Kawarai, F. Zou, T. Katayama, C.T. Baldwin, R. Cheng, H. Hasegawa, and *et al.* 2007. The neuronal sortilin-related receptor SORL1 is genetically associated with Alzheimer disease. *Nat. Genet.* 39:168-177.

Rojas, R., S. Kametaka, C.R. Haft, and J.S. Bonifacino. 2007. Interchangeable but essential functions of SNX1 and SNX2 in the association of retromer with endosomes and the trafficking of mannose 6-phosphate receptors. *Mol. Cell. Biol.* 27:1112-1124.

Rong, J., J.R. McGuire, Z.-H. Fang, G. Sheng, J.-Y. Shin, S.-H. Li, and X.-J. Li. 2006. Regulation of intracellular trafficking of huntingtin-associated protein-1 is critical for TrkA protein levels and neurite outgrowth. *J. Neurosci.* 26:6019-6030.

Roth, M.G. 2004. Phosphoinositides in constitutive membrane traffic. *Physiol. Rev.* 84:699-730.

Rothman, J.H., I. Howald, and T.H. Stevens. 1989. Characterization of genes required for protein sorting and vacuolar function in the yeast *Saccharomyces cerevisiae*. *EMBO J.* 8:2057-2065.

Rothman, J.H., and T.H. Stevens. 1986. Protein sorting in yeast: mutants defective in vacuole biogenesis mislocalize vacuolar proteins into the late secretory pathway. *Cell.* 47:1041-1051.

Roux, A., K. Uyhazi, A. Frost, and P. De Camilli. 2006. GTP-dependent twisting of dynamin implicates constriction and tension in membrane fission. *Nature*. 441:528-531.

Salazar, M.A., A.V. Kwiatkowski, L. Pellegrini, G. Cestra, M.H. Butler, K.L. Rossman, D.M. Serna, J. Sondek, F.B. Gertler, and P. De Camilli. 2003. Tuba, a novel protein containing Bin/Amphiphysin/Rvs and Dbl homology domains, links dynamin to regulation of the actin cytoskeleton. *J. Biol. Chem.* 278:49031-49043.

Saraste, J., and E. Kuismanen. 1984. Pre- and post-Golgi vacuoles operate in the transport of Semliki Forest virus membrane glycoproteins to the cell surface. *Cell*. 38:535-549.

Saxton, M.J. 1987. Lateral diffusion in an archipelago. *Biophys. J.* 52:989-997.

Schiestl, R.H., and R.D. Gietz. 1989. High efficiency transformation of intact yeast cells using single stranded nucleic acids as a carrier. *Curr. Genet.* 16:339-346.

Schiller, M.R., A. Blangy, J. Huang, R.E. Mains, and B.A. Eipper. 2005. Induction of lamellipodia by Kalirin does not require its guanine nucleotide exchange factor activity. *Exp. Cell. Res.* 307:402-417.

Schiller, M.R., F. Ferraro, Y. Wang, X.-m. Ma, C.E. McPherson, J.A. Sobota, N.I. Schiller, R.E. Mains, and B.A. Eipper. 2008. Autonomous functions for the Sec14p/spectrin-repeat region of Kalirin. *Exp. Cell Res.* 314:2674-2691.

Schröder, M., and R.J. Kaufman. 2005. The mammalian unfolded protein response. *Annu. Rev. Biochem.* 74:739-789.

Schwarz, D.G., C.T. Griffin, E.A. Schneider, D. Yee, and T. Magnuson. 2002. Genetic analysis of sorting nexins 1 and 2 reveals a redundant and essential function in mice. *Mol. Biol. Cell*. 13:3588-3600.

Seaman, M.N.J. 2004. Cargo-selective endosomal sorting for retrieval to the Golgi requires retromer. *J. Cell Biol.* 165:111-122.

Seaman, M.N.J., E.G. Marcusson, J.L. Cereghino, and S.D. Emr. 1997. Endosome to Golgi retrieval of the vacuolar protein sorting receptor, Vps10p, requires the function of the VPS29, VPS30, and VPS35 gene products. *J. Cell Biol.* 137:79-92.

Seaman, M.N.J., J.M. McCaffery, and S.D. Emr. 1998. A membrane coat complex essential for endosome-to-Golgi retrograde transport in yeast. *J. Cell Biol.* 142:665-681.

Seaman, M.N.J., and H.P. Williams. 2002. Identification of the functional domains of yeast sorting nexins Vps5p and Vps17p. *Mol. Biol. Cell.* 13:2826-2840.

Seet, L.-F., and W. Hong. 2006. The Phox (PX) domain proteins and membrane traffic. *Biochim. Biophys. Acta.* 1761:878-896.

Semenza, J.C., K.G. Hardwick, N. Dean, and H.R.B. Pelham. 1990. ERD2, a yeast gene required for the receptor-mediated retrieval of luminal ER proteins from the secretory pathway. *Cell.* 61:1349-1357.

Sever, S., A.B. Muhlberg, and S.L. Schmid. 1999. Impairment of dynamin's GAP domain stimulates receptor-mediated endocytosis. *Nature.* 398:481-486.

Shao, Y., W. Akmentin, J.J. Toledo-Aral, J. Rosenbaum, G. Valdez, J.B. Cabot, B.S. Hilbush, and S. Halegoua. 2002. Pincher, a pinocytic chaperone for nerve growth factor/TrkA signaling endosomes. *J. Cell Biol.* 157:679-691.

Shaw, P.J. 2005. Molecular and cellular pathways of neurodegeneration in motor neurone disease. *J. Neurol. Neurosurg. Psychiatry.* 76:1046-1057.

Shi, H., R. Rojas, J.S. Bonifacino, and J.H. Hurley. 2006. The retromer subunit Vps26 has an arrestin fold and binds Vps35 through its C-terminal domain. *Nat. Struct. Mol. Biol.* 13:540-548.

Shimada, A., H. Niwa, K. Tsujita, S. Suetsugu, K. Nitta, K. Hanawa-Suetsugu, R. Akasaka, Y. Nishino, M. Toyama, L. Chen, Z.-J. Liu, B.-C. Wang, M. Yamamoto, T. Terada, A. Miyazawa, A. Tanaka, S. Sugano, M. Shirouzu, K. Nagayama, T. Takenawa, and S. Yokoyama. 2007. Curved EFC/F-BAR-domain dimers are joined end to end into a filament for membrane invagination in endocytosis. *Cell.* 129:761-772.

Shin, N., N. Ahn, B. Chang-Ileto, J. Park, K. Takei, S.-G. Ahn, S.-A. Kim, G.D. Paolo, and S. Chang. 2008. SNX9 regulates tubular invagination of the plasma membrane through interaction with actin cytoskeleton and dynamin 2. *J. Cell Sci.* 121:1252-1263.

Shin, O.-H., and J.H. Exton. 2001. Differential binding of Arfaptin 2/POR1 to ADP-ribosylation factors and Rac1. *Biochem. Biophys. Res. Commun.* 285:1267-1273.

Simpson, J.C., T. Nilsson, and R. Pepperkok. 2006. Biogenesis of tubular ER-to-Golgi transport intermediates. *Mol. Biol. Cell.* 17:723-737.

Sivadon, P., F. Bauer, M. Aigle, and M. Crouzet. 1995. Actin cytoskeleton and budding pattern are altered in the yeast rvs161 mutant: the Rvs161 protein shares common domains with the brain protein amphiphysin. *Mol. Gen. Genet.* 246:485-495.

Skehel, P.A., R. Fabian-Fine, and E.R. Kandel. 2000. Mouse VAP33 is associated with the endoplasmic reticulum and microtubules. *Proc. Natl. Acad. Sci. USA.* 97:1101-1106.

Skehel, P.A., K.C. Martin, E.R. Kandel, and D. Bartsch. 1995. A VAMP-binding protein from *Aplysia* required for neurotransmitter release. *Science.* 269:1580-1583.

Smith, H.E., and S. Ward. 1998. Identification of protein-protein interactions of the major sperm protein (MSP) of *Caenorhabditis elegans. J. Mol. Biol.* 279:605-619.

Söllner, T., S.W. Whiteheart, M. Brunner, H. Erdjument-Bromage, S. Geromanos, P. Tempst, and J.E. Rothman. 1993. SNAP receptors implicated in vesicle targeting and fusion. *Nature.* 362:318-324.

Soulet, F., D. Yarar, M. Leonard, and S.L. Schmid. 2005. SNX9 regulates dynamin assembly and is required for efficient clathrin-mediated endocytosis. *Mol. Biol. Cell.* 16:2058-2067.

Soussan, L., D. Burakov, M.P. Daniels, M. Toister-Achituv, A. Porat, Y. Yarden, and Z. Elazar. 1999. ERG30, a VAP-33-related protein, functions in protein transport mediated by COPI vesicles. *J. Cell Biol.* 146:301-311.

Spires, T.L., H.E. Grote, S. Garry, P.M. Cordery, A. Van Dellen, C. Blakemore, and A.J. Hannan. 2004. Dendritic spine pathology and deficits in experience-dependent plasticity in R6/1 Huntington's disease transgenic mice. *Eur. J. Neurosci.* 19:2799-2807.

Strochlic, T.I., T.G. Setty, A. Sitaram, and C.G. Burd. 2007. Grd19/Snx3p functions as a cargo-specific adapter for retromer-dependent endocytic recycling. *J. Cell Biol.* 177:115-125.

Suetsugu, S., K. Murayama, A. Sakamoto, K. Hanawa-Suetsugu, A. Seto, T. Oikawa, C. Mishima, M. Shirouzu, T. Takenawa, and S. Yokoyama. 2006. The Rac binding domain/IRSp53-MIM homology domain of IRSp53 induces Rac-dependent membrane deformation. *J. Biol. Chem.* 281:35347-35358.

Sutton, R.B., D. Fasshauer, R. Jahn, and A.T. Brunger. 1998. Crystal structure of a SNARE complex involved in synaptic exocytosis at 2.4Å resolution. *Nature.* 395:347-353.

Takei, K., V.I. Slepnev, V. Haucke, and P. De Camilli. 1999. Functional partnership between amphiphysin and dynamin in clathrin-mediated endocytosis. *Nat. Cell Biol.* 1:33-39.

Tarricone, C., B. Xiao, N. Justin, P.A. Walker, K. Rittinger, S.J. Gamblin, and S.J. Smerdon. 2001. The structural basis of Arfaptin-mediated cross-talk between Rac and Arf signalling pathways. *Nature*. 411:215-219.

Teuling, E., S. Ahmed, E. Haasdijk, J. Demmers, M.O. Steinmetz, A. Akhmanova, D. Jaarsma, and C.C. Hoogenraad. 2007. Motor neuron disease-associated mutant vesicle-associated membrane protein-associated protein (VAP) B recruits wild-type VAPs into endoplasmic reticulum-derived tubular aggregates. *J. Neurosci.* 27:9801-9815.

The Huntington's Disease Collaborative Research Group. 1993. A novel gene containing a trinucleotide repeat that is expanded and unstable on Huntington's disease chromosomes. *Cell*. 72:971-983.

Traer, C.J., A.C. Rutherford, K.J. Palmer, T. Wassmer, J. Oakley, N. Attar, J.G. Carlton, J. Kremerskothen, D.J. Stephens, and P.J. Cullen. 2007. SNX4 coordinates endosomal sorting of TfnR with dynein-mediated transport into the endocytic recycling compartment. *Nat. Cell Biol.* 9:1370-1380.

Tsuda, H., S.M. Han, Y. Yang, C. Tong, Y.Q. Lin, K. Mohan, C. Haueter, A. Zoghbi, Y. Harati, J. Kwan, M.A. Miller, and H.J. Bellen. 2008. The amyotrophic lateral sclerosis 8 protein VAPB is cleaved, secreted, and acts as a ligand for Eph receptors. *Cell*. 133:963-977.

Tsuda, T., S. Munthasser, P.E. Fraser, M.E. Percy, I. Rainero, G. Vaula, L. Pinessi, L. Bergamini, G. Vignocchi, D.R.C. McLachlan, W.G. Tatton, and P. St George-Hyslop. 1994. Analysis of the functional effects of a mutation in SOD1 associated with familial amyotrophic lateral sclerosis. *Neuron*. 13:727-736.

Valdez, G., W. Akmentin, P. Philippidou, R. Kuruvilla, D.D. Ginty, and S. Halegoua. 2005. Pincher-mediated macroendocytosis underlies retrograde signaling by neurotrophin receptors. *J. Neurosci.* 25:5236-5247.

Van Aelst, L., T. Joneson, and D. Bar-Sagi. 1996. Identification of a novel Rac1-interacting protein involved in membrane ruffling. *EMBO J.* 15:3778-3786.

van Buul, J.D., M.J. Allingham, T. Samson, J. Meller, E. Boulter, R. García-Mata, and K. Burridge. 2007. RhoG regulates endothelial apical cup assembly downstream from ICAM1 engagement and is involved in leukocyte trans-endothelial migration. *J. Cell Biol.* 178:1279-1293.

Vedrenne, C., D.R. Klopfenstein, and H.-P. Hauri. 2005. Phosphorylation controls CLIMP-63-mediated anchoring of the endoplasmic reticulum to microtubules. *Mol. Biol. Cell*. 16:1928-1937.

Vergés, M., F. Luton, C. Gruber, F. Tiemann, L.G. Reinders, L. Huang, A.L. Burlingame, C.R. Haft, and K.E. Mostov. 2004. The mammalian retromer regulates transcytosis of the polymeric immunoglobulin receptor. *Nat. Cell Biol.* 6:763-769.

Vigorito, E., S. Bell, B.J. Hebeis, H. Reynolds, S. McAdam, P.C. Emson, A. McKenzie, and M. Turner. 2004. Immunological function in mice lacking the Rac-related GTPase RhoG. *Mol. Cell. Biol.* 24:719-729.

Vincent, S., P. Jeanteur, and P. Fort. 1992. Growth-regulated expression of *rhoG*, a new member of the *ras* homolog gene family. *Mol. Cell. Biol.* 12:3138-3148.

Voeltz, G.K., W.A. Prinz, Y. Shibata, J.M. Rist, and T.A. Rapoport. 2006. A class of membrane proteins shaping the tubular endoplasmic reticulum. *Cell.* 124:573-586.

Wacker, I., C. Kaether, A. Krömer, A. Migala, W. Almers, and H.-H. Gerdes. 1997. Microtubule-dependent transport of secretory vesicles visualized in real time with a GFP-tagged secretory protein. *J. Cell Sci.* 110:1453-1463.

Wang, D., M. Guo, Z. Liang, J. Fan, Z. Zhu, J. Zang, Z. Zhu, X. Li, M. Teng, L. Niu, Y. Dong, and P. Liu. 2005. Crystal structure of human vacuolar protein sorting protein 29 reveals a phosphodiesterase/nuclease-like fold and two protein-protein interaction sites. *J. Biol. Chem.* 280:22962-22967.

Wassmer, T., N. Attar, M.V. Bujny, J. Oakley, C.J. Traer, and P.J. Cullen. 2007. A loss-of-function screen reveals SNX5 and SNX6 as potential components of the mammalian retromer. *J. Cell Sci.* 120:45-54.

Watanabe, N., P. Madaule, T. Reid, T. Ishizaki, G. Watanabe, A. Kakizuka, Y. Saito, K. Nakao, B.M. Jockusch, and S. Narumiya. 1997. p140mDia, a mammalian homolog of *Drosophila* diaphanous, is a target protein for Rho small GTPase and is a ligand for profilin. *EMBO J.* 16:3044-3056.

Waters, M.G., T. Serafini, and J.E. Rothman. 1991. 'Coatomer': a cytosolic protein complex containing subunits of non-clathrin-coated Golgi transport vesicles. *Nature*. 349:248-251.

Weir, M.L., H. Xie, A. Klip, and W.S. Trimble. 2001. VAP-A Binds promiscuously to both v- and t-SNAREs. *Biochem. Biophys. Res. Commun.* 286:616-621.

Weissenhorn, W. 2005. Crystal structure of the endophilin-A1 BAR domain. *J. Mol. Biol.* 351:653-661.

Wennerberg, K., S.M. Ellerbroek, R.-Y. Liu, A.E. Karnoub, K. Burridge, and C.J. Der. 2002. RhoG signals in parallel with Rac1 and Cdc42. *J. Biol. Chem.* 277:47810-47817.

Wennerberg, K., K.L. Rossman, and C.J. Der. 2005. The Ras superfamily at a glance. *J. Cell Sci.* 118:843-846.

Worby, C.A., and J.E. Dixon. 2002. Sorting out the cellular functions of sorting nexins. *Nat. Rev. Mol. Cell Biol.* 3:919-931.

Wyles, J.P., C.R. McMaster, and N.D. Ridgway. 2002. Vesicle-associated membrane protein-associated protein-A (VAP-A) interacts with the oxysterol-binding protein to modify export from the endoplasmic reticulum. *J. Biol. Chem.* 277:29908-29918.

Wyles, J.P., and N.D. Ridgway. 2004. VAMP-associated protein-A regulates partitioning of oxysterol-binding protein-related protein-9 between the endoplasmic reticulum and Golgi apparatus. *Exp. Cell Res.* 297:533-547.

Xin, X., Y. Wang, X.-m. Ma, P. Rompolas, H.T. Keutmann, R.E. Mains, and B.A. Eipper. 2008. Regulation of Kalirin by Cdk5. *J. Cell Sci.* 121:2601-2611.

Yamaki, N., M. Negishi, and H. Katoh. 2007. RhoG regulates anoikis through a phosphatidylinositol 3-kinase-dependent mechanism. *Exp. Cell Res.* 313:2821-2832.

Yarar, D., M.C. Surka, M.C. Leonard, and S.L. Schmid. 2008. SNX9 activities are regulated by multiple phosphoinositides through both PX and BAR domains. *Traffic.* 9:133-146.

Yarar, D., C.M. Waterman-Storer, and S.L. Schmid. 2005. A dynamic actin cytoskeleton functions at multiple stages of clathrin-mediated endocytosis. *Mol. Biol. Cell.* 16:964-975.

Yarar, D., C.M. Waterman-Storer, and S.L. Schmid. 2007. SNX9 couples actin assembly to phosphoinositide signals and is required for membrane remodeling during endocytosis. *Dev. Cell.* 13:43-56.

Youn, H., M. Jeoung, Y. Koo, H. Ji, W.R. Markesbery, I. Ji, and T.H. Ji. 2007a. Kalirin is under-expressed in Alzheimer's disease hippocampus. *J. Alzheimers. Dis.* 11:385-397.

Youn, H., I. Ji, H.P. Ji, W.R. Markesbery, and T.H. Ji. 2007b. Under-expression of Kalirin-7 increases iNOS activity in cultured cells and correlates to elevated iNOS activity in Alzheimer's disease hippocampus. *J. Alzheimers. Dis.* 12:271-281.

Zerial, M., and H. McBride. 2001. Rab proteins as membrane organizers. *Nat. Rev. Mol. Cell Biol.* 2:107-117.

Zhao, L., and S.L. Ackerman. 2006. Endoplasmic reticulum stress in health and disease. *Curr. Opin. Cell Biol.* 18:444-452.

Zhong, Q., C.S. Lazar, H. Tronchère, T. Sato, T. Meerloo, M. Yeo, Z. Songyang, S.D. Emr, and G.N. Gill. 2002. Endosomal localization and function of sorting nexin 1. *Proc. Natl. Acad. Sci. USA*. 99:6767-6772.

Zimmer, M., A. Palmer, J. Köhler, and R. Klein. 2003. EphB-ephrinB bi-directional endocytosis terminates adhesion allowing contact mediated repulsion. *Nat. Cell Biol.* 5:869-878.